
Thanapong Suwanasri

**Investigation on No-load Mechanical
Endurance and Electrical Degradation
of a Circuit Breaker Model under
Short Circuit Current Interruption**

Investigation on No-load Mechanical Endurance and Electrical Degradation of a Circuit Breaker Model under Short Circuit Current Interruption

Von der Fakultät für Elektrotechnik und Informationstechnik
der
Rheinisch-Westfälischen Technischen Hochschule Aachen
zur Erlangung des akademischen Grades eines
Doktors der Ingenieurwissenschaften
genehmigte Dissertation

vorgelegt von

Thanapong Suwanasri, M.Sc.
aus Bangkok, Thailand

Berichter: Univ.-Prof. Dr.-Ing. Armin Schnettler
Univ.-Prof. Dr.-Ing. Hans-Jürgen Haubrich

Tag der mündlichen Prüfung: 8. Februar 2006

Diese Dissertation ist auf den Internetseiten der Hochschulbibliothek der
RWTH Aachen online verfügbar.

Acknowledgement

This thesis has been written during my time (2001-2005) as a scientific staff at the Institute of High Voltage Technology of Aachen University of Technology. Within these years, I have received a lot of help and support from many parties and I would like to express my deep appreciation to them.

First of all I would like to thank Univ.-Prof. Dr.-Ing. Armin Schnettler for offering me the opportunity to pursue my doctoral degree under his supervision, his professional guidance, patience, encouraging, enthusiasm and support. Furthermore I am extremely grateful to Univ.-Prof. Dr.-Ing. Hans-Jürgen Haubrich, who kindly accepted the responsibility for being a co-supervisor.

My appreciation is extended to Univ.-Prof. Dr.-Ing. Rolf H. Jansen for his encouraging and offering a chance for Thai students to study at RWTH-Aachen University. Financial support from Siemens AG (Germany) during this research project is specially acknowledged.

My thanks are also extended to my colleagues, especially Dr.-Ing. Christian Cornelissen, Dipl.-Ing. Robert Dommerque, Dipl.-Ing. Lutz Hulka, Dipl.-Ing. Michael Schmale, Dipl.-Ing. Michael Schwinne, Dipl.-Ing. Christoph Kahlen and all the other colleagues for their impressive friendship and help during my work at the Institute of High Voltage Technology.

I am indebted to all staffs in the workshop, especially Leo Künzer and Helmut Liedecke, for their valuable help and prompt support throughout my work with their great patience in the preparations of testing facilities in a laboratory.

My greatest gratitude must go to my parents and my brother, who has taken a good care of my parents all the time and especially during my time in Germany, and my best friend Miss Ruchada Wissanu Wong. Their love, greatest motivation and constant support have played a vital role behind my work and make me proud and honor of being a part of the family.

Last but not least, I wish to thank Mr. Pornchai, Mr. Tonglor, Kittipong, Chadchai, Chanchai, Cattareeya, friends in Aachen and in Thailand and the others who have not been mentioned here for their encouragement as well as support.

Aachen, in February 2006

Thanapong Suwanasri

Abstract

The demand on reducing circuit breaker failure, extending service life, increasing equipment reliability and lowering the related operating and maintenance costs are nowadays of prime importance for the electricity supply network. According to statistics, the major failure mode is originated from operating mechanism, whereas interrupter has the highest percentage of failure in high voltage component. Thus, the method to facilitate the assessment of internal mechanical conditions by using commercially available devices without opening major parts and the experimental investigation on electrical erosion inside the interrupter were performed in this work.

The experimental investigation on the mechanical endurance of operating mechanism up to 6,000 no-load switching was performed with 110kV puffer type circuit breakers due to its requirement of large driving energy for hydraulic operating mechanism. The conventional measurement, e.g. coil current, contact timing, dynamic contact resistance and pumping motor current as well as additional vibration technique were carried out in both laboratory and field test. The investigation on electrical erosion focusing on aging of nozzle and electrode under current interruption was performed with a reduced-size SF₆ self-blast circuit breaker model and synthetic test circuit, providing the current density comparable to that in the real circuit breaker, because of the extensive use of nozzle ablation, the possibility for parameters variation and the reduction of cost and time.

For mechanical investigation, the parameters were measured at the beginning as a reference and also thereafter every 500 switching under normal and variable operating conditions, e.g. variation of auxiliary supply voltage, hydraulic oil pressure and SF₆ gas pressure. The test result was verified by that from two of the same type circuit breakers and the theoretical calculation for vibration result in the frequency-domain analysis. Subsequently, the on-site measurement before and after maintenance and some simulated defects were executed. The electrical aging investigation was performed by successive tests with constant energy stresses until interrupting failure occurred. The effect of current amplitude, nozzle diameter, expansion volume, arcing time and recovery voltage on mass losses, geometry changes of nozzle and its influence on pressure build-up were investigated.

The analysis of vibration signals in a combination with the other supervised parameters provides the useful information regarding the significant events occurring inside during circuit breaker operation, e.g. motion start of mechanism and within pole, contact touching and motion stop. The deviations of these measured values from the reference according to number of no-load switching operations, variable operating conditions and some incorporated defects were comprehensively determined. The relationship between the gradual changes in technical status of the supervised components and the number of no-load operations is helpful for selecting the proper maintenance method.

Regarding the electrical erosion of the nozzle and the electrodes, the mass losses per switching and per energy; and the geometry change of nozzle especially between the arcing column and the expansion chamber were investigated. Moreover, volume loss and mass loss along the nozzle column; its effect on the pressure build-up reduction; and the dependences of mass losses on interrupting current amplitude, $\int i dt$ and $\int i^2 dt$; have been determined. Furthermore by applying the wear equivalent law, the allowable number of interruption in function of the breaking current to rated short-circuit current ratio and the remaining lifetime can be determined. This result will be used to verify the accuracy of simulation tools in order to visualize the aging process, to evaluate the interrupter condition and to minimize the expensive experiment tests.

Untersuchungen zur mechanischen Leerlauf-Dauerbeständigkeit und der elektrischen Abnutzung eines Leistungsschaltermodells bei Lichtbogenbeanspruchungen

Kurzfassung

Die Verringerung der Komponentenausfallrate, die Verlängerung der Nutzungsdauer, die zunehmende Zuverlässigkeit und die Senkung der Betriebs- und Instandhaltungskosten spielen heute eine wichtige Rolle für das elektrische Versorgungsnetz. Bei Hochspannungs-Leistungsschaltern ist statistisch der Antrieb die Hauptursache eines Fehlers, während die Unterbrechereinheit die höchste Ausfallrate der Aktivteile aufweist und bei modernen SF₆-Selbstblasschaltern zudem einem Degradationseffekt unterliegt. Demzufolge wurden in dieser Arbeit der innere mechanische Zustand eines Leistungsschalters mit Hilfe handelsüblicher Diagnoseverfahren bestimmt und experimentelle Untersuchungen der elektrischen Abnutzung innerhalb einer Unterbrechereinheit durchgeführt.

Bei der experimentellen Untersuchung der mechanischen Leerlauf-Dauerprüfung mit bis zu 6.000 Schaltungen wurde ein 110kV-Blaskolben-Leistungsschalter mit hydraulischem Antrieb genutzt, da dieser Schaltertyp eine relativ große Antriebskraft besitzt und somit üblicherweise eine höhere Ausfallrate aufweist. Messungen der Spulenströme, der Schaltzeiten, des dynamischen Kontaktwiderstandes und des Pumpenmotorstroms sowie die Vibrationscharakteristiken wurden im Labor und bei den Vor-Ort-Messungen durchgeführt. Die experimentelle Bestimmung der Abnutzung der Düsen und der Elektroden bei Lichtbogenbeanspruchungen wurde mit einem SF₆-Selbstblasschalter-Modell untersucht. Dabei wurden die geprüften Stromdichten denen kommerzieller Selbstblasschalter angepasst.

Für die mechanische Untersuchung wurden die Messgrößen zu Beginn der Untersuchungen als Referenz herangezogen. Nach jeweils 500 Schaltungen unter normalen und variablen Betriebsbedingungen, d.h. Variation der Versorgungsspannung, des Hydraulikdruckes und des SF₆-Druckes, wurden die aufgenommenen Parameter mit den Referenzwerten verglichen. Zusätzlich konnten die Analyseergebnisse mit denen gleicher Leistungsschaltertypen und mit theoretischen Berechnungen der Vibrationscharakteristiken verglichen und verifiziert werden. Anschließend wurden Vor-Ort-Messungen vor und nach einer Wartung sowie zusätzlich Messungen mit künstlich eingebrachten Defekten durchgeführt. Die Untersuchungen zur Düsen- und der Elektrodenabnutzung wurden in sequentiellen Versuchen mit konstanter Lichtbogenenergie so lange durchgeführt, bis das Schaltermodell sein Ausschaltvermögen verloren hatte. Die Einflüsse von Stromstärke, Düsendurchmesser, Druckkammervolumen, Lichtbogenzeit und Wiederkehrspannung auf die Massenverluste, Geometrieänderung der Düse und den Druckaufbau wurden dabei untersucht.

Die Analyse der Vibrationssignale im Zusammenhang mit anderen gemessenen Parametern kann Informationen über auftretende signifikante Ereignisse, z. B. die Betätigung des Einschaltmagnets, die Bewegung des Hilfskontakts, die Hauptkontaktberührung und das Erreichen des Schalterendzustands liefern. Die Abweichungen dieser gemessenen Werte von den Referenzwerten konnte eindeutig der Anzahl der Leerlauf-Schaltungen, den variablen Betriebsbedingungen und einigen simulierten Defekten zugeordnet werden.

Im Bezug auf die Lichtbogenbelastung wurden die Massenverluste pro Schaltung und pro Energie, die Geometrieänderung insbesondere zwischen Lichtbogenkanal und Schaltkammer untersucht. Die Volumen- und Massenverluste entlang des Düsenkanals, der Einfluss des Düsenaufbrandes auf die Reduzierung des Druckaufbaus sowie die Massenverluste als Funktion der Stromstärke wurden ermittelt. Durch diese Kenntnisse und die Anwendung des Abnutzungsäquivalent-Gesetzes kann die zulässige Schaltanzahl als Funktion des Verhältnisses von Abschaltstrom bezogen auf den Nennkurzschlussstrom und die Restnutzungsdauer bestimmt werden. Die gewonnenen experimentellen Daten werden zur Kalibrierung bzw. Verifizierung der CFD-Simulationen eingesetzt, mit deren Hilfe eine Zustandsbewertung der Schaltkammer ohne erheblichen experimentellen Versuchsaufwand erfolgen kann.

Table of Contents

1	Introduction.....	1
1.1	Introduction to the Topic	1
1.2	Knowledge Status	5
1.3	Objective of the Thesis	9
2	Basic Theory	12
2.1	Operating Principle of SF ₆ Circuit Breakers.....	12
2.2	Switching Phenomena and Switching Requirements	15
2.2.1	Switching Phenomena.....	15
2.2.2	Switching Requirements	17
2.3	Degradation and Monitoring Techniques	19
2.3.1	Equipment Failure and Basic Knowledge of Maintenance	19
2.3.2	Degradation and Failure Patterns.....	21
2.3.3	Condition Monitoring and Maintenance.....	24
2.3.4	Reliability and Availability.....	26
2.4	Ablation-controlled Arc and Material Properties	29
2.4.1	Ablation-controlled Arc.....	29
2.4.2	Arc Modelling and Material Properties	30
2.5	Choice of SF ₆ Circuit Breaker Monitoring.....	37
3	Investigations of No-load Mechanical Endurance of an Industrial Type Circuit Breaker	38
3.1	Experiment Set-up and Test Arrangement.....	38
3.1.1	Experiment Set-up.....	39
3.1.2	Measurement Techniques and Method	42
3.1.3	Theoretical Calculation of Circuit Breaker Pole Vibration	47
3.2	Experimental Results	48
3.2.1	Comparison of Results at Rated Operating Condition.....	48
3.2.2	Comparison of Various Operating Conditions and Artificial Defects....	54
3.3	Summary	60

4	Investigations on Current Interruption Using an SF₆ Circuit Breaker Model.....	61
4.1	Experiment Set-up and Test Arrangement.....	61
4.1.1	Circuit Breaker Model.....	62
4.1.2	Synthetic Test Circuit and Measurement Techniques.....	63
4.1.3	Example of the Measured Result and the Gas Flow Observation.....	64
4.1.4	Experiment Methods	65
4.2	Measured Parameters and Characteristics of Synthetic Test Circuit	69
4.3	Circuit Breaker Model Degradation.....	72
4.3.1	Determination of Mass Loss and Ablation Factor	72
4.3.2	Determination of Nozzle Geometry Change.....	75
4.3.3	Influence of Nozzle Widening on the Pressure Build-up and Gas Flow	78
4.4	Impact from the Other Parameters on the Degradation	82
4.5	Summary and Outlook	85
5	Withstand Capability of Circuit Breaker Model to Breaking Current....	86
5.1	Method to Determine the Allowable Number of Interruptions and the Remaining Lifetime of Circuit Breaker	86
5.1.1	Interrupting Current Consideration	87
5.1.2	$\int i dt$ and $\int i^2 dt$ Consideration.....	89
5.2	Result from Measurement with Circuit Breaker Model.....	92
6	Conclusions	96
7	Zusammenfassung.....	99
8	References	102
9	List of Abbreviations and Symbols.....	114
10	Appendix	117
	Curriculum Vitae	125

1 Introduction

1.1 Introduction to the Topic

High voltage circuit breakers have been extensively used in electrical power systems in order to making, carrying and breaking the current in normal operating condition as well as in abnormal conditions within specific time. The abnormal or fault current in electrical power systems can be ranged from some of 10kA in subtransmission and transmission network up to more than 100kA in the generating parts. The present and future demands on the current carrying capacity and interrupting capacity are of prime importance for circuit breaker selection. Because a principal function of circuit breakers is to provide the means for short circuit current interruption, its failure in operation could lead to unfavorable consequences.

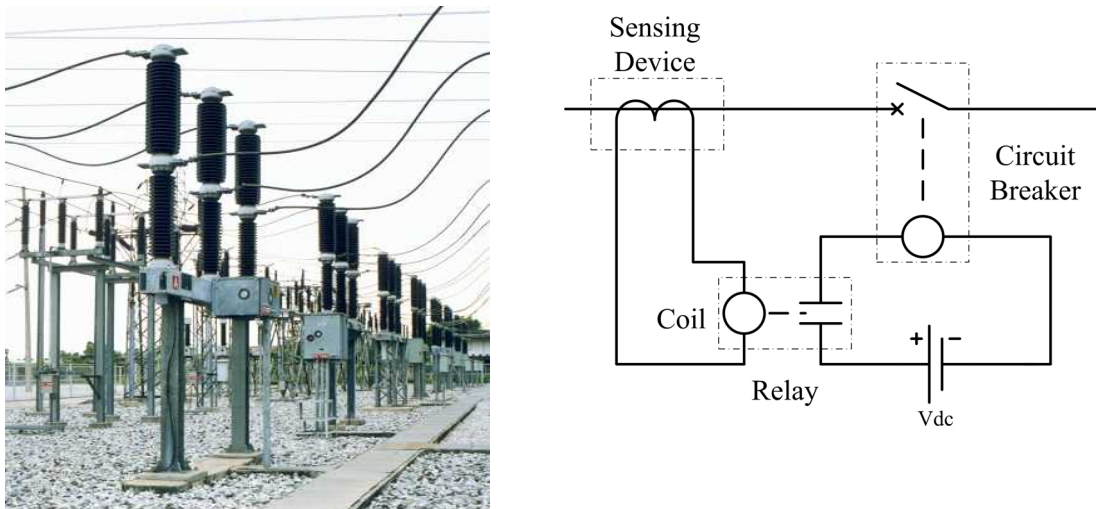


Figure 1.1: 110kV circuit breaker and overview of related components

Generally, a circuit breaker has to work together with other devices as a team as shown in Figure 1.1 in order to interrupt the current. It usually consists of sensing device such as a current transformer, and protective relay. A current transformer (CT) usually supplies the secondary current (1A or 5A) to protective relays. In case an abnormal condition occurs, the relay will receive a current from CT higher than pick up setting and send a command to the trip coil of the circuit breaker. After the trip coil of circuit breaker receives the current, the circuit breaker will operate to interrupt the abnormal current. Therefore failures of any associated devices or failure in circuit breaker itself could result in misoperation and subsequently damaging effects as a whole.

SF₆ circuit breakers are the most widely used ranging from medium voltage to extra high voltage with two or more interrupters in series [Loo02]. Around 1952, the application of SF₆ gas as an arc-quenching medium has been initiated. SF₆ is used as a good insulating and arc quenching medium not only because it is a colourless, non-toxic, non-flammable, chemically inert at low temperature gas, but it also has no reaction with metals, plastic and other substances, electronegativity property,

high dielectric strength and fast dielectric recovery during current zero period due to its low thermal time constant. During current interruption process, many decomposition products of SF_6 such as SF_4 , SF_2 , H_2S , HF , SOF_2 , SOF_4 and S_2F_{10} depending on the arc current as well as contact and nozzle ablation occur due to the high temperature from power arc. Most of the decomposition products recombine within a very short time in the order of 10^{-6} to 10^{-7} seconds. Nevertheless, SF_6 has high global warming potential, liquefaction problem and long lifetime of 3,000 years [Cig00b], the alternative of SF_6 , such as SF_6 mixture diluted by N_2 [Gar76b], [Son02] or CF_4 , or the use of CO_2 is considered to substitute the pure SF_6 in circuit breaker.

In the early days, SF_6 circuit breakers were the two-pressure type. The interrupting function was performed by a high velocity flow of SF_6 through the orifice of a PTFE nozzle located inside the arc-extinguishing chamber. Later on, it was superseded by SF_6 puffer circuit breakers, which gains the advantages in a compact chamber. SF_6 puffer circuit breakers use the axial convection as a predominant heat transfer mechanism. However, rather complex driving mechanisms for higher ratings have become an obstacle in circuit breaker development, regarding higher reliability and more economical designs, to satisfy the steadily increasing demands. Thus, the third generation using self-blast principle was introduced. Initially during high current period the hot gas, caused by a part of arc energy and expanding into the expansion chamber during arc clogging period, together with the ablated mass inflow result in the higher gas pressure in the expansion chamber. Later on when nozzle throat becomes liberated by a reduction of the arc diameter at lower instantaneous current values, the pressure difference between the expansion chamber and the arcing column generates a gas flow through the nozzle along the arc. Hence, the interrupting conditions in self-blast circuit breakers are much more dependent on the interrupting current than those in the puffer type circuit breakers. By using self-generated pressure the required driving energy is significantly reduced in comparison to the puffer type, thus a relatively simple spring mechanism can be used. Nevertheless, intensive use of the nozzle ablation seems to be unavoidable in order to obtain the required build-up pressure in expansion chamber [Gaj98]. Nowadays, high-voltage self-blast single interrupter circuit breakers are produced up to a rating of 245kV, 63kA [Sed03].

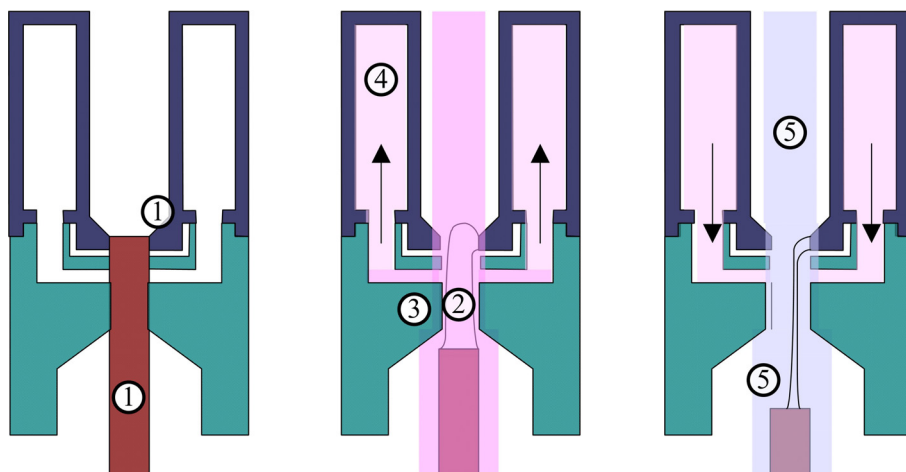


Figure 1.2: Operating principle of self-blast circuit breaker

For the sake of simplicity, Figure 1.2 is always used to explain the operating principle of self-blast circuit breaker by many authors [Kri99], [Puf01]. After contact (1) separation, the arc (2) occurs and it is forced into a narrow, cylindrically shaped nozzle (3) made of PolyTetraFluoroEthylene (PTFE) or Teflon and it becomes ablation controlled. The vaporized nozzle material generates a high-pressure stagnation point at the nozzle centre, which forces hot gas into the expansion chamber (4). In the expansion chamber, the mixing process between incoming hot gas with vaporized nozzle and electrode material and the existing cold gas occurs and causes a pressure rise in the expansion chamber. When the current approaches its natural current zero, the ablation vanishes and the pressure between nozzle area decreases. The pressure inside the expansion volume, which is now higher than the pressure between the nozzles, flows back providing the extinguishing flow (5).

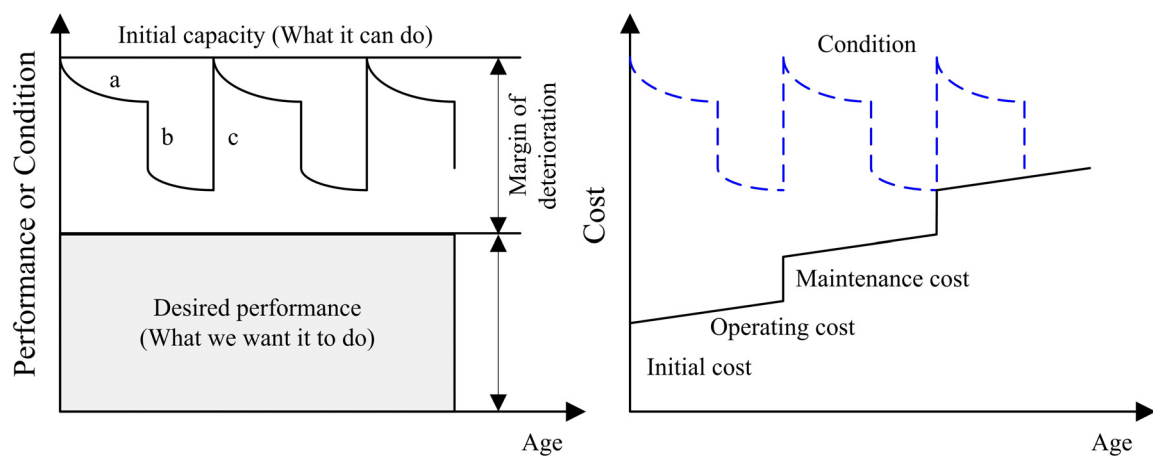


Figure 1.3: Margin of deterioration [Mou97], condition-age relationship and related cost

After circuit breakers have been installed in service, their current interruptions lead to an electrical degradation of interrupting unit, especially nozzle and electrode. Their ablated mass and geometry change result in lower pressure build-up, contaminated insulating gas and less interrupting capability. In principle, according to Figure 1.3 (left), the condition degradation is caused by many kinds of stresses (b) imposed by the electrical network, e.g. overvoltage due to switching of inductive and capacitive load, interrupting of terminal fault and short line fault. Moreover, external stresses mostly from the nature, such as lightning impulse voltage, temperature, UV-rays, pollution flashover, etc. also affect the degradation. These stresses (b) and aging (a) not only cause the deterioration in circuit breaker performance from initial capability, but they also increase operating and maintenance costs, reduce reliability and affect safety and environmental concerns. Occasionally, circuit breakers may not have operated for several months, but they still have to provide the reliable interruptions of any fault current at all time. Therefore, maintenance activity (c) has played a vital role in order to maintain the performance within acceptable limit as shown in Figure 1.3 (left). The related expenses such as initial investment, operating and maintenance costs are shown in Figure 1.3 (right).

In the past, corrective and preventive maintenance strategies have been broadly applied to maintain the asset. The main idea of preventive maintenance is that every asset has a useful lifetime. Consequently, the same typical lifetime patterns have been applied to a group of similar assets with similar operating circumstances. Indeed, each asset has its own individual useful lifetime. Therefore, the too-early replacement of asset results in waste of money and asset life, while the too-late replacement brings about poor reliability and increases the associated cost.

Because of the inadequacy to serve the growing demand in the past, the assets were replaced before their deteriorating condition or performance became an issue. Nowadays, many assets are rated sufficiently to fulfil a low growing demand up to the expiry of their lifetimes. Cost reduction such as minimization of operating and maintenance costs and investment of spare parts, and the optimization of using assets until their end of lifetime are now the major concerns of utilities to be able to compete in the liberalized electricity market. Besides, life extension by proper maintenance or the use of diagnostic tools to keep track of asset conditions is also one of prime interest. For that reason, condition-based maintenance is now taking over the traditional preventive maintenance. The condition assessment by using on-line monitoring has been applied to develop an understanding about the condition of asset in a large population with similar circumstances by examining a representative sample.

According to the second survey by CIGRE' [Hei94] about the reliability and failure mode of high voltage circuit breakers shown in Figure 1.4, the common failure causes of SF₆ single pressure circuit breakers are 43% in operating mechanism and 26% in high voltage component. The particular consideration on high voltage components shows that 45% of failure stems from interrupter unit, which is approximate 12% of total failures. Thus, failures of operating mechanism and interrupter unit deserve to be focused.

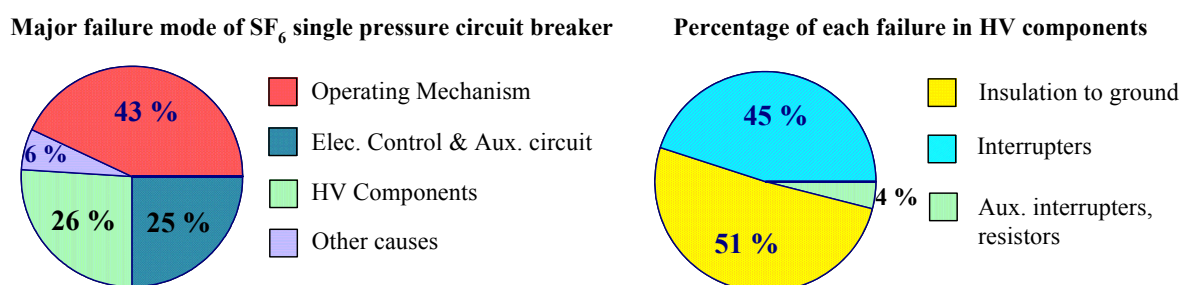


Figure 1.4: Failure statistic of SF₆ single pressure circuit breaker

The mechanical life test, i.e. the number of no-load operations that the mechanism and contacts can operate without undue wear, has been performed to investigate the endurance of operating mechanism. Because of no current flowing through the contacts during testing, the only loading is purely mechanical. However, the knowledge about the deteriorating or gradual changes in mechanical condition after number of no-load operations is still limited. By using diagnostic devices together with non-invasive techniques, the technical state of observed components can be determined from the outside measurement without any disassembly. The relationship between the technical status changes from the pre-determined reference

base line of the supervised components and the number of no-load operation should provide the useful information to adopt the proper maintenance method. Moreover, switching of load and fault current results in an electrical aging of components in the interrupter unit, especially nozzle and contact which are directly exposed to powerful arc radiation. The investigation on electrical degradation after each interruption in terms of component wear, physical changes as well as its influence on gas flow characteristic with a circuit breaker model and a synthetic test circuit offers the possibility to verify and adjust the accuracy of simulation tools, which subsequently will be a powerful tool to visualize the aging process inside the interrupter unit.

1.2 Knowledge Status

After the first generation of two-pressure type SF₆ circuit breaker, the puffer type, which generates the gas blast by means of puffing principle consisting of piston and cylinder built into a circuit breaker interrupter [Bro84], has been vastly used for several decades. Unfortunately, the puffer type circuit breaker may fail to interrupt at very high current due to clogging processes, which not only shuts off the escaped gas, but also resists the imposed movement and under severe conditions can reclose the break [Gre91]. For this reason, it requires a powerful mechanism to continue the opening stroke, which is not practical for a high voltage circuit breaker with higher rated current. Besides reliability, a desire to achieve higher voltage rating per break, smaller and cheaper circuit breaker is also an interesting point for circuit breaker development [Ike84], [Suz92].

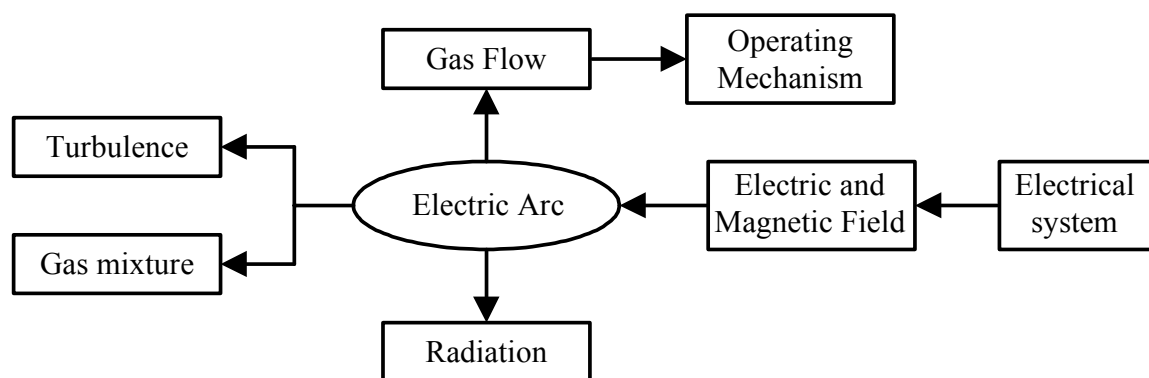


Figure 1.5: Overview of switching phenomena inside circuit breaker

In order to understand the complex phenomena inside self-blast circuit breakers during current interruption as shown in Figure 1.5, many theoretical and numerical calculations and experimental investigations have been continually conducted. The theoretical descriptions and investigations of cylindrical-form arcs in a tube of ablative wall dealing with stationary two-temperature or isothermal two-zone arc model, axial convection and radiative energy transfer could be found in [Lee75], [Her77], [Nos77], [Nie78], [Kov84], [Ruc86], [Biz97], [Blu97]. The two-zone model represents the physical behaviour of an ablation-controlled arc by a hot, conducting, radiation emitting, cylindrical plasma column surrounding by a non-conductive colder vapour layer. It is also assumed that the temperature jumps drastically from one zone to the other. Consequently, the conservation equations of

mass, momentum and energy can be solved for the relationship of various parameters such as gas flow velocity, pressure, density, current and electric field. Meanwhile, the other theoretical descriptions of arc modeling were also introduced [Fan86]. The further development of the two-zone model for ablation-controlled arc in long cylindrical nozzle [Mül93a] as well as the studies of arc during high current phase [Gle88a] were reported. This two-zone arc model along with thermodynamic property of turbulence gas flow was implemented in CFD (Computational Fluid Dynamics) algorithm for simulation of current interruption during high current phase [Cla97c]. Unfortunately, the two-zone arc model is suitable only for the high current period. The modeling during current-zero period is also inevitably significant, because the residual plasma inside the nozzle throat and influence of turbulence gas flows are responsible for the thermal and dielectric recovery capability of a circuit breaker. Thus, many researchers try to predict the arc behaviour during current-zero period [Gar76a], [Gle88b], [Zha02b]. Theoretical investigations have been performed to study the dielectric recovery of insulating gas [Per72a], [Per72b], [Mit86], electron-ion recombination rate constant [Bar97] and dielectric recovery of residual SF₆ plasma [Yan01].

In SF₆ self-blast circuit breakers, the interactions of switching arc, gas flow, pressure build-up, nozzle material and interrupting geometry are really complex. Additionally, its interrupting capability depends primarily on the state of extinguishing gas, which is not only determined by pressure, but also by temperature and mass fraction of all ablated materials. Therefore, various experimental investigations have been performed with circuit breaker models to investigate the interrupting capability influenced by nozzle erosion [Mei86], by using different nozzle materials [Mül93b], [Cla97a], [Kri99], different volumes and configurations of expansion chamber [Yos02], arc-gas interaction [Yos02], [Sed03], gas flow velocity and pattern [Puf01] and the use of high-speed camera to observe the arc in the extinction area [Kie93] etc. These investigations provide the understanding of hot and cold gas mixture in the expansion chamber, effective energy removal from the arc extinction area, recovery of dielectric strength and high voltage withstand in that area after arc extinction. Besides, the experiment with full power short circuit interruption testing is also very costly. So it is necessary to utilize data obtaining from the large number of reduced power test in order to determine the circuit breaker design parameters [Per78].

Numerical analysis such as CFD-calculations, have been used to calculate temperature, mass fraction of ablated nozzle materials, turbulence activity, density and velocity of the mixing phenomena in the expansion chamber, which are difficult to access from the measurement, of both model and industrial-type circuit breaker [Wen93], [Cla97b], [Yan99a], [Yan99b], [Zha00], [Jai01], [Bae02], [Xin02], [deH03]. The mathematical models to calculate the distribution of emission and absorption in plasma, which generally depends on the concentration of chemical species occurring in the plasma, were introduced. The calculations for the radiation emitted by an SF₆ arc have been developed, such as the net emission coefficient of radiation [Aub94], the Method of Partial Characteristics (MPC) [Ray95], [Bou96], [Kom97], [deH01], [Kim02]. The good agreement between experiment and

simulation ensures the use of calculated results and information from numerical model as a design aid [Sca92].

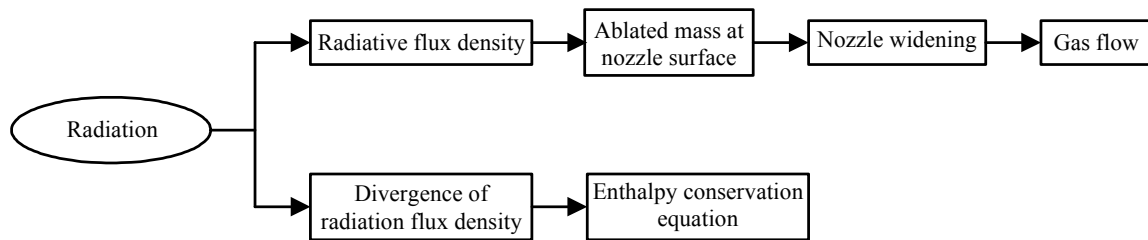


Figure 1.6: Nozzle ablation due to the arc radiation

According to Figure 1.6, pressure built-up in the expansion chamber is normally generated when the hot PTFE vapour heats up and compresses the gas in the expansion volume. This ablated PTFE vapour generated by strong arc radiation adds mass, momentum and energy to the system and consequently modifies the arcing environment. Furthermore, it also affects the composition of the gas and residual plasma left in the arc extinction area, which determines the dielectric strength of the gap. Therefore, investigations on nozzle ablation effect and the mixing process of PTFE vapour with SF_6 were carried out [Jon86], [Zha02a], and recently the computation of the nozzle ablation factors and nozzle throat diameter enlargement was presented [Osa03]. The Cu vapour contamination with SF_6 gas increases the electrical conductivity, which has a negative effect on the interruption performance of circuit breaker, while PTFE vapour contamination does not have deleterious effect on arc-interruption. The effect of CuW and PTFE vapour contaminations on the transient behaviour of SF_6 arcs, such as transport and thermodynamic properties, was reported [Air76], [Jon88a], [Gon96], [Pau97], [Cou98]. The influence of metal vapour such as copper, silver and aluminum, on pressure in the expansion volume was investigated in terms of initial and average rate of rise of pressure [Jai99]. Various decomposition products appear in the form of gaseous and powdery products. Switching dust caused by arc erosion of contact consists of CuF_2 , WOF_4 and WO_2F_2 etc. [Cam89]. The erosion of contacts and nozzles leads to increasing ohmic resistance of the current carrying path followed by an increasing temperature. Degradation process of grease caused by SF_6 dissociation products was also performed [Suz82]. Apart from those degradations, they are also subjected to various stresses [Bec01]. The two severe cases are short-line fault, demanding a high thermal interruption performance due to the high rate of rise of the recovery voltage (RRRV), and terminal-fault, demanding a high dielectric interruption performance because of the high recovery voltage peak. Accordingly, interruption ability as a function of pressure and dI/dt for both severe cases [Swa77], [Ari90] as well as arc resistance measurement around current zero to determine the limit capacity of circuit breakers for short line fault [Kno99] have been investigated.

To discover the subassemblies of the circuit breaker that deserve more attention regarding the improvement of quality assessment, design, testing, maintenance, diagnostics etc., the second international survey limited to only single pressure SF_6 circuit breakers was conducted [Jan94], [Jan96]. According to [Jan94], the average

number of operating cycles is 42 cycles per year and the average interval between scheduled maintenance is 8.3 years. The operating mechanism is the subassembly with the most failures. The dominant failure modes are “Does not open or close on command” and “Locked in open or closed position”. The components in the interrupter unit, which limit the service life, are nozzle and arcing contact. The dependence of switching capability on the ablation and the geometry change of the nozzle caused by radiation was presented in [Aub02], [Tel02]. Load current, no-load line switching and current lower than 30% of rated short circuit current do not cause significant wear in the interrupter. Unfortunately, information concerning the numbers and type of operating cycles, e.g. load switching, no-load switching, capacitive current switching, making or breaking short circuit current, are scarcely collected. Otherwise, it would be a helpful guideline for maintenance staff to adopt the proper maintenance measures.

Mechanical and electrical endurance tests are used to verify the service life of circuit breaker, which has often been set at 25 years, but normally circuit breakers rated 110 to 145kV have been removed from service after 35 to 40 years and 30 to 35 years for 230kV [Cig00a]. Electrical endurance test generally determines the cumulative kA that may be interrupted during the lifetime of circuit breaker without maintenance. This test can be carried out at reduced recovery voltage because transient recovery voltage (TRV) does not affect ageing due to very low power dissipation [Pon93]. In [Sto88] the electrical endurance test with double flow single break 145kV circuit breaker showed the erosion of arcing contact and nozzle after current interruptions. Because of directly exposed to powerful arc radiation during current interruption, nozzle wear can be seen from an increasing bore diameter and modification of blowout conditions. Therefore, by proper maintenance, use of diagnostic tools, standardized extended test programs [IEC04] and sporadic repairs to keep any deviation of interrupting characteristics within acceptable tolerances [Men92] an extension of service can be achieved. A diagnostic system allowing the diagnosis of internal operating conditions of circuit breakers from the outside measurement without any disassembly was proposed [Noa88], [Jon94]. The technical diagnostic of the circuit breaker is realized through the supervision of some parameters such as coil current, dynamic contact resistance, contact timing, contact travel, vibration measurement etc. These selected parameters should offer specific information about the technical state of the supervised equipment. The radiated emission from the arc was also observed by using optical fibre-based system to provide monitoring information during circuit breaker operation [Jon88b], [Col94]. Aspect about the knowledge of contact wear determined by current and arcing time measurement and dynamic contact resistance measurement [Jea88], [Hof92], [Fuj98], [Ada03] states that the accumulated value of I^2t at each opening could provide a valid indication of the arcing contact wear. Using of vibration measurement as a non-invasive technique to access the mechanical conditions of circuit breaker was performed by many researchers [Lai88], [Ohs89], [Dem92], [Hes92], [Run92], [Pol95], [Run99], [Hua03], [Suw03], [Suw04]. An extensive field-testing with 31 circuit breakers was conducted in [Run96]. The use of on-line monitoring system is proposed [Bar88], [Hof92], [Vou94], [Van02], [Neu04] as well as statistical methods to evaluate the circuit breaker condition. The requirement

and reliability of the monitoring device are mentioned in [Jan92]. For that reason, not only the traditional preventive maintenance can be turned into a condition-based maintenance for the individual circuit breaker, but the maintenance costs can also be reduced by extending the period between maintenance and restricting to only necessary work. However, this demands comprehensive and accurate records of performance in various stages of circuit breaker operation [Faw78].

Practically, by implementing the simple diagnostic and monitoring methods, such as pressure and gas density, contact resistance, timing and contact travel, the mechanical and electrical degradation can not be clearly determined. Meanwhile, the using of existing data to evaluate the electrical wear, such as the evaluation of accumulated fault current and time from the recorded data of digital protection relay [Bar88], [Hof92], [Neu90], is limited by the determination of mass loss, the influence of current interruption on geometry change of the components inside the interrupting unit and their further consequences on the interrupting performance as well as current transformer saturation. Furthermore, the reliability of the monitoring system, durability, lifetime and resistance to electromagnetic interference still require the further improvement.

Up till now, the use of non-invasive diagnostic tools to access the internal mechanical condition and keep track of its deterioration during mechanical test, especially when reaching the limit-life, is not completely available. Additionally, the electrical erosion and degradation of components inside the interrupter unit, i.e. nozzle and electrode dominated by the direct contact with power arc, after each current interruption in term of mass loss per switching, ablation factor, physical change and its influence on gas flow and pressure build-up is not clearly determined. These will be extensively performed in this work.

1.3 Objective of the Thesis

The purpose of this study is to find a non-invasive method to access the internal mechanical condition of a circuit breaker during no-load mechanical endurance test and with simulated defects; to investigate the degradation in electrical condition after each short circuit current interruption; and to find a method to predict the erosion and its remaining lifetime. The gained experimental results concerning mass loss per switching and ablation factor of nozzle and electrode, physical changes of nozzle as well as its influence on the build-up pressure will be further used to verify and adjust the accuracy of simulation tools in order to visualize and evaluate the aging process inside circuit breakers.

The experimental investigations of no-load mechanical endurance test are performed with three industrial-type circuit breakers, which are 110kV SF₆ puffer type circuit breakers with hydraulic operating mechanism. One of them is used as a reference and the investigation is performed up to 6,000 switching operations under several operating conditions, e.g. variation of auxiliary power supply voltage and motor supply voltage, SF₆ and hydraulic oil pressure change. The non-invasive techniques and vibration measurement are applied. At the beginning of the test, the measurement results of the first circuit breaker are compared with the other two of

the same type circuit breakers to ensure the reliability of the result. After that, some artificial defects are incorporated into reference circuit breaker to observe the sensitivity of monitored parameters to the imposed defects.

The analysis using the combination of appropriate measured parameters including event-timing extraction of vibration signals provides the possibility to detect the occurrence of significant events inside circuit breakers. By observing the changes of these supervised parameters, any change from the reference fingerprint implies the change in circuit breaker condition or an early indication of a potential problem. The knowledge about the deteriorating or gradual changes in mechanical condition after a number of no-load operations will subsequently be the useful information to adopt the proper maintenance measure.

The investigation on current interruption using an SF₆ circuit breaker model is carried out to gain the understanding about the degradation of electrical condition. Instead of using a real circuit breaker and high power short-circuit laboratories, which is very costly and laborious in order to access the components inside the interrupter unit, a reduced-size circuit breaker model and a synthetic test circuit are used, providing the possibilities for parameters variations, such as nozzle diameter, expansion chamber volume, current amplitude and recovery voltage. Since the experiment is designed to avoid complicated measurement, only arc current, voltage across nozzle and across electrode and pressure in expansion chamber are measured. From the recorded current and voltage waveforms, the current amplitude, $\int i dt$, $\int i^2 dt$ and energy over nozzles and over electrodes of each interruption can be simply derived. Because nozzle ablation and electrode erosion occur during each current interruption, the mass loss of nozzles and electrodes including nozzle geometry changes especially around the nozzle edge between arcing column and expansion chamber and mass loss and volume loss along nozzle column per switching are determined. Consequently, the ablation factor, i.e. mass loss per energy, of nozzles and electrode as well as the dependence of mass loss on current amplitude, $\int i dt$, $\int i^2 dt$ can be determined. The impact of nozzle geometry change after each interruption on gas flow and pressure build-up is also investigated. The deviation of maximum pressure, pressure at current zero and time to reach those pressures after each successive interruption can be observed from the recorded waveform of pressure build-up inside the expansion chamber. Practically, a circuit breaker has to provide the reliable interruption under varying current amplitude up to its rated short-circuit current. Hence the impact of the interrupted current amplitude on the electrical degradation is the primary investigation. Each test condition is carried out successively by imposing constant energy over one pair of nozzle and electrode until a thermal failure occurs. By this way, the number of allowable interruption under different current amplitudes can be determined. The influences of arcing time, reduced expansion volume and higher recovery voltage on degradation and pressure build-up are also additionally observed. To obtain the statistically reasonable result, the repetitive testing of each test condition is necessary, and should be performed under the same testing environment.

Furthermore, by knowing the mass loss or wear limit the allowable number of interruptions in function of breaking current to rated short-circuit current ratio and

remaining lifetime can be estimated. Further investigations to improve and verify the accuracy of the nozzle ablation and contact erosion models in the CFD simulation need to be performed as shown in Figure 1.7. The good agreement between experiment and simulation ensures the use of calculated results and information from simulation to visualize and evaluate the aging process inside the interrupter unit. With the aid of simulation tools, the expensive and demanding experiment testing could be avoided or at least minimized. It is expected that this method will become an economically effective method for circuit breaker condition evaluation and diagnostic.

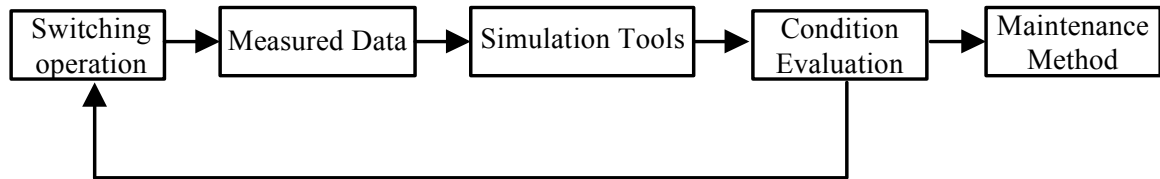


Figure 1.7: Diagram of circuit breaker diagnostic

2 Basic Theory

The operating principle of SF₆ circuit breakers for both puffer and self-blast types is described in the first part. After that, switching phenomena and switching requirement for arc extinction, thermal and dielectric recovery are presented in the second part. The degradation and monitoring techniques, such as maintenance techniques, failure patterns, principle of condition monitoring and maintenance, reliability and availability concept, are subsequently discussed in the third part.

Eventually, the ablation-controlled arc, arc modeling and material properties of SF₆, PTFE and SF₆-PTFE mixture used to calculate and describe the switching arc phenomena inside the interrupter unit are presented. The choice of circuit breaker monitoring is discussed in the last section.

2.1 Operating Principle of SF₆ Circuit Breakers

Formerly, SF₆ circuit breakers were of the two-pressure type [Flu77]. Its structural design was based on bulk oil circuit breaker. The extinguishing chamber and the contacts of each phase were located in the earthed steel tank filled with SF₆ around 3 bars absolute. During interruption, the high velocity flow of SF₆ from the high-pressure storage tank through the orifice of a PTFE nozzle located inside the arc-extinguishing chamber was performed. Because SF₆ was stored in the tank with high pressure, there was the possibility of SF₆ liquefaction during low temperature period. Further disadvantages of the two-pressure type circuit breaker were the need to store large quantities of high-pressure gas for a long period, gas leakage, complexity resulting from using the blast valves and large chamber size.

The SF₆ puffer type circuit breaker overcame the above-mentioned problem of the two-pressure type with only one compact chamber. The pressurization to produce sufficient flow is achieved by piston and cylinder compression, assembled as an integral part of the moving contact, during contact separation. Its operating principle can be described as follows:

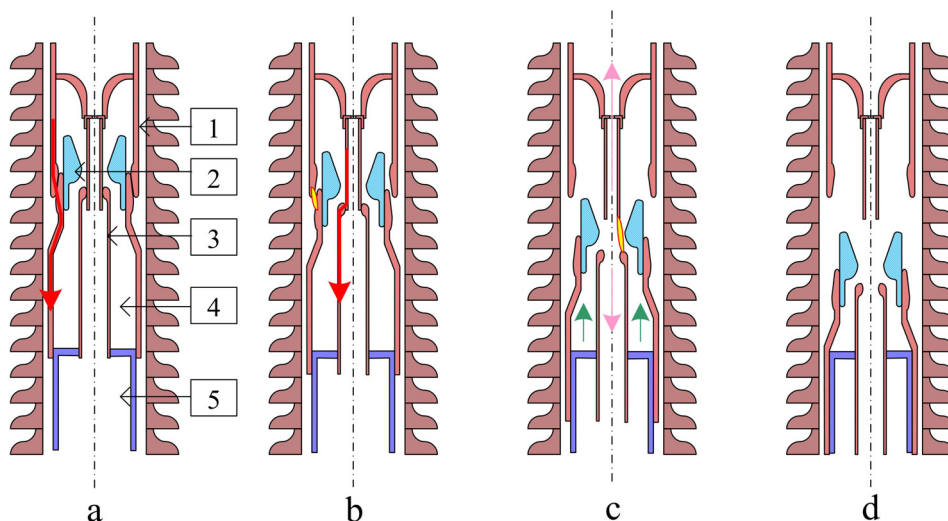


Figure 2.1: Operating principle of puffer type circuit breaker

- a. In Figure 2.1 a, the interrupter is in closed position and the current practically flows through the terminal pad, contact support, fix contact (1), moving contact, guide tube and terminal pad, respectively.
- b. In Figure 2.1 b, at the first breaking period, the moving contact connected with the operating rod is now moving downward and the current now flows through the arcing contacts (3).
- c. In Figure 2.1 c, along with contact opening, the blast cylinder is moved towards the fixed piston (5) and compresses the trapped SF₆ in the compression chamber (4). Immediately after contact separation, when the fixed contact (1) is still inside the insulating nozzle (2) throat, the arc is blocked. After the nozzle throat separates from the fixed contact, it still can be temporarily closed by the large diameter arc owing to higher instantaneous values of the current called “nozzle clogging” [Nos77]. In this situation, gas flow is minimized and the arc energy inside the nozzle cannot be effectively evacuated.
- d. By reduction of arc diameter at lower instantaneous current values [Cao91], the nozzle throat becomes liberated. The relatively high-density gas, compressed along the whole stroke of an opening operation, flows turbulently through the nozzle and causes rapidly convective heat transfer from the arc to the surrounding colder SF₆ gas. Figure 2.1d shows the position of each component after successful current interruption.

For the conventional puffer type circuit breaker, a considerable amount of mechanical energy is needed during opening operation to compress the gas and create an efficient gas flow for arc energy removal. According to Cigre’ statistic [Hei94], observing the behavior of high-voltage circuit breaker in actual service, the most malfunctions are of mechanical nature. Hence, the development of circuit breakers during the last 20 years have focused on alternative interrupting principles, which require lower mechanical energy for their operation [Gaj98]. This leads to simple operating mechanisms and less mechanical stress on kinetic chain. Lower mechanical stress means less wear, higher reliability, lower operating cost and longer mechanical lifetime. Moreover, the small moving masses and low contact velocity should be developed in order to reduce mechanical operating energy. For that reason, self-blast circuit breakers have been introduced by utilizing the arc energy to build up the gas pressure necessary for the arc extinction and dielectric recovery.

The basic feature of a self-blast circuit breaker is that the gas pressure needed for the flow of the arc-extinguishing medium SF₆ is created by the thermal energy of the arc itself. Its operating principles can be described as follows:

- a. In Figure 2.2 a, the interrupter is in closed position and the current flows through terminal pad, contact support, fix contact (1), moving contact, guide tube and terminal pad, respectively.
- b. At the first breaking period by opening of main contact, the arc occurs between fixed and moving main contacts. The moving contact connected with operating rod is now moving downward and compresses the gas in the

compression chamber by fixed piston (7). As soon as the pressure inside the compression chamber (6) is higher than that in expansion chamber (4), the valve (5) opens and the compressed gas flows out. After that, the current now changes to flow through arcing contacts (3) as shown in Figure 2.2 b.

- c. After the separation of the arcing contacts, the arc occurs and the nozzle is subsequently blocked. In this high current phase as shown in Figure 2.2 c, there is only little gas flow through the throat of the hollow arcing contact because it is mainly filled by the arc. The ohmic heating of the gas in the steadily increasing volume between the fixed and moving arcing contacts builds up a pressure, which forces the heated gas to flow into the expansion chamber. After that, the valve (5) is closed because the pressure in the expansion chamber is now higher than that in the compression chamber, in which the gas is further compressed due to the moving of the contact. The pressure build-up in the nozzle area (2) is predominantly enhanced by the evaporation of material from the insulating nozzle wall.
- d. The insulating gas is heated until the fixed arcing contact leaves the bottleneck of nozzle and the arc diameter decreases because the current is now approaching current zero. The stored pressure in the expansion chamber is now forced to flow back through the nozzle and extinguish the arc.
- e. When the decreasing pressure inside the expansion chamber by outflow of gas is lower than that in the compression chamber, the valve opens again. Then, the compressed cold gas flows out and supports to extinguish the small conducting arc current. At last, the interruption process is complete as shown in Figure 2.2 d.

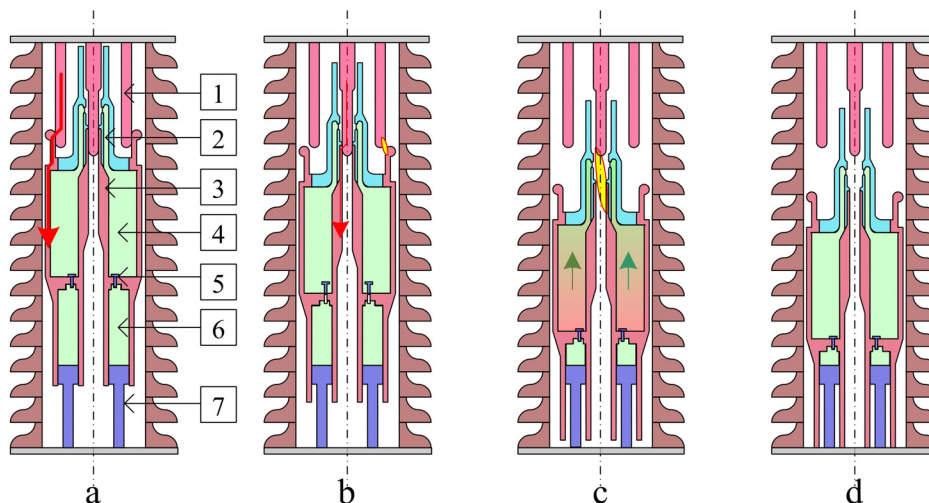


Figure 2.2: Operating principle of self-blast with auxiliary puffer circuit breaker

The more intensive the heating, the higher the gas pressure and more intensive gas flow become more pronounced in case of interrupting higher short-circuit current. However, the gas temperature in the expansion chamber is higher than that of conventional puffer type owing to ohmic heating. This is one of the major limitations of self-blast circuit breakers because the high temperature of the gas reduces the recovery voltage withstand of the area between the open arcing contacts. For higher breaking currents, it causes the increasing in gas heating and

higher gas temperature. For this reason, the interrupting capacity is limited not only by the thermal breaking capability, but also by the recovery of dielectric strength.

In case of breaking low current, the arc energy is not sufficient to create the required pressure build-up to extinguish the arc. An additional gas flow must be driven by mechanical compression. The shape of the expansion chamber should be optimized to achieve the good mixing between the existing cold gas and the inflowing hot gas, which means the effective use of the cold gas and results in the increasing quality of the interrupting process [Yos02], [Sed03].

2.2 Switching Phenomena and Switching Requirements

2.2.1 Switching Phenomena

According to circuit breaker functions, when it is in closed position, it has to carry a current with a wide variety of amplitude ranging from load current to rated short-circuit current with negligible voltage drop across its contacts. While in the opened position, there is no current flowing through the contact, but the full rated system voltage and often the rated impulse withstand voltage appear across its contacts. This statement implies that a circuit breaker is stressed by current in closed position and by voltage in opened position, which occur in separate time. Nevertheless, circuit breaker is not only in closed or opened position all the time, but it also changes its position or status from one to the other, which is called switching operation.

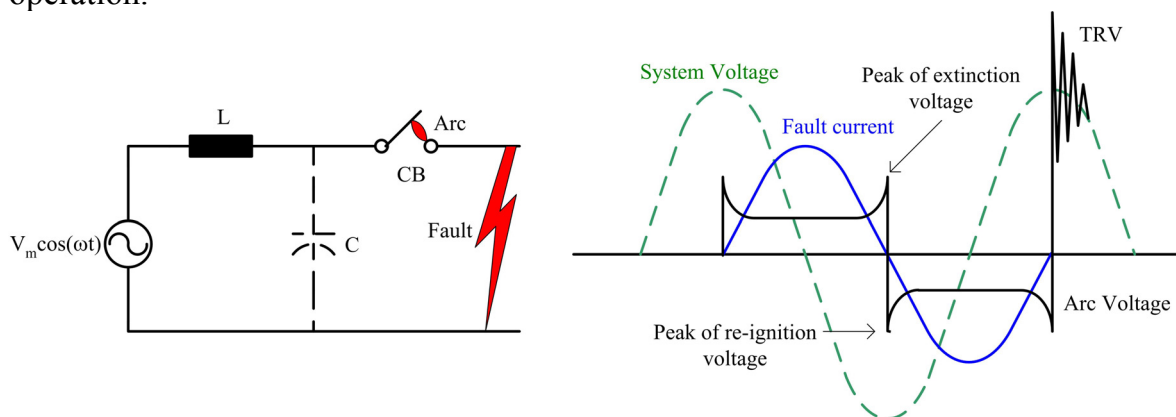


Figure 2.3: Arc voltage characteristic and current interruption process

According to Figure 2.3, the simple circuit consisting of only a reactance and a stray capacitance is used to describe the fault current interruption of a circuit breaker. Refer to the above current and voltage waveforms, after receiving the trip signal from the protective relay, the contact of the circuit breaker opens and an arc is initiated. This arc is subsequently quenched by an insulating gas flow. While the fault current approaches zero, the arc voltage increases rapidly to the peak value of the so-called extinction voltage. This extinction voltage can distort the current waveform. If this extinction voltage peak is equal to the system voltage maintaining the arc, the current may be forced to zero before the natural current zero of system frequency. At the point very close to natural current zero, the recovery voltage can generate an electric field stress, which is high enough to re-establish the arc. The

current will remain at zero until the arc voltage in the negative direction, called re-ignition voltage, reaches the peak value. When the arc is established once more, the voltage across the contact falls to an almost constant value, which is only sufficient to maintain the arc, until the next current zero. If the contact gap is now able to fully recover and the re-establishment of the arc is prevented, the transient recovery voltage appears across the opening contacts and a small current, called the post arc current, may flow for a few microseconds after current interruption. If the contact gap can withstand the transient recovery voltage (TRV), no restriking occurs. When the normal system voltage comes across the open contact, the interruption process is eventually complete. Therefore, the sequence of current interruption process can be described as follows: contact separation - arc occurs - current zero - transient recovery voltage - post arc current and power frequency voltage across the opened contact of circuit breaker.

However, in the complex power system with the presence of system resistances (R), the interrupted current usually consists of the additional DC component (second term of Equation 2.1) as shown in Figure 2.4 and it can be expressed as

$$i(t) = \frac{V_m}{\sqrt{R^2 + \omega^2 L^2}} \left[\sin(\omega t + \theta - \varphi) - \sin(\theta - \varphi) e^{-\alpha t} \right] \quad (2.1)$$

where $\alpha = \frac{R}{L}$ and $\tan(\varphi) = \frac{\omega L}{R}$

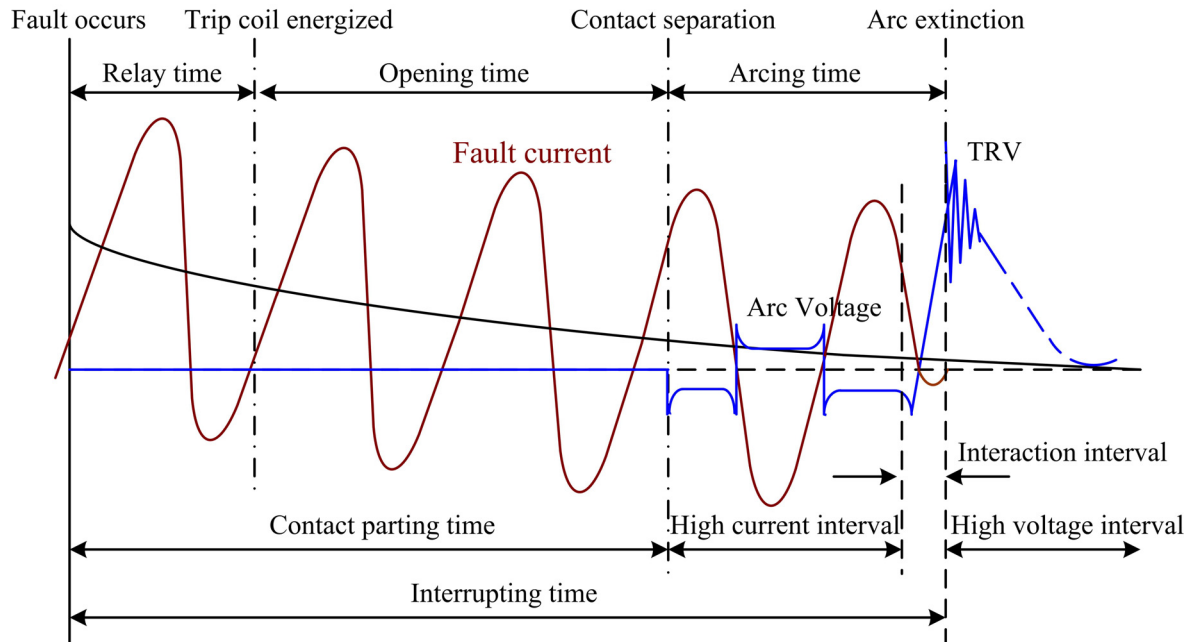


Figure 2.4: Interruption time relationships and three basic intervals of interrupting process

According to Figure 2.4, the interrupting time consists of relay time, opening time and arcing time, while the contact parting time consists of relay time and opening time. The relay time consisting of the time for sensing device, e.g. CT, to detect the abnormal current and operating time of protective relay, is defined as the time from the instance of fault initiation until the trip coil is energized. The operating time is

the time from the moment that trip coil is energized until the time when contact is galvanically separated. Therefore it consists of the time needed to release the latch, time for mechanical parts movement and time for moving contact movement. The arcing time is defined from the moment of galvanically contact separation until arc extinction, which consists of high current interval and interaction interval. Nevertheless, for any current interruption process three intervals, as defined in IEC 427 and ANSI/IEEE C37.081 [ANS81], are of prime interest. These intervals can be described as follows:

1. *High current interval* The high current interval starts from the moment that contact begins to separate until the significant change in arc voltage occurs. This interval occurs before the interaction and high voltage interval. Within this interval, the short circuit current flows through the circuit breaker with relatively small voltage drop across its contacts. The energy supplied from the arc causes the ionisation of insulating gas, vaporization of nozzle wall and electrode material, pressure build-up etc.
2. *Interaction interval* The interaction interval is counted from the beginning of the significant change in arc voltage before current zero to the time when the current, including the post arc current if it occurs, stops to flow through the circuit breaker. Depending on the residual conductivity inside the contact gap after current zero, the post arc current may continually flow. Within this interval, the stress from current is changing to voltage stress. As the current decreases to zero, the arc voltage rises and distorts the current waveform. The post arc conductivity after current zero may influence the voltage across the circuit breaker and the energy supplied to the ionised contact gap. The mutual interaction between the system and the circuit breaker immediately before and after current zero is of prime importance for switching operation [IEEE81].
3. *High voltage interval* The high voltage interval starts from the moment that the current, including the post arc current if it occurs, stops to flow through the circuit breaker up to the end of the recovery voltage transient. Within this interval, the circuit breaker is considered as a passive element in the system and its contact gap is stressed by the recovery voltage.

These three intervals follow each other immediately and they continuously cover the whole interrupting process. Among these three intervals, the interaction interval is the most complicated one. The steep rise of arc voltage during this interval influences the shape and the rate of change of current immediately before current zero [Ana99].

2.2.2 Switching Requirements

In SF₆ circuit breakers, the interrupting process is done by blowing of SF₆ gas through the nozzle towards the arc. The current interruption or arc extinguishing can be accomplished only at current zero with extensive energy removal from the arc. The essential transition process from high-conductivity plasma to insulating gas condition can be separated into two phases:

Thermal phase

The cross section of the conducting arc depends on the current amplitude. Therefore, with sinusoidal current waveform, the arc cross-section changes with time. Because of the thermal capacity of the arc, the changing of arc cross-section along current waveform has time delays. Then at current zero, the thin conducting arc column still exists and it is cooled by the outflow of gas from expansion chamber before current zero. Immediately after current zero the transient recovery voltage with a high rate of rise of recovery voltage in a few kV/ μ s stresses across the open contact and causes a current flow through the remaining electrical conducting arc, called the post arc current. This highly unreliable post arc current [Sch02], typically in the order of 1-10A, is hardly to measure. The decaying arc channel is now re-established by ohmic heating. The energy balance only in some microsecond period plays a vital role on success or failure of interruption, called the thermal interruption mode [Rag77]. The energy balance equation can be determined by power input due to the post arc current and the recovery voltage; thermal inertia and losses due to turbulent shear transfer as power absorption [Ana99]. The most severe stress for thermal interruption failure occurring in practical experience is the short line fault (SLF) at relatively short line in some km away from circuit breaker terminal [Gar97].

Dielectric phase

After effective cooling of gas flow, the conducting plasma column vanishes, the temperature between contact gap decreases and no current flows. Then, the contact gap enters into the dielectric recovery period. The contact gap, consisting of deionised electrons under elevated temperature and reduced density, has a lower dielectric withstand voltage. The time need for the full dielectric recovery of the contact gap is called dielectric phase and it is ranged in hundred microseconds [Bra82], [Rya89]. Within this dielectric phase, the interrupter has to withstand a voltage up to several hundred kV within a few hundred microseconds. Because at this time the post arc conductivity no longer exists, the success or failure of interruption does not depend anymore on energy balance. Nevertheless, it depends on the release of electrons caused by the electric field [Ana99], which according to Townsend equation can be written as

$$\frac{\partial n_e}{\partial t} = -\frac{\partial n_e V_e}{\partial Z} + (\alpha - \eta)n_e V_e \quad (2.2)$$

where

- n_e is the number of electrons
- α is the ionisation coefficient
- η is the attachment coefficient
- V_e is the drift velocity of electrons
- Z is the distance along the axis of contacts

Since α and η are coefficients of ionisation and attachment respectively, they depend on the gas density and the electric field. However, as the length of the

contact gap increases, the field distribution becomes more inhomogeneous and the streamer discharge appears. The further increasing of recovery voltage results in more rigorous streamers, which finally leads to the rapid increase of current, arc discharge and the restrike within the contact gap.

The transient recovery voltage imposed by electrical system across the open contacts can reach a high peak value U_c . If U_c is higher than the withstand voltage of contact gap, the circuit breaker gap fails through dielectric breakdown called dielectric failure. This can be recognized by arc reignition and a very sudden collapse of the reignition voltage. The critical fault, that can cause dielectric failure, is usually the so-called terminal fault (TF), which occurs at circuit breaker terminal.

2.3 Degradation and Monitoring Techniques

2.3.1 Equipment Failure and Basic Knowledge of Maintenance

Deterioration and functional failure

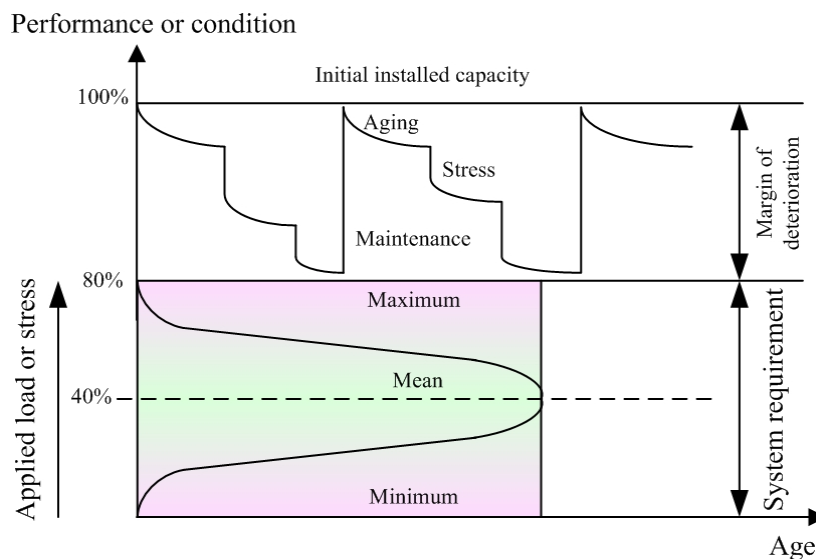


Figure 2.5: condition degradation and example of variable applied stress

In case of circuit breakers, their initial capacity, e.g. rated load, interrupting rating, rated voltage, impulse withstand voltage (BIL, SIL) etc., is carefully selected to cover maximum system requirements and allows for some margin of deterioration as shown in Figure 2.5. When it is put in service, stresses from the system it connected with as well as the aging of the circuit breaker itself cause it to deteriorate. The maintenance activity is performed to ensure that its capacity stays above the maximum system requirement, but it cannot raise the capacity above the initial installed capacity. This means that it must be maintained within the margin of deterioration zone. Generally, the variable stress or loading applied to a circuit breaker depends on the system requirements, e.g. load current variation according to time of the day or seasons, higher interrupting rating requirement due to the connection of new power plant etc. Whenever the system requirement is higher than

the actual performance of circuit breaker, it is unable to fulfill its required function. This is called functional failure.

Evident and hidden failure

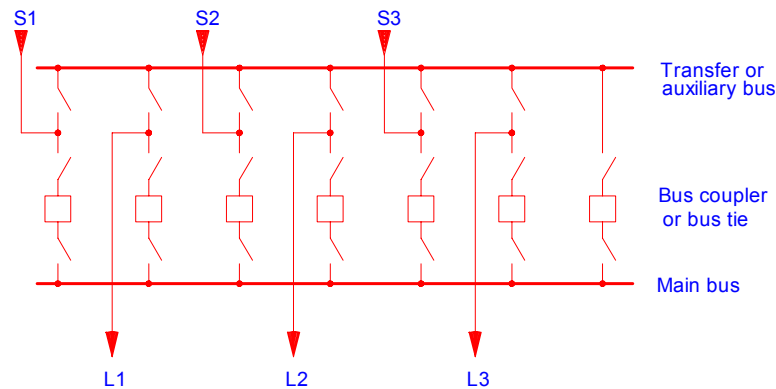


Figure 2.6: Evident failure and hidden failure

For instance, if we consider a 230kV substation with main and transfer scheme as shown in Figure 2.6, the failure of any circuit breaker in any bay from S_1 to S_3 and L_1 to L_3 is considered as evident failure because its failure will finally become evident to operating personal under normal condition. The consequence of this failure has no adverse effect on safety and operational capability of this substation because the tie-bay circuit breaker can take over the required function from the failed circuit breaker. The only consequences associated with this failure are direct costs of repair. While failure of tie-bay circuit breaker is considered as hidden function because its failure, if it occurs, will not become evident to operating personal under normal condition [Mou97].

Preventive maintenance and maintenance development

The relationship between failure rate and the lifetime of a large sample of a homogeneous component population according to the traditional view of failure can theoretically be illustrated as shown in Figure 2.7. After being put in service at time T_0 , this population has relatively low and constant failure rate λ , which is called useful life period. Within this period, the equipment can be utilized with full advantage. However, a small percentage of equipment will fail during this period, called premature failure. When the equipments reach the wear-out time T_w , wear-out becomes manifest and the failure rate increases quite rapidly. About one-half of survived equipment after time T_w will fail during T_w and T_M period. Therefore, the time T_M is defined as the mean wear-out life or average life of the population. However, the early failure during burn-in period (dash line) actually occurs in practice owing to the failure of substandard or weak parts.

This view of failure based on the assumption that most items operate reliably until end of useful life and then wear-out, and the belief that the equipment has life form a basic rule of preventive maintenance. This suggests that the equipment overhauls or component replacements should be done at fixed interval, not later than the end of its useful life even if it has not failed. However, the equipment nowadays is

generally far more complex and leads to various failure patterns. These will be discussed in the next section.

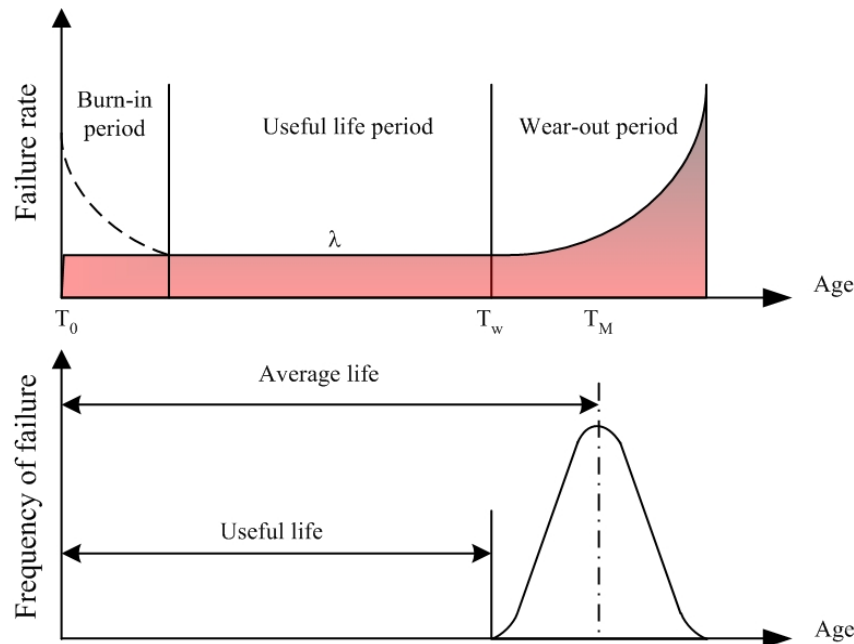


Figure 2.7: The traditional view of failure

2.3.2 Degradation and Failure Patterns

In practice, the equipment is always subjected to a wide variety of stresses after putting into service. These stresses cause the equipment to deteriorate by lowering its capability, or more accurately, its resistance to stress. The equipment fails on one hand when its resistance drops to the extent that it can no longer meet the system requirement. The falling capability of equipment can be caused by deterioration, dirt, disassembly or human error etc. On the other hand, the equipment may also failed by the increase of system requirement above the actual equipment performance such as the increase in system fault level from 31.5kA to 40kA caused by the connection of new power plant. Thus, in order to select the proper maintenance techniques it is necessary to know the relationship between age and failure, which can be separated into two categories as follows:

Age-related failure patterns

The prediction of equipment life could be performed with great accuracy, if the deterioration is directly proportional to the applied stress and the stress is applied regularly throughout the life of equipment. Unfortunately, in practice two identical equipments putting into service at the same time under the same working condition will fail at different age, which is not only because a little variation of their initial resistance to failure, but they are also subjected to different stresses at different time throughout their lives. Even though any equipment has its individual end of lifetime, the failure of a large population will gather around the mean life or the so-called average life of the equipment with typical characteristics of a normal or Gaussian distribution as long as they deteriorate in this manner (see Figure 2.7). If

the average life can be determined, the preventive maintenance can be effectively applied.

The failure pattern according to age-related failure should show the rapid increase in failure rate and probability of failure when the equipments get older, especially after the useful life. Therefore, in Figure 2.8 pattern A, B and C on the left hand side can be classified as age-related failure pattern.

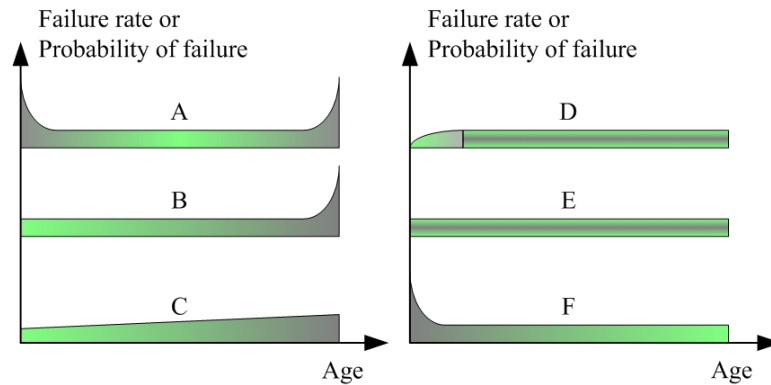


Figure 2.8: Six patterns of failure [Mou97]

Non age-related failure patterns

The increase in equipment complexity, such as more associated components and the variation of applied stresses in service, are the primary reasons of non-age-related failure. Generally, the stresses in service occur irregularly and the condition or performance does not deteriorate proportionally to the stresses. For instance, the dependence of condition deterioration of three different components on the identically applied stresses together with normal aging is illustrated in Figure 2.9. For component A, B and C each high stress causes only temporarily reduction, permanent reduction to some extent and acceleration of the decline of its condition respectively. When these components are used together in any equipment, their failures will occur randomly and the relationship between age and failure seems to be unpredictable.

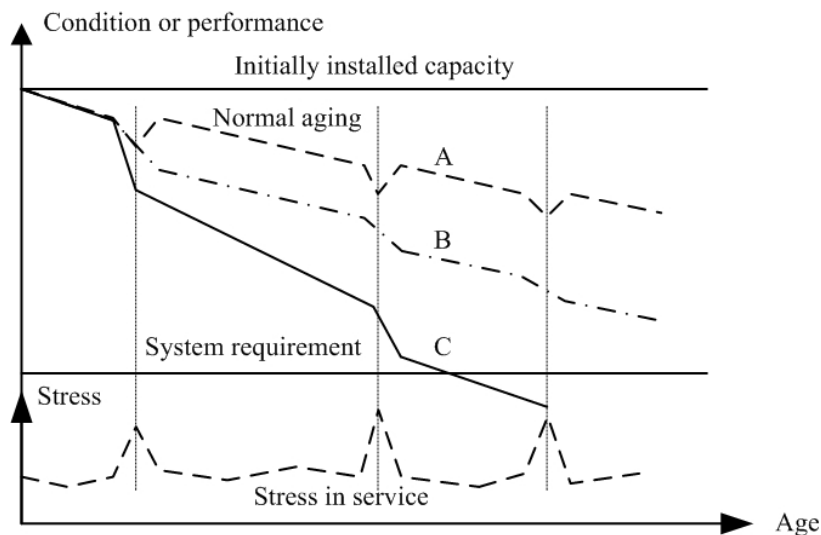


Figure 2.9: Example of condition deterioration owing to stresses and aging [Smi93]

Failure pattern D, E and F in Figure 2.8 are non age-related because after the initial period the failures occur randomly without any relationship between failure and operating age. Therefore, it is impractical to apply preventive maintenance with this kind of equipment. The condition-based maintenance is now preferred for the equipment with non age-related failure patterns.

Failure patterns

Failure pattern A

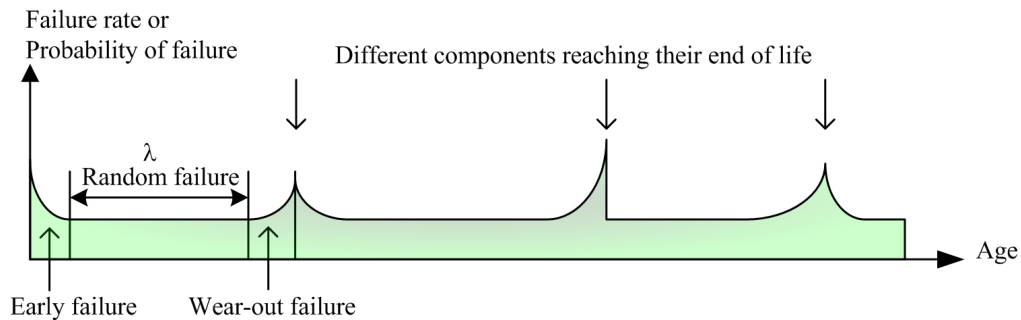


Figure 2.10: The practical view of the well-known bathtub curve

The practical view of the failure pattern A or the bathtub curve is shown in Figure 2.10. Generally, it consists of three periods, which are burn-in, useful life and wear-out periods. During burn-in period, the early failure maybe caused by commissioning work such as incorrect set-up or incorrect start-up, or unnecessary invasive routine maintenance, poor design, poor quality manufacture and incorrect operation. During useful life the failure rate is constant, whereas during wear-out period the failure rate increases due to aging phenomena. Most of the equipment is generally replaced before they reach wear-out period.

Failure pattern B

Failure pattern B is an age-related failure. Without consideration of premature failure during useful life, the distribution of failure frequencies is plotted against age for 100 samples of equipment in Figure 2.11 a. The frequency of these failures is likely to conform to a normal distribution gathering around the mean life or the average life. The mean time between failures of the equipment in this example case is 25 years.

In Figure 2.11 b the survival distribution or number of remaining equipment can be simply derived based on the above failure frequency distribution. The probability of failure shown in Figure 2.11 c is the probability that any equipment, which has survived to the beginning of this year, will fail during this year.

Failure pattern C, D, E and F

Failure pattern C shows a steadily increasing probability of failure, but the wear-out period cannot be exactly determined. Failure pattern D has a slowly increase in probability of failure for a certain period and then constant. The constant probability of failure implies that equipment can fail at any time and the failure occurs

randomly. For this reason, Failure pattern D and E is non age-related and has no useful life. Thus, preventive maintenance is not applicable to this type of equipment. Failure pattern F is quite different from the other because it starts with high failure rate during burn-in period and then drops eventually to a constant value. The highest failure rate occurring when the equipment is new or just after overhaul is known as early failure. The causes of early failure are poor design, manufacturing defectives, incorrect installation, incorrect commissioning, incorrect operation, unnecessary maintenance and excessively invasive maintenance.

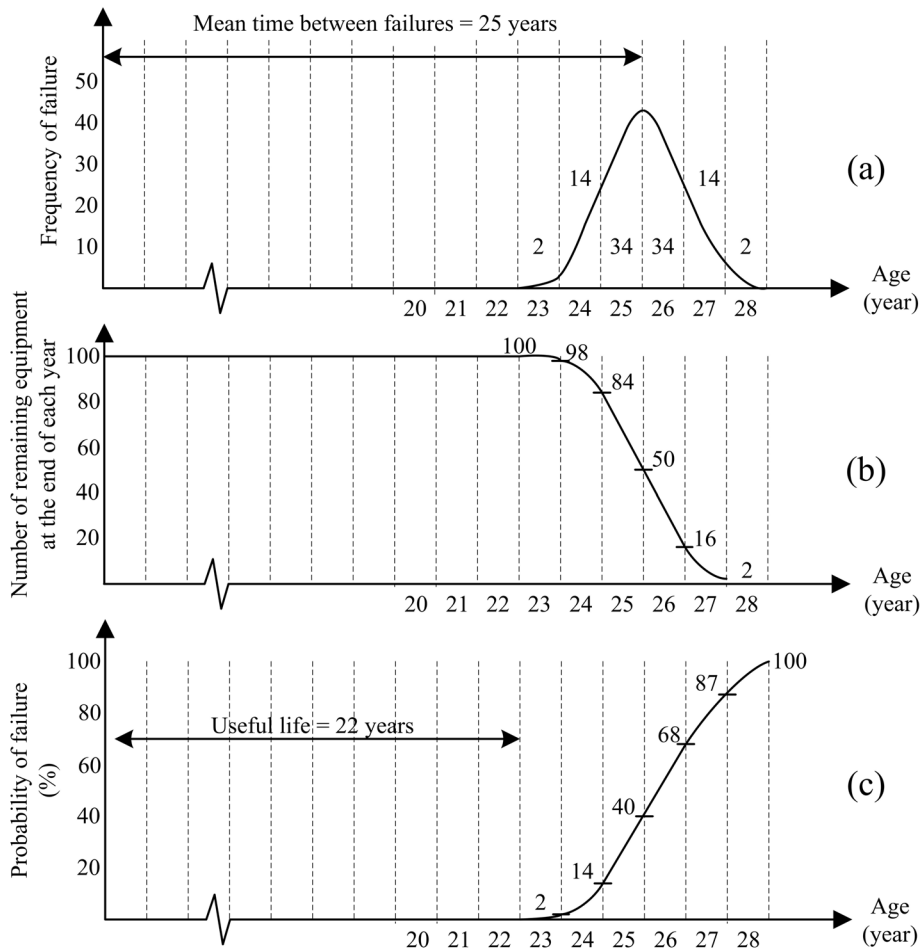


Figure 2.11: Example case for failure pattern B

2.3.3 Condition Monitoring and Maintenance

According to the last section, the equipment with non age-related failure pattern has no average life and the relationship between failure and operating age cannot be determined. However, when failures are nearly to occur or in the process of occurring, some kind of detectable information, if the appropriate diagnostic tools are applied, should be capable to identify the deterioration in condition.

The purposes of monitoring system according to [IEEE00] are to determine the condition of a specific equipment and its associated components, to improve equipment utilization by prolonging the potential life time of equipment and economics of equipment operation, to reduce failure rate, to increase reliability and

availability, to optimize maintenance activity and cost reduction, to facilitate the provision of spare parts and to develop an understanding of the condition of a large population of equipments in similar circumstances by examining a representative sample of the population. The requirements of monitoring devices [Jan92], [Nel01] are simple in application and interpretation, economical in initial cost and installation, reliable in operation, able to detect a wide range of equipment failure modes and able to be used by non-professional staff. The condition monitoring of high voltage circuit breakers can be divided into manual, temporary and continuous including on-line condition monitoring. The complexity of the monitoring system depends on type and rating of equipment, its importance in the system and user preferences. According to [Hof92], the condition monitoring is recommended to apply with the circuit breakers, which located in critical locations in the network where an outage can create a high disturbance cost, in extremely polluted environment, in extreme climate conditions and seldom operated circuit breakers.

Principle of condition monitoring, diagnostic test and maintenance planning

Condition monitoring and diagnostic systems, see appendix A for definition, normally form as an information chain. Monitoring or diagnostic system starts with the sensors located on the equipment, data acquisition, signal processing, feature extraction and decision-making. Then, the output from a monitoring system, whether it is periodic or continuous monitoring, in-service or out-of-service diagnostic tests, will be sent to user-interface unit, where the results are presented to the user.

In general, the function of each component in condition monitoring and diagnostic system can be described as follows:

Sensor is a device that transforms one physical quantity (input) into another (output), usually into an electrical one. The requirement for a sensor is high reliability, constant long term behaviour and immune to electromagnetic disturbance.

Data acquisition processes the output from binary or analog sensors to suit for digital signal processing by filtering, analog to digital (A/D) conversion and immediate storing data, usually in compressed form, before processing.

Signal processing and feature extraction are the process to determine the characteristics values of the signal such as crest-value, value at the same time point, etc., and to derive and find the relation between these values. The monitored parameters and extracted features should be sensitive enough to behaviour changes of failure part.

Decision-making is the analysis process. The detected changes of signatures, obtained in subsequent operation of equipment, from normal operating condition, which used as a basis for comparison and stored in database, will be analyzed. Any exceed-acceptable limit value will be evaluated to determine the condition of the equipment.

User-interface presents the result information, mostly as colour band or scale, which is easy for interpretation, to a human operator.

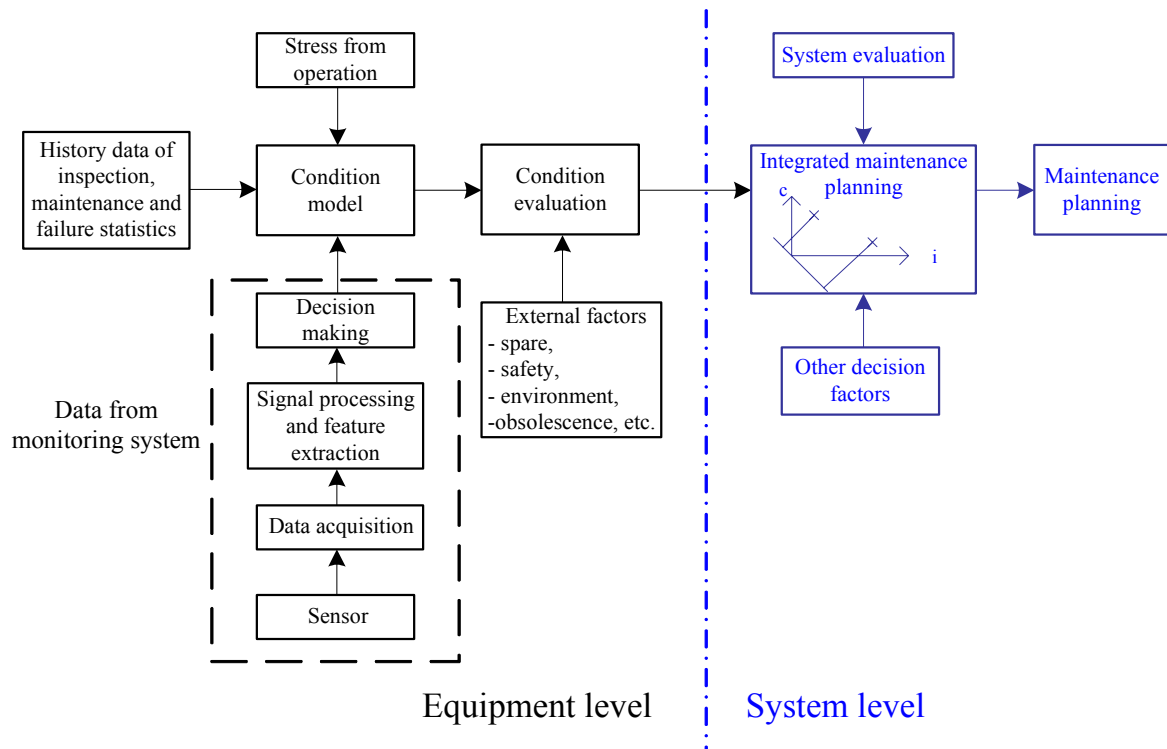


Figure 2.12: Overview of maintenance system [FGH01]

From Figure 2.12 at equipment level on the left hand side, e.g. circuit breaker, the combined information among condition monitoring and diagnostic test; failure statistics and history data of inspection and maintenance; and stress in operation such as number of switching operations and short-circuit current interruption, is primarily used to determine the deterioration of circuit breaker according to stress and aging. Then, it will be further evaluated to model the changes of condition with time. After the condition of circuit breaker is known, it will be considered together with external factors such as availability of spare parts, safety and environmental impact, technology obsolescence and financial constraints. If the condition exceeds the acceptable limit, the action plan is proposed.

The determined condition of circuit breakers from equipment level together with their importance in the system, e.g. acceptable limit of failure rate and reliability of the circuit, system configuration and type of redundancies, interrupted power, kind of customer, social impact, etc., and other decision factors, e.g. available material and personnel, cost, etc., will be evaluated together in the integrated maintenance planning. The evaluated result will be proposed as maintenance planning. This procedure is known as a Reliability-Centred-Maintenance (RCM) strategy [Bal98].

2.3.4 Reliability and Availability

In [IEEE95], a failure is defined as termination of the ability of an item to perform its required functions. The possible causes of circuit breaker failure are shown in Figure 2.13. The examples of interrupter failure are unacceptable tolerances of excessively worn arcing contacts, main contacts and nozzle, insufficient gas pressure build-up, loss or degradation of SF₆, abnormal contact velocity, etc. In

order to prevent failure, a circuit breaker should be kept sealed tight, dry, clean and minimized frictions by visual inspection, exercising and proof testing.

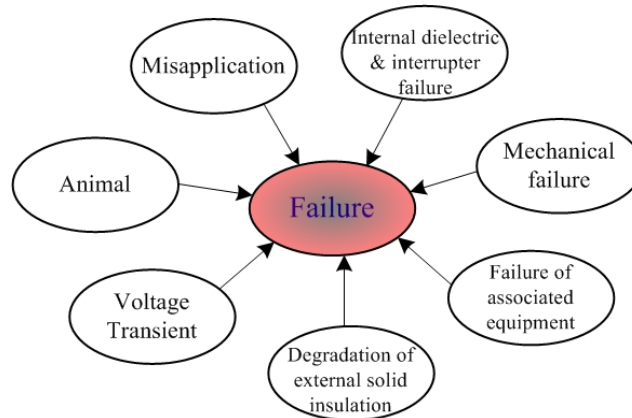


Figure 2.13: Possibility of circuit breaker failure

The basic concept of reliability with the definition [IEEE97], listed in Appendix A, is presented here. When a fixed number N_0 of circuit breakers are put in service, after a time t , N_s circuit breakers survive and N_f fail. Thus, the reliability at time t is defined as

$$R(t) = \frac{N_s}{N_0} = \frac{N_s}{N_s + N_f} \quad (2.3)$$

By substituting N_s with N_f in the numerator of equation 2.3 the unreliability (Q) of the probability of failure is obtained and the summation of R and Q is equal to one.

The probability of failure per one circuit breaker is called the failure rate or λ . For constant λ , it can be written as the following:

$$\lambda = \frac{1}{N_0} \frac{N_f}{t} \quad (2.4)$$

The relationship between reliability and a constant failure rate

$$R(t) = e^{-\lambda t} \quad (2.5)$$

The failure density function

$$f(t) = \lambda e^{-\lambda t} \quad (2.6)$$

The mean time between failure (MTBF)

$$MTBF = \int_0^{\infty} t \lambda e^{-\lambda t} dt = \frac{1}{\lambda} \quad (2.7)$$

The cumulative probability of failure or unreliability

$$F(t) = \int_0^t \lambda e^{-\lambda t} dt = 1 - e^{-\lambda t} \quad (2.8)$$

The following example explains some basic idea about reliability concept by assuming that ten circuit breaker poles have been in service for ten years. The total year in service of circuit breaker poles in this period is 10 circuit breaker poles x 10 years = 100 years. The interrupting unit of each circuit breaker pole has been checked once in 5 years for 10 years period. Thus, the failure finding interval (FFI) is 5 years. Over the ten-year period, the interrupters have been found to be in a failed state on 4 occasions. Therefore, the mean time between failure (MTBF) of the interrupting unit is 100 years in service / 4 failures = 25 years. In this case, the failure-finding interval of 5 years is equal to 20% of the MTBF of 25 years. Since we do not know exactly when each interrupter failed, the assumption on the average is applied. Hence, each interrupter was out of service for 2.5 years before or after failure finding. This means that over the 10 year period, our interrupters were in a failed state for a total of: 4 interrupters x 2.5 years each in a failed state = 10 years. So the unavailability of our interrupters is 10 years in a failed state / 100 years in service = 10% or 90% availability. The unavailability equation can be arranged in the simple form as

$$\text{Unavailability} = \frac{\text{Number of failure}}{\text{Total year in service}} \times \frac{\text{FFI}}{2} = \frac{\text{FFI}}{2 \times \text{MTBF}} \quad (2.9)$$

If we are not satisfied with an availability of 90% and would like to increase it to 95%. The associated unavailability is 5%. Thus, the checking interval needs to be changed from once in 5 years to $2 \times 5\% \times 25 \text{ years} = 6 \text{ months}$.

To achieve a higher degree of reliability, circuit breakers should be simple in design and consists of fewer parts. From two international enquiries on the reliability of high voltage circuit breaker 63 kV and above, conducted by CIGRE WG 13.06 and reported in [Hei94] and [Jan96] for used in improvement the reliability of circuit breaker and in substation and system studies, the failure rate, downtime data, average number of operation and major failure mode were determined. The first enquiry included 20,000 circuit breakers of all technologies and covered the year 1974 through 1977. While the second enquiry included only 18,000 single pressure SF₆ circuit breakers for the year 1988 through 1991 and shows the improvement of single pressure SF₆ circuit breaker over the old technology, which results in lower major failure rate and higher maintainability. The reliability improvement is much higher in higher voltage range due to changed designs. The total major failure rate is considerably reduced from 0.0158 per year (First enquiry) to 0.0067 per year (Second enquiry). The estimated interval between scheduled overhaul shows an average of 8 years and a median value of 6 years. In operating mechanism, the highest risk of a major failure in a hydraulic mechanism is "locked in open or closed position" and "does not open or close on command" for spring mechanism.

Figure 2.14 shows the major failures of circuit breaker rated by failure characteristic from the first and second enquiry. The number on the x-axis means that (1) Does not close on command; (2) Does not open on command; (3) Closes without command; (4) Open without command; (5) Does not make the current; (6) Does not break the current; (7) Fail to carry current; (8) Breakdown to earth; (9) Breakdown between poles; (10) Breakdown across open pole (internal); (11) Breakdown across open pole (external); (12) Locking in open or closed position and

(13) Others. In [IEEE00], the failure modes and causes are completely identified. The technical life of circuit breaker is far more than 25 years, as normally expected and stated in [Cig00a] for 41 years. Hence, the verification of the mechanical and electrical endurance limits is of prime importance.

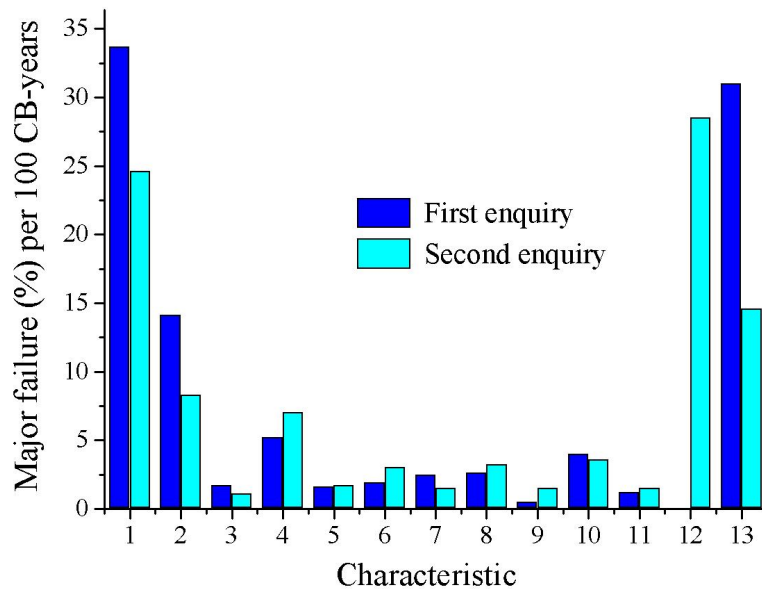


Figure 2.14: Major failures of circuit breaker from the first and second enquiry [Jan96]

2.4 Ablation-controlled Arc and Material Properties

2.4.1 Ablation-controlled Arc

Ablation-controlled arc is a basic approach for the high current arc in gas circuit breakers. The arc is governed by a radiative transfer, as the dominant radial energy transport mechanism to convey the ohmic power to evaporate material, and the axial convection generated by arc-induced wall vaporization. The arc, which is ignited in a narrow cylindrical open at both ends nozzle with fictitious current density (ratio of current to nozzle cross section) above 10A/mm^2 , is called ablation stabilized arc [Nie78], [Ruc86], [Mül93a], [Mül93b], [Mül94].

An electric arc is formed in a confined cylindrical wall made from insulating material with low thermal conductivity. Because the diameter of free-burning arc is much greater than the diameter in the cylindrical nozzle, during high current the diameter of the arc approaches that of the wall. The temperature of the arc core inside the cylindrical nozzle is around $25,000\text{K}$, which is clearly higher than that of free burning arc with the same current amplitude. The radiation energy from the arc is principally dissipated by wall absorption and ablation of wall material, which subsequently forms the main component of the arc plasma [Mül88].

As the cylinder ablates, a high-pressure region forming in the tube causes a pressure gradient, which expels plasma to both ends of the tube. Due to symmetrical configuration the pressure is highest at the tube centre. The arc plasma is assumed to be in local thermodynamic equilibrium. The vapour sheath existing concentrically between the tube wall and the arc column is an electrical insulation and has a temperature around 3,000-4,000K. The energy of hard photon from the arc with short wavelength $\lambda < \lambda_p$ (threshold wavelength approximately 220nm [Ruc86]) can directly disrupts the molecular chemical bonds at the surface of arcing channel, while the long wave radiation $\lambda > \lambda_p$ penetrates into the wall, heats up the material to evaporation and sublimation temperature respectively and causes damages deeper inside the volume of nozzle [Mül93b]. At both ends of nozzle, the ohmic input energy is transported to outside by radiation and convection.

2.4.2 Arc Modelling and Material Properties

The success or failure of current interruption depends predominantly on the close interaction between arc, radiation, ablation and gas flow. This makes it difficult to predict the conditions at current zero without the possibility to investigate the transient behaviour of a circuit breaker. The application of computational simulation on gas flow conditions [deH03] is essential in order to gain the visualization of the process inside expansion chamber and to understand the physical interactions and to reduce the expenses, time and effort spent in experimental investigation. The simulation tool based on computational fluid dynamics (CFD) algorithm evaluated during the last years at the Institute for High Voltage Technology, RWTH-Aachen is a powerful tool to facilitate the investigation of physical phenomena inside high voltage self-blast circuit breakers. The thermodynamic properties of an arc and its surroundings are vital for computation of energy transport. Furthermore, the physical characteristics of the insulating gas and effect of vaporized nozzle material deserve to be considered.

The simulation can be divided into two significant parts:

- a. *High current simulations* serve for the investigation of mixing processes of hot and cold gas in the expansion chamber and the exhaust volume respectively [Cla97b], [Cla97c]. The mixing process of ablated nozzle material and cold SF₆ inside the storage and exhaust volume is recently investigated, but the temperatures inside an interrupter under fault conditions is difficult to measure. Moreover, the gas state is inhomogeneous because it composes of the hot regions with a high PTFE mass fraction and the existing cold regions consisting of nearly pure SF₆.
- b. *Low current simulations* are used to investigate the influence of the cooling gas state on the extinguishing process. It requires an arc modelling, which is very different from that during high current period. Cylindrical symmetry and an isothermal plasma zone can no longer be supposed and the flow simulation has to be combined with electric and magnetic field calculations to obtain the structure of the electrical potential, the current density and the Lorentz forces [Cla97b].

The high current period, where the main energy input into the interrupter occurs, lasts for some 10ms, whereas the low current period lasts only some 10 μ s. Therefore, high- and low current simulations can be performed separately.

2.4.2.1 The Two-Zone Model

One of the improvement methods over the previous one is the two-zone model. The two-zone model describes the ablation controlled arc in narrow, cylindrically shaped insulating nozzles as a cylindrical conductive plasma column surrounded by a non-conductive vapour layer [Nie78]. Both zones are assumed to be isothermal and the velocity distribution is independent from the radius. A schematic representation of an arc burning inside cylindrical insulating nozzle is shown in Figure 2.15. According to [Mül93a] it is assumed that the entire injected ohmic energy input is completely converted to radiation. The fraction ϑ is emitted out of the arc and divided into 3 parts as follows:

1. A part ϑ_w evaporates on the surface and causes the increase in nozzle radius.
2. A part ϑ_t penetrates deeply into the nozzle wall.
3. A part ϑ_0 leaves the system through the wall as a leakage power.

The remaining of the radiation power $(1 - \vartheta)$ heats up the vaporized nozzle material entering to the arc from vapour temperature T_v to the arc temperature T_a . The energy escaped from the system is principally by convection of flowing plasma and vapour, forced by high-pressure stagnation point in the nozzle centre, through both nozzle outlets with sonic velocity.

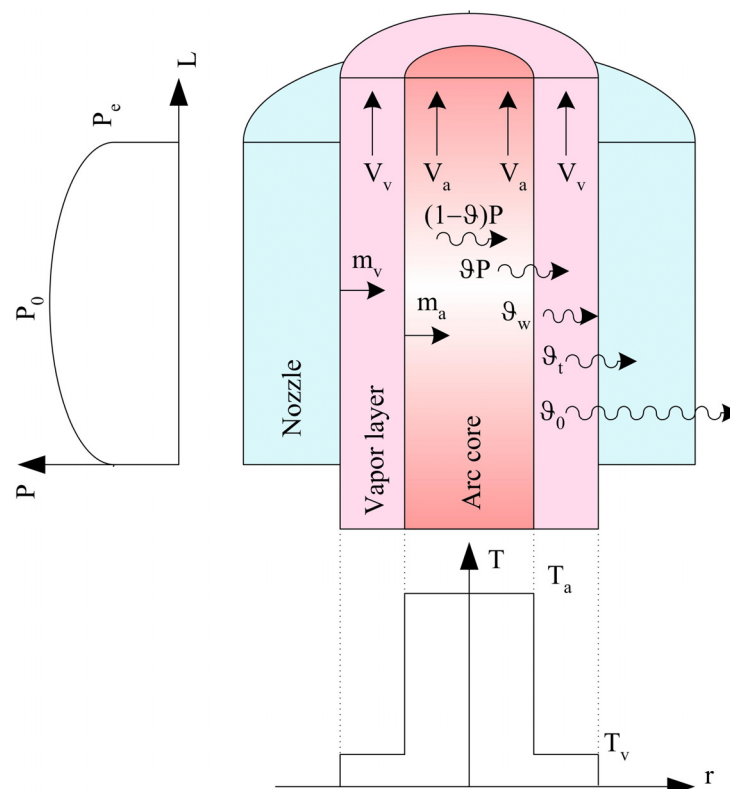


Figure 2.15: Schematic presentation of the two-zone model

The conditions of plasma and vapour are determined by plasma temperature, vapour temperature and axial pressure profile as shown in Figure 2.15. The temperature profile of arc and vapour is rectangular because the temperature of arc and vapour are assumed to be independent on the positions both in axial and radial directions. Furthermore, only laminar flow with no radial pressure gradient is supposed. The axial pressure distribution shows that the maximum pressure (P_0) occurs at nozzle centre, while the pressure at both nozzle ends (P_e) is half of this maximum pressure.

An analytical solution of the fundamental equation system for mass, momentum and energy conservation has been used to calculate central pressure, arc voltage, plasma temperature and ablating mass flux with the assumption of thermodynamic equilibrium. The simplifications and assumptions to solve the differential equation system [Mül93a], [Kri99] are as follows:

1. The nozzle and arc are in cylindrical shape.
2. The velocity distribution in both zones is equal.
3. The local thermodynamic equilibrium (LTE) governs in both zones with two different temperatures for plasma and vapour, which are independent from the axial coordinate.
4. The energy transport by diffusion and conduction is neglected.
5. The pressure is not a function of the radius.
6. The influence of magnetic pressure on pressure build-up is negligible.
7. The arc is considered as a quasi-stationary arc during high current period.
8. The electrical conductivity σ and the specific enthalpy h don't change along the axial coordinate.
9. The arc is modelled as a grey-body radiator, which can be explained by Stefan-Boltzmann law.

Therefore, the radiation power P_r is given by

$$P_r = S\beta\epsilon T_a^4 \quad (2.10)$$

The ablation causing the increase in nozzle diameter is defined as

$$\dot{m}_w = \frac{g - g_0}{h_v} UI \quad (2.11)$$

For the whole ablation, it is expressed by

$$\dot{m}_v = \frac{g - g_0}{h_v} UI \quad (2.12)$$

where S is surface
 β is the Stefan-Boltzmann constant
 ϵ is the gray factor

T_a is the arc temperature

h_v is the vapour enthalpy

U is arc voltage

I is arc current

With the above simplification and assumption, the conservation equations for mass, momentum and energy have been solved in [Mül94] to determine the following:

Arc voltage by Ohm's law

$$U = \frac{LI}{\sigma\Phi\pi R^2} \quad (2.13)$$

The maximum pressure at nozzle center

$$P_0 = \frac{(1-g)c_a}{(h_a - h_v)\pi R^2} \left[\delta \left(\frac{h_a - h_v}{1-g} \right) \frac{c_v}{c_a} + 1 \right] UI \quad (2.14)$$

The arc temperature

$$T_a = \sqrt[4]{\frac{UI}{2\pi\sqrt{\Phi}RL\beta\varepsilon}} \quad (2.15)$$

The sum of evaporated mass

$$M = \delta \int_0^t UI dt \quad (2.16)$$

After ablation at surface and in depth, the radius of the nozzle can be written as:

$$R = \sqrt{R_0^2 + \frac{1}{\pi L \rho_0} \left(\delta \int_0^t UI dt \right)} \quad (2.17)$$

where L is tube length, σ is electrical conductivity

Φ is contraction number, i.e. ratio of arc cross sectional area to nozzle cross sectional area

R is nozzle radius

Index a is for arc, v is surrounding vapor

c is sound velocity, h is specific enthalpy

δ is ablation factor, i.e. ratio of ablated mass to supplied energy

R_0 is R at $t=0$, ρ_0 is density of solid material

With this equation system from equation 2.13 to 2.16 and the known ablation factor, the maximum pressure, temperature, energy and ablated mass can be successfully determined.

2.4.2.2 Material Properties

The thermodynamic properties of arc and its surrounding are important in the energy transport computation. Therefore, the physical properties of insulating gas SF₆ and the effect of ablated nozzle material should be clearly understood.

Fundamental properties of SF₆

Pure SF₆ is colorless, odorless, nontoxic and nonflammable. Its specific density at 20°C and 1 bar pressure is 6.135g/litre. The molecular weight is 146.05. Its boiling point is -60°C at 1 bar pressure. It can be liquefied by compression and may be conveniently stored as a liquid. However, liquefaction in a circuit breaker, mostly at -25°C with 6 bar nominal filled pressure for puffer type, must be avoided. The sonic conductivity of SF₆ is remarkably low. The speed of sound in SF₆ at 30°C and 1 bar pressure is 138.5m/s.

SF₆ is chemically inert up to 150°C and will not attack metals, plastics and other substances used in circuit breaker. However, under arc with high temperature, it decomposed into various components principally SF₄ and SF₂ together with small amount of S₂, F₂, S, F, etc. Figure 2.16, the relative particle density of SF₆, shows that between temperatures 1,000K to 3,000K SF₆ gradually dissociated into SF₄ and SF₂ with the good insulating property. Free fluorine atoms (F) take place at temperature above 1,000K. Free sulfur atoms (S) occur at temperature above 3,000K. The ionized sulfur atoms (S⁺) appear when temperature is higher than 3,000K. When temperature is higher than 6,000K, the ionized fluorine atoms (F⁺) come out. At this stage, the gas is conductive and beyond 20,000K SF₆ gas is completely ionized.

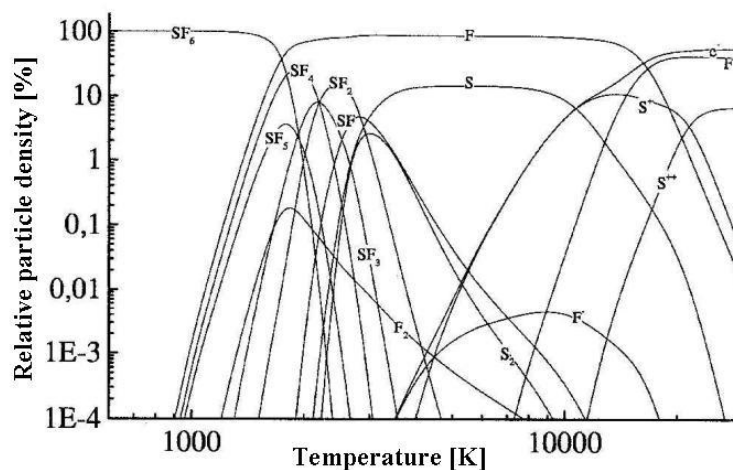


Figure 2.16: Relative particle density of SF₆ [Kri99]

When these particles are combined with moisture, they become corrosive for both glass and metal. The whitish powder also occurs by the combination of such elements with vaporized metals. However, this whitish powder has good insulating properties, the contacts of circuit breaker must be designed to ensure self-cleaning on current carrying surfaces. The maximum dissociation at 2,000°C yields the good thermal conductivity and low electrical conductivity, because the dissociated and

ionized SF_6 will transport the heat convectively and diffusively by free dissociation energy recombination in colder region. This means that the heat from arc can be dissipated radially with very steep temperature gradient. These chemically active impurities recombine within short period 10^{-6} to 10^{-7} second after arc extinction. The remaining of impurities can be further eliminated by absorbing materials such as alumina located inside the pressure vessel of circuit breaker. Alumina also absorbs moisture inside the pressure vessel.

SF_6 is the superior gas as an insulating and arc-quenching medium because of its fast dielectric strength recovery after current passes through zero. Its electrical properties are as follows: 89kV/cm.bar dielectric breakdown strength, less than 10^{-7} dielectric loss factor, between 15.6-19.3eV ionization energy, 22.4eV dissociation energy and 1.002 relative permittivity ϵ_r .

Fundamental properties of PTFE

PolyTetraFluoroEthylene (PTFE) under commercial name TEFLON is an aliphatic partly crystalline synthetic material belonging to thermoplastic material group with good thermal, electrical and chemical properties. It is nonflammable with 2.18g/cm^3 density. The solid bonding between C and F atoms is 504kJ/mol bonding energy. Its chemical property is persistent until 300°C . Above 300°C , PTFE is not liquid but in gel form. The crystalline melting temperature is 327°C and decomposition temperature is between 570°C to 600°C . For the transition from solid to vapour, the material has to be heated up first up to the decomposition temperature. Then, additional energy is used for phase transition and finally to bring the gas up to vapour temperature. The surface resistance is around $10^{16}\Omega$. The breakdown strength is between 60 to 80kV/mm. The dielectric loss factor ($\tan \delta$) is 5×10^{-4} . The relative permittivity ϵ_r is 2.1. The heat conductivity is 0.4 W/(mK) and 1.0 J/(gK) specific heat capacity (C_p).

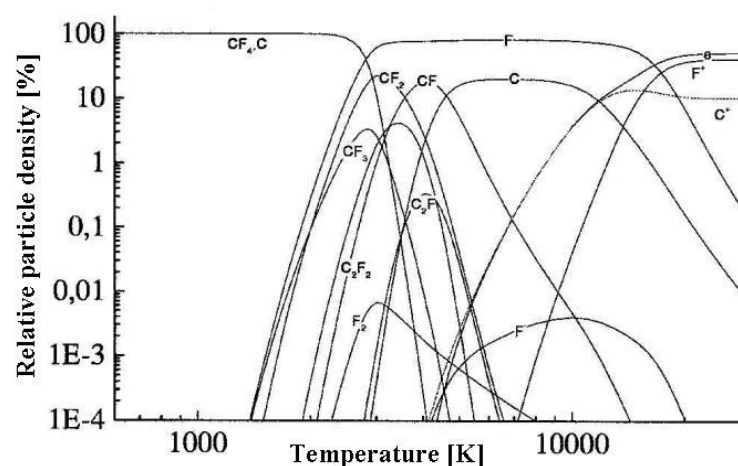


Figure 2.17: Relative particle density of PTFE [Kri99]

Figure 2.17 shows the decomposition of PTFE, which before consists mainly of CF_4 and free carbon atom (Graphite). The sublimation temperature is roughly 3,600K. The decomposition of vaporized PTFE, which are now C and F atoms, has comparable characteristics with that of SF_6 decomposition products both in

electrical and thermal conductivity [Yan99a]. Therefore, the mixing of ablated PTFE with SF₆ gas, especially in expansion chamber of circuit breaker, does not degrade the insulating and extinguishing properties of SF₆ gas.

SF₆-PTFE mixture

In practical current interruption, SF₆ gas is decomposed and it is contaminated by the ablated nozzle material and electrode vapour [Air76], [Pau97]. The SF₆-PTFE mixture is very complicated because the dissociation of SF₆ as well as PTFE has to be taken into account. A 1:1 mixture of SF₆ and PTFE from [Ruc86] in Figure 2.18 shows that the presence of additional fluorine from the SF₆ prevents the formation of graphite at temperature below 4,000K. The onset of dissociation is shifted from 1,500K for pure SF₆ to 2,500K for SF₆-PTFE because of the presence of stable CF₄ in the plasma mixture. The electrical conductivity of SF₆-PTFE mixture is similar to that of SF₆ for temperature above 6,000K, whereas below this temperature SF₆ has a slightly higher conductivity [Rya89].

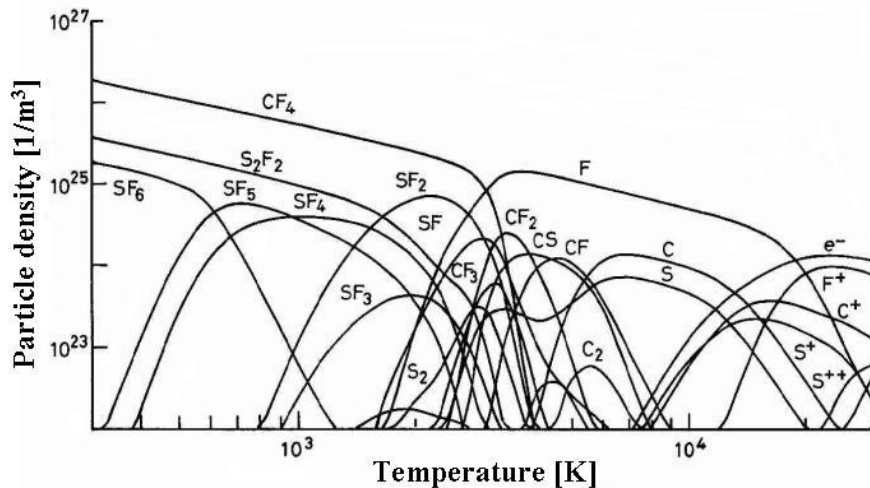
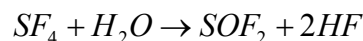


Figure 2.18: Particle density of 1:1 mixture of SF₆-PTFE [Ruc86]

These mixtures are of primary concern for the reliability and lifetime of circuit breaker. The short lived products can influence the interrupting capabilities both in the thermal and dielectric phases of the circuit breaker, while the long lived products, mostly aggressive gases, result in the corrosion in the circuit breaker.

- Short-lived product* The main short-lived products are CF₂, C₂F₄ and C₂F₆.
- Long-lived product* The main stable composition products of SF₆ arc are CF₄, CS₂, SOF₂, S₂F₂ and HF. The SOF₂ molecule is formed according to the reaction



It is obvious that the SOF₂ molecule is formed only if H₂O is present. Therefore, the moisture content during assembly of circuit breaker has to be carefully controlled.

2.5 Choice of SF₆ Circuit Breaker Monitoring

The mentioned statistics should be used as a guideline for selecting the components that should be monitored. A number of detection systems still remain mostly in a laboratory investigation. Moreover, the required reliability and high sensitivity add more complexity and make it vulnerable to the disturbances from external sources. Thus, a monitoring system should select the most basic and important functions, minimize the number of monitored parameters and be kept simple, straightforward.

The mechanical parameters that should be monitored are listed as follow:

- Close and trip coils because of its relatively simple task.
- Contact make and contact break by monitoring the voltage across the contacts should provide an approximation indication of contact touch, but this changes influenced by a contact erosion is not possible.
- Contact travel and velocity should be possible to infer the deterioration of linkages and increased friction.
- Charging motors by measuring the starting and running currents, running time and frequency of operation. The deviation from a baseline data should indicate leaks in a hydraulic system.
- Contact temperature by optical methods should indicate a number of possible problems, such as broken contact fingers, oxide formation, etc.

The interrupter wear owing to current interruptions consists mainly of the nozzle ablation and the contact erosion. The nozzle ablation is caused by the energy from the radiated power from the arc as well as a thermal conduction, when arc plasma makes contact with the nozzle wall. However, the radiative transfer is responsible for initiating nozzle ablation [Rya89]. For PTFE nozzle, a non-uniform absorption with depth was determined from the optical measurement. Thus, the absorption of most radiation is highly localized close to the surface, and causes the ablation, which is governed by the fracture of various molecular bonds, the formation of chemical fragments etc. This process depends on the spectral content of the radiation. The most severe ablation occurs around the nozzle throat owing to the highest flux density at the wall. The amount of ablation increases with the fault current and with the multiple of half-cycle arcing [Rya89].

The contact erosion caused primarily by the vaporization of the cathode and the anode electrodes. The determination can not be made directly, but indirect methods using measurements of current and arcing time can be performed by using a conventional instrument, such as current transformer. The arcing time can be extracted from the contact separation or contact travel measurement. The product of the current and the arcing time should provide a related parameter of contact erosion and nozzle ablation to ampere-seconds of arcing.

3 Investigations of No-load Mechanical Endurance of an Industrial Type Circuit Breaker

Up till now, the preventive maintenance is predominantly used to maintain circuit breakers after specific time interval or after specific number of operations. Even though nowadays, the higher degree of circuit breaker reliability have been achieved by using circuit breaker of simple design and consisting of fewer parts [Pfl78] and reducing of using lubrication in design phase for higher reliable operating mechanism [Faw78], failures still exist and sometimes cause costly consequences. Therefore, maintenance is inevitably needed. However, this task is very costly, time-consuming and sometimes can incorporate unintentional defects due to excessively invasive maintenance. The condition monitoring and diagnostic tests, especially with non-invasive techniques, have been developed with aiming to facilitate maintenance activity. Manual diagnostic tests can be performed both during in-service and out-of-service test. In-service tests, such as compressor operating characteristics, etc., and out-of-service test, such as dynamic and static contact resistance, main and auxiliary contact timing measurement, etc., are generally carried out during routine test. Some techniques have been developed so far by many researchers, such as measurement of enclosure vibration to detect abnormal contact condition inside GIS [Ohs89], development of acoustic analysis by measuring vibration signals of circuit breaker in laboratory and in field test [Run92], [Run96]. Unfortunately, until now the service experience with condition monitoring is too limited to draw final conclusions about the possibilities to improve maintenance activity because of lacking of knowledge about the acceptable limits of circuit breaker condition.

Referring to chapter 2, the failure pattern A and B during random failure and the period reaching wear-out zone is of significant importance for the circuit breaker degradation evaluation. The experiment under no-load, i.e. no current running through the contacts at the time and only pure mechanical loading, up to 6,000 switching operations is setup to investigate the degradation of mechanical components during random failure period. The variable operating conditions and the artificial defects are performed to investigate the conditions when reaching and in the wear-out zone, respectively. The deviation of monitored parameters from reference values due to variable operating conditions and defects and their sensitivity are also discussed.

3.1 Experiment Set-up and Test Arrangement

To maintain circuit breakers on a condition-based basis, a comprehensive knowledge is needed for both normal and abnormal operating conditions. From this reason, the experiment in this part, designed to use non-invasive techniques without opening major parts, was performed with three of 110kV SF₆ puffer type circuit breaker with hydraulic operating mechanism. One of them was investigated by doing no-load switching up to 6,000 switching operations and measured various parameters after every 500 switching operations under normal and variable

operating conditions that could probably occur in service, e.g. variation of control voltage supplied from station service power source or battery from the secondary circuit, motor supply voltage variation, SF₆ pressure change due to leakage or over-filling and hydraulic oil pressure change caused by seal and gasket aging. Since these problems can cause deterioration in operation efficiency, their effects are deserved to investigate. The monitored or measured parameters [Swe02], as suggested by Cigre' study committees 13 and 23, were close and trip coil current, hydraulic pumping motor current and time, main contact timing, dynamic contact resistance. In addition, vibration analysis, one of the well-developed diagnostic techniques [Hoi99], [Run99] and used for many years to diagnose rotating machine condition [Kol00], has been applied to measure the vibration characteristics of poles, operating mechanism and pumping motor as well. The measured values at the beginning of the test were used as a reference base line. The test and measurement of the first circuit breaker was performed at the institute laboratory because of the readily controlled conditions for testing and imposing abnormalities. The measurement results of the first circuit breaker have been compared with another two of the same type circuit breakers. The measurement of the second circuit breaker, still in service in a high voltage substation, were carried out before and after maintenance, while the testing of the third circuit breaker in a storage room was done under normal operating condition.

3.1.1 Experiment Set-up

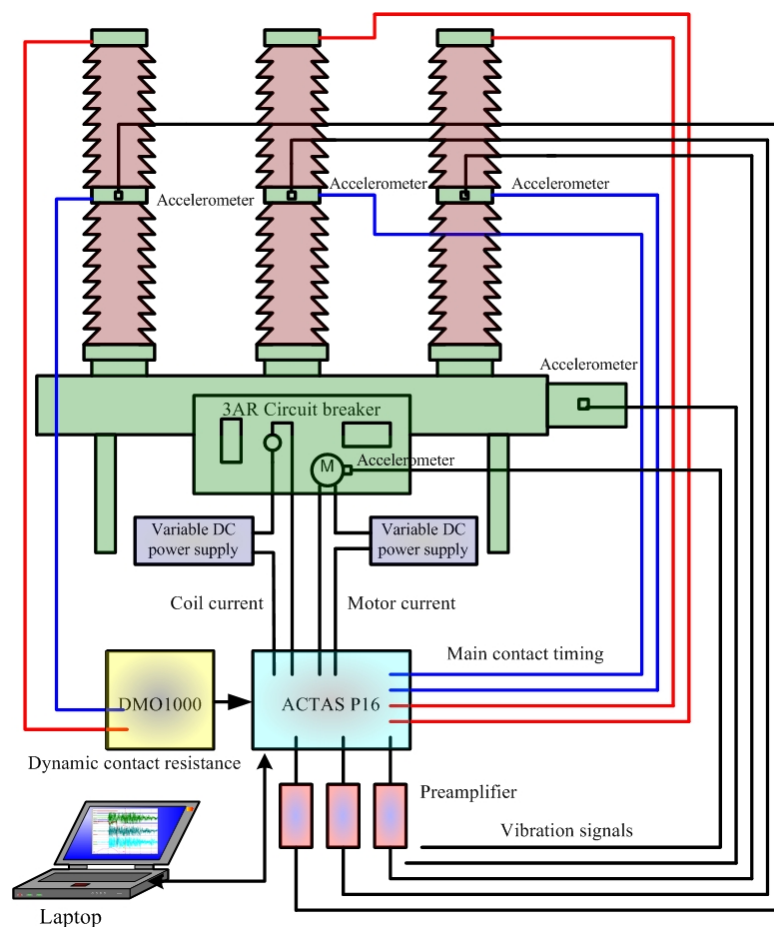


Figure 3.1: Experiment set-up

The main components of the test system and their details were described as follows:

- 3 of 110kV, 1250A, and 31.5kA puffer type SF₆ circuit breakers with three-pole-operated hydraulic operating mechanism.
- 5 accelerometers type 4501 (B&K) mounted externally at the middle of each pole, hydraulic pumping motor and hydraulic operating mechanism of the circuit breaker.
- 1 small accelerometer type 4374 (B&K) mounted at the middle of pole A to compare the signal with above sensor type.
- 3 preamplifiers type 2626 (B&K) for vibration signal conditioning with optical cable connection to accelerometer.
- 1 circuit breaker testing device ACTAS P16¹.
- 1 dynamic resistance measurement device DMO1000¹.
- Measurement cables and coaxial cable for serial connection between notebook and measurement device.
- 1 notebook as a control unit with ACTAS software program.
- 1 PC for evaluating and analysing measurement results and data storage.
- 2 variable DC or AC power supply for control circuit and pumping motor.
- SF₆ storage and filling unit.

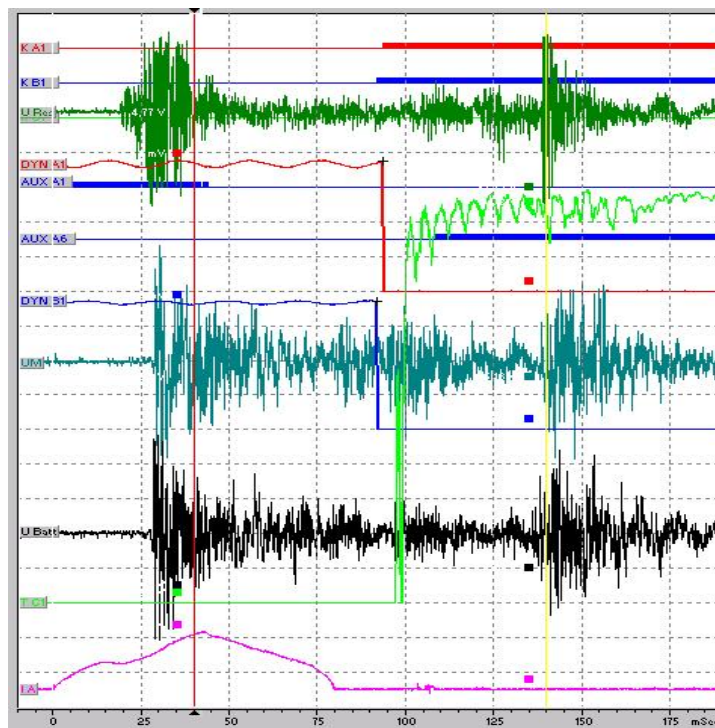


Figure 3.2: Vibration signals and other measured parameters recorded during closing operation

During the tests, the close and trip coil current were used as command signal to initiate circuit breaker operation and trigger data acquisition. The transfer of commands, parameters and data between notebook and ACTAS testing device was

¹ KoCoS Meßtechnik AG, Südring 42, D-34497 Korbach, Germany

carried out via a fast serial port connection. In each measurement, the following parameters, shown in Figure 3.2, were recorded:

- Close and trip coil current
- Main contact timing
- Auxiliary contact timing
- Dynamic contact resistance of each poles
- Pumping motor current and operating time
- Vibration measurement of each pole, operating mechanism and pumping motor

The first circuit breaker (CB1) was mainly served throughout the study. The above-mentioned parameters were measured since the beginning up to 6,000 switching operations. After 6,000 switching operations, the artificial defects were incorporated. After that, various measured parameters were evaluated and compared with those before defects. The detected changes of signatures from the initial or normal condition were used to evaluate the changing of circuit breaker condition and the capability of diagnostic tools. On site measurements were done with the second circuit breaker (CB2), which is in service in a high voltage substation. The third circuit breaker (CB3) was tested under normal condition and compared with the first circuit breaker. The overview of the test plan is summarized in Table 3.1.

Circuit breaker and measurement	Nr. of SW before testing	Test conditions	Voltage	Oil Pressure (bar)	SF ₆ (bar)	Nr. of SW per test
The First circuit breaker (Reference) Measurement <ul style="list-style-type: none"> ▪ At the beginning as reference base line ▪ After every 500 switching operations ▪ Up to 6000 switching operations The artificial defects after 6,000 swichtings <ul style="list-style-type: none"> ▪ Operation without connecting rod (1) ▪ Without bush in connecting rod (2) ▪ Fix contact pole B damaged (3) ▪ Operation until connecting rod is broken (4) 	200	Normal or rated operation	100%	320	6.5	15
		Variable supply voltage	115%	320	6.5	15
			70%	320	6.5	15
		Variable oil pressure	100%	280	6.5	5
			100%	250	6.5	5
		Variable SF ₆ pressure	100%	280	8	5
			100%	250	5.5	5
		Variable motor supply voltage	115%	320	6.5	5
			100%	320	6.5	5
70%	320	6.5	5			
Each defects	100%	320	6.5	5		
The second circuit breaker Measurement <ul style="list-style-type: none"> ▪ Before and after maintenance 	440	Normal operation	100%	320	6.5	10
The third circuit breaker Measurement in the storage room	1050	Normal operation	100%	320	6.5	10
		Variable supply voltage	115%	320	6.5	10
			70%	320	6.5	10

Table 3.1: Overview of the test plan

Referring to Figure 2.8 for failure pattern A and B, the period of reaching the wear-out zone are considered in order to simulate the artificial defects into the first circuit breaker. The arrangement of defect severity, the requirement of diagnostic tool as well as expected results are also summarized in Table 3.2.

Simulated defects	Time of occurrence in failure pattern	Objective of simulated defects	Severity of defect	Expected measurement result
Remove bush of the rod	During random failure	Mechanical degradation	low	difficult to detect
Fix contact damage	Reaching wear-out	Contact erosion by arc	high	difficult to detect
Cut connecting rod	Wear-out zone	Mechanical failure	very high	should be detectable
Remove connecting rod	Failure occurs	Severe mechanical failure	extremely high	should be detectable

Table 3.2: Summary of simulated defects



Remove connecting rod of Pole A



Remove bush of connecting rod of Pole A



Fix contact of Pole B manipulated to damage



Cut connecting rod of Pole A

Figure 3.3: Example of some incorporated artificial defects.

3.1.2 Measurement Techniques and Method

Coil control unit

The testing device is equipped with IGBTs working as a fast switch with a high degree of switching precision. The turn-on and turn-off delay is around $1 \mu\text{s}$ for activating the coils. The measurement of coil current is carried out by using integrated shunt resistors. The close and trip coil currents are captured as analog

signal. Actually, the coil current indicates not only the condition of the coil itself, but also the condition of the latches [Cle96]. The close coil current waveform shown in Figure 3.4 indicates the events occurring during circuit breaker operations. This can be described as follow:

At $t = 0$ ms, the close signal is initiated and current begins to flow through close coil until it reaches the first peak I_1 at time t_1 . At time t_1 , armature begins to move. Then, the circuit breaker has been unlatched and the armature moves to the end position at time t_2 [Kez02]. Therefore, the time between t_1 and t_2 indicates the speed of armature movement. Next, the current rises again to the second peak I_2 at time t_3 and the rate of rise depends on the coil inductance, while the amplitude of current at the second peak depends on the coil resistance. At time t_3 , the auxiliary NC contact is opened as seen from the voltage change of binary signal from initial level to 0V. After t_3 the voltage is removed from the coil and current decays gradually. At time t_4 , the main contact inside the interrupter is closed and it is followed by the auxiliary NO contact closing at time t_5 . The same description can also be applied to trip coil current during opening operation. This corresponds to [deG96], which mentioned that the improperly maintained latch could cause the coil to draw more current and change in coil current waveform.

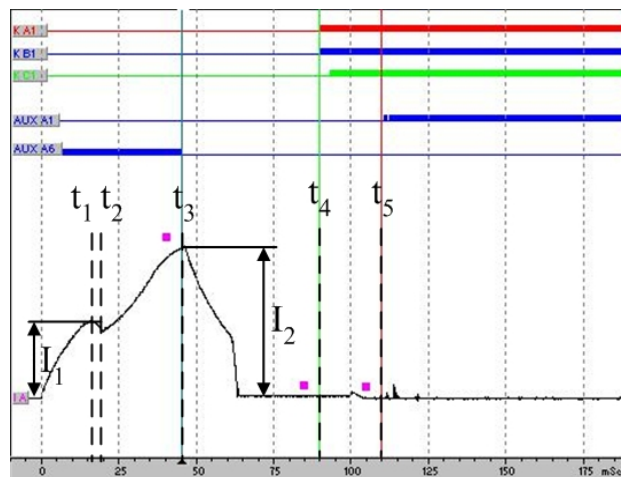


Figure 3.4: Events occurring during closing operation extracted from coil current waveform

Main contact status measurement

The measurement of main contact status are determined by capturing the resistance of a measurement loop with 12Vdc power supply. The threshold of main contact status depending on the loop resistance are define as follows: $R < 30\Omega$ main contact closed, $R > 30k\Omega$ main contact open. The signals for main contact status are recorded as binary inputs.

Auxiliary contacts measurement

Auxiliary contacts equipped with circuit breakers are normally used for signalling in telecontrol systems, station control system as well as protective systems. The power supply of 30 Vdc is applied to two types of auxiliary contact, normally closed and

normally open, in order to test their switching function, timing and synchronizing with respect to main contact.

Pumping motor current measurement

The motor current is measured by using resistive shunt. The values of peak amplitude of starting current, running current and operating time can be extracted from the measured current waveform.

Dynamic resistance measurement

This measurement captures the characteristic of the main contact resistance during switching operation, which makes it possible to identify the relationship between main contact resistance and travel. The test system feeds a pure direct current of approximately 1,000A from its own power supply through the main contacts, while at the same time the current and voltage drop across travelling contact are captured. Then, the dynamic contact resistance is calculated from measured voltage drop and current.

Vibration analysis

The vibration signals during closing and opening operations are recorded by using accelerometers and a data acquisition system. The vibration signatures are compared with the reference, which has been recorded earlier from the same circuit breaker under normal operating condition. The aiming is that the irregularities or abnormal conditions should be able to detect from changes extracted from the recorded vibration signatures.

Vibration measurement consists of the following components:

Sensor

The piezoelectric accelerometer is used to measure the vibration signal propagating to the external structure via various parts of the internal mechanism and insulating medium. The accelerometer consists of two small polarized ceramic plates with opposite polarity. It was temporarily mounted with adhesive glue on circuit breaker enclosure surface. It produces a charge in proportional to the acceleration (pC/ms^{-2}) to which the transducer is subjected. To gain the proper result, the direction of main sensitivity axis should be in the same direction of observed object movement. The output signal from the accelerometer is transmitted to a preamplifier via special noise reduction cable. The cable should be properly clamped to prevent the possibility of dynamically induced noise being generated by the cable movement.

Preamplifier and signal conditioner

The capacitive output impedance of the accelerometer is quite high and it can not be directly connected to the measurement device. Preamplifier and signal conditioner device are needed in order to match the impedance and amplify the signal to reasonable value. Before measurement, the charge generated by

each accelerometer must be set individually (sensitivity pC/g) according to a pre-defined value in its specification. The transfer factor was adjusted to produce output signal of 1V/ms^{-2} throughout the test. The maximum output signal was +10V and -10V.

Data acquisition

The sampling rate was set at 10kHz. The total record time was set at 200ms for closing operation and 150ms for opening operation. To avoid an error introduced in digital signal analysis caused by improper sampling time, called aliasing [Nor89], the signal should be sampled at a rate of at least twice the highest frequency of the signal, which is 5kHz for vibration signals. Otherwise, the digital representation will cause high frequencies to appear as low frequencies, when the sampling rate is too slow to catch the details of the analog signal. The total sampling time could also introduce erroneous frequencies to appear in the digital representation because the signal is assumed to be periodic within the sample record length. Thus, the actual frequency will leak into a number of fictitious frequencies, called leakage problem. Leakage can be corrected to some degree by using proper window function involving multiplying the original analog signal by a weighting function, which forces the signal to be zero outside the sampling period. Rectangular window, which is suitable for transient signal, was used throughout the analysis.

Signal analysis

The acquired vibration signals were further analyzed in both time-domain and frequency-domain.

In time-domain analysis, the event timing extraction by using Discrete Envelope Statistics (DES) [Pol95] was employed to determine the times at which important events occur during switching operation. The method of DES can be obtained as follows: in case that we have the acceleration signal $f(t)$, then the vibration envelope is

$$F(t) = \sqrt{f^2(t) - f(t-1) * f(t+1)} \quad (3.1)$$

Where t is each sample point. Equation 3.1 is used to reduce high frequency harmonics fluctuation. After that $F(t)$ will be passed to approximately 100Hz low pass filter and then the envelope of the acceleration signal can be used for timing analysis with the aid of the other measured parameters as shown in Figure 3.5.

By considering the envelope of acceleration signals, which are signal envelope of pole A (dash line) and of operating mechanism (solid line), together with coil current (dot line) and dynamic contact resistance (dash-dot line) waveforms, as shown in Figure 3.5 for closing operation, the timing of important events can be clearly determined. At point 1, the closing command is sent to close coil. Then, motion of operating mechanism starts first and shortly later the motion within pole occurs as shown at point 2. The amplitude of the pole envelope reaches the value of around 5.8g in a few

milliseconds later due to the accelerated motion of moving parts. Next, the arcing contact touches the fix contact at point 3 with around 2.6g of pole envelope amplitude owing to weaker impact. No significant change occurs in the signal envelope of operating mechanism because this event is far away from sensor location. Eventually, the motion of operating mechanism stops first, the arcing contact is then fully touched the fixed contact and shortly later the moving contact reaches the end as shown at point 4. Finally, the envelope amplitude declines gradually. Unfortunately for opening operation, only motion start event can be extracted from the signal envelope. Thus, this method is suitable for closing operation.

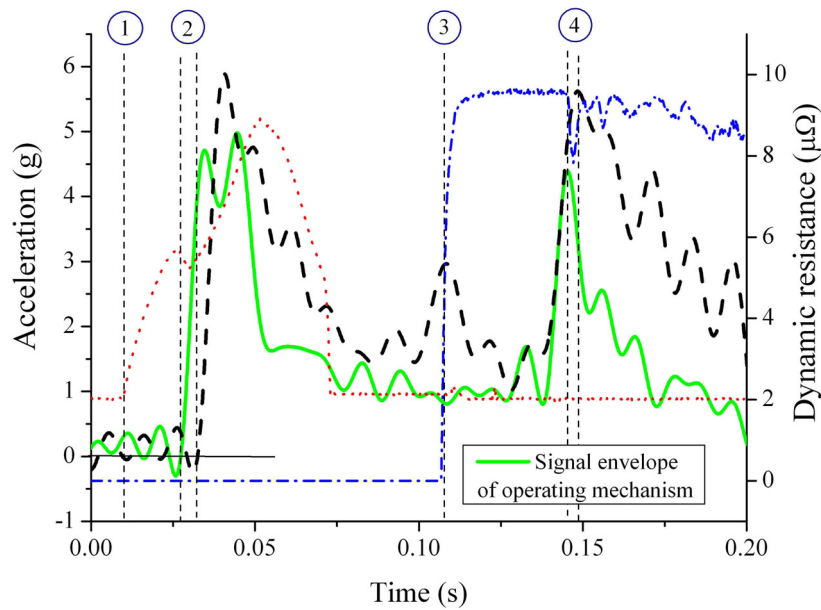


Figure 3.5: Example of signal envelope for event timing extraction

In frequency-domain analysis, the vibration signal after preamplifier was passed to digital band pass filter of 30-10,000Hz to eliminate noise above and below a specified frequency range and remove DC-offset from the measured signal. The 20 points adjacent average was also applied to remove high frequency noise. After that, the signal was analyzed by a fast fourier transform (FFT). For Discrete Fourier Transform (DFT) of a dataset $x(n)$ with index n in the range $0 \leq n \leq N-1$, the forward Discrete Fourier Transform (DFT) is defined as

$$X(k) = \sum_{n=0}^{N-1} x(n)e^{-j\frac{2\pi}{N}kn} \quad \text{for } 0 \leq n \leq N-1 \quad (3.2)$$

3.1.3 Theoretical Calculation of Circuit Breaker Pole Vibration

The whole structure of a circuit breaker can be drawn as a spring mass model as shown in Figure 3.6 (a) and the simplified model in Figure 3.6 (b) by using the estimation method developed in [Kir98].

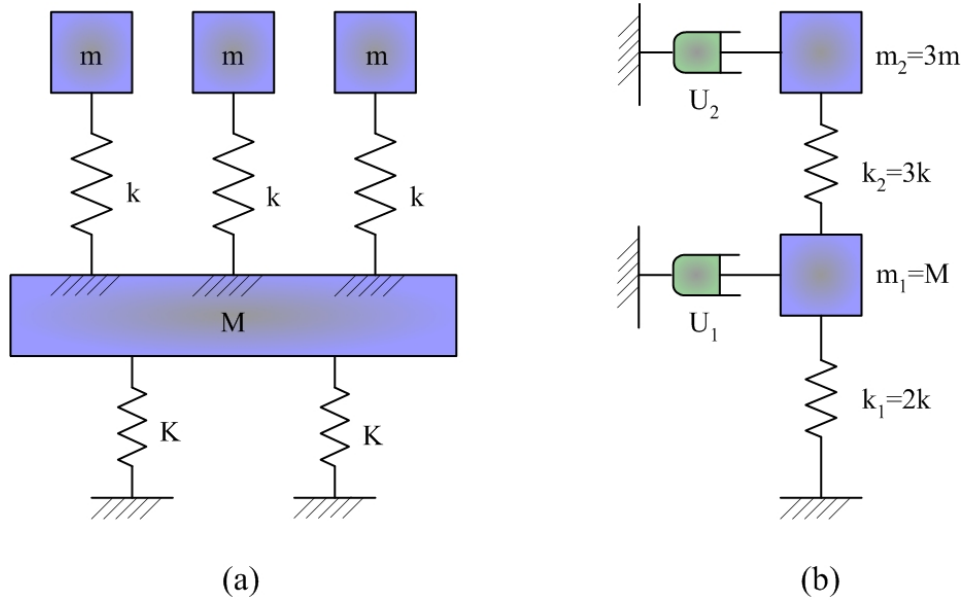


Figure 3.6: (a) Spring mass model, (b) Simplified model [Kir98]

Considering that $m_2 = \text{total weight} - \text{base mass} = 2,190\text{kg} - 1,575\text{kg} = 615\text{kg}$
 $m_1 = M_{\text{base}} = 1,575\text{kg}$
 $k_1 = 3,000,000 \text{ N/m}$ for porcelain (k is stiffness of the spring)
 $k_2 = 2,950,000 \text{ N/m}$ for steel

Equation of motion

$$\ddot{x}_1 + d\dot{x}_1 + ax_1 - bx_2 = q.\sin(\omega t) \quad (3.3)$$

$$\ddot{x}_2 + e\dot{x}_2 + cx_2 - cx_1 = 0 \quad (3.4)$$

where $a = \frac{(k_1 + k_2)}{m_1}$, $b = \frac{k_2}{m_1}$, $c = \frac{k_2}{m_2}$, $d = \frac{U_1}{m_1}$, $e = \frac{U_2}{m_2}$, $q = \frac{Q}{m_1}$

By neglecting damping U , the natural frequencies are

$$f_{1,2} = \sqrt{\frac{(a+c)}{2} \pm \sqrt{\left(\frac{(a+c)}{2}\right)^2 + b.c}} \quad (3.5)$$

Substitute the value of a , b and c in Equation 3.5 and then the natural frequency of pole vibration is 97.56Hz.

However, the circuit breakers in service are always connected by conducting wires at their terminal pads. This mass of wires will add to the mass m_2 and causes the change in the vibration characteristics of the poles.

3.2 Experimental Results

The evaluation of the test result is divided into two parts. The first part is the comparison of test results of three circuit breakers under rated operating condition, which is 100% of rated voltage of auxiliary power supply for close and trip coil circuit and pumping motor power supply, 320 bar hydraulic oil pressure and SF₆ 6.5 bar. Then, the results measured from the first circuit breaker in every after 1,000 up to 6,000 no-load switching operations are compared with the reference result measured at the beginning of the test. The second part is the comparison of test results from the first circuit breaker under variable operating conditions and defects.

3.2.1 Comparison of Results at Rated Operating Condition

The comparison of measured results from three circuit breakers is presented first and follows by the results during the test periods of the first circuit breaker. The presented values or waveforms of each result are the average value of five closing or opening operations. From Figure 3.7 as seen from coil current waveforms, the close or trip command is sent at 10ms after recording time starts. Therefore the real value of time presented in the subsequent figures, e.g. closing time or opening time of main contact, must be subtracted by this 10ms to avoid misunderstanding when reading the value directly from the graphs.

Coil current

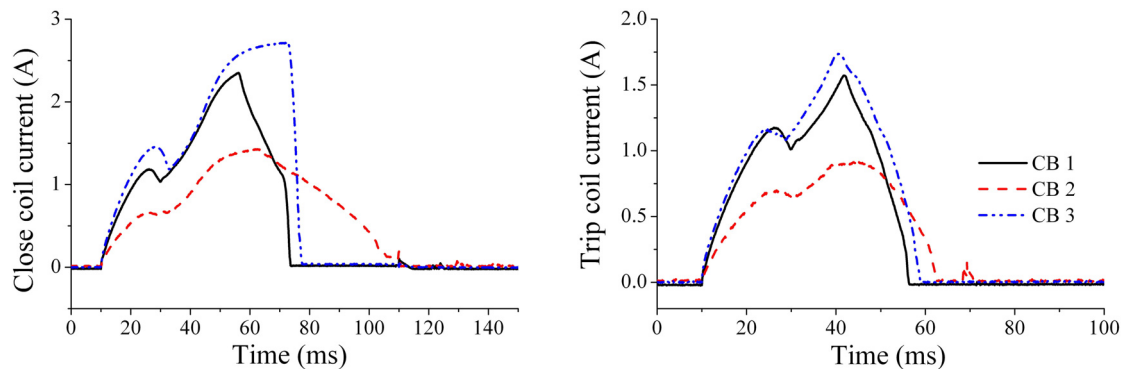


Figure 3.7: Close and trip coil current of three circuit breakers at the beginning of the test

At the beginning of the test (the first 5 switching operations of CB2 and CB3), shown in Figure 3.7, each circuit breaker has a different waveform of close coil current. Because of relatively slow in the first closing operation of CB2 & 3, close coil current of both circuit breakers was supplied longer than usual, but waveform of CB3 was cut off after 75ms due to the operation of add-in protective device. For trip coil current, waveform of CB1 and CB3 looks slightly similar because of equal in rated supply voltage 110Vdc, but different from waveform of CB2 using 220Vac supply voltage.

At the end of the test (the last 5 switching operations of CB2 and CB3), each circuit breaker also has a different waveform of close coil current. Slightly change in

waveform of CB2 and CB3 are caused by faster in closing time when compared with the beginning. For trip coil current, waveform of CB3 has become slightly lower in both peak values and looks nearly similar to waveform of CB1, while waveform of CB2 remains unchanged.

Since maintenance of CB2 causes a reduction in closing time, the faster in second peak occurrence and the shorter in time of current flow can be seen from close coil waveform when compared with those before maintenance.

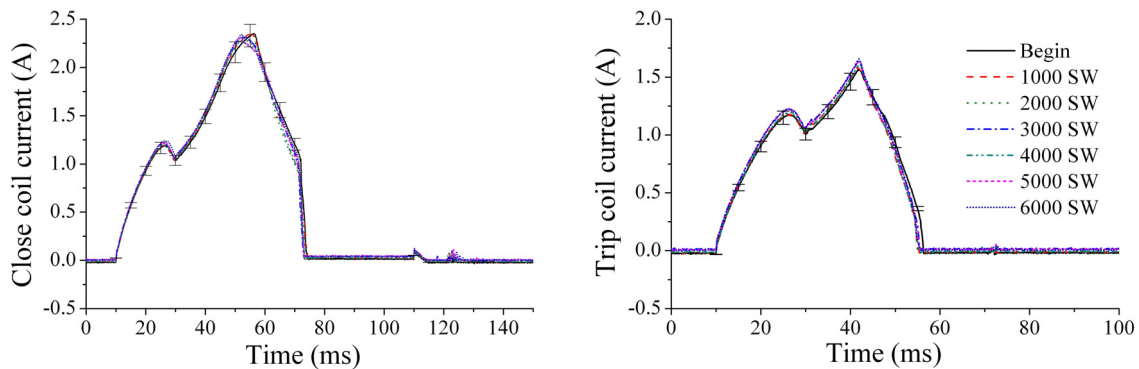


Figure 3.8: Close and trip coil current of the first circuit breaker at the beginning to 6,000 switching operations (5% error bar of I at the beginning)

During the test period of CB1 (0-6,000 no-load switching test), waveform of trip coil current does not change for the first peak and the second peak, waveform of close coil current does not change in first peak, but second peak occurs 5ms or 9% faster with roundness around peak value after 2,000 switching operations. As mentioned in section 3.1.2 and Figure 3.4, first peak of both coil currents occurs at the same time and has the same value, while second peak occurs when auxiliary contact starts to change its status.

Operating time

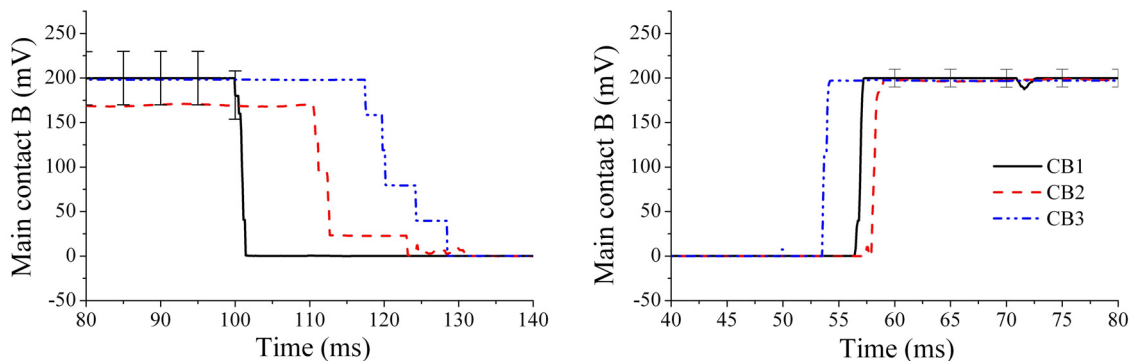


Figure 3.9: Closing (left) and opening time (right) of three circuit breakers at the beginning of the test (15% error bar of CB1 for closing and 5% for opening)

At the beginning of the test, the closing time of CB3 was the slowest (110-120ms), CB1 was the fastest (90ms) and CB2 was in the between (100-105ms). For the first closing operation of CB2 and CB3 closing time was not only longer, but voltage drop across main contact of CB2 was also lower. However, after some switching

operations it subsequently reached the normal closing time. According to [deG96] for field experience, the very first short is also often missed, but it provides a good indication of the operating time after a certain standing period. Opening time of CB3 is the fastest (44ms), while that of CB1 and CB2 is nearly the same (47ms).

At the end of the test, the closing time of CB1 was around 2ms slower than that from the beginning. All of three CBs had closing time within the allowable limit (93ms). The closing time of CB2 after maintenance was 10ms faster than before maintenance. Opening time was unchanged during test period of CB1, before and after maintenance of CB2 and during 15 switching operations of CB3.

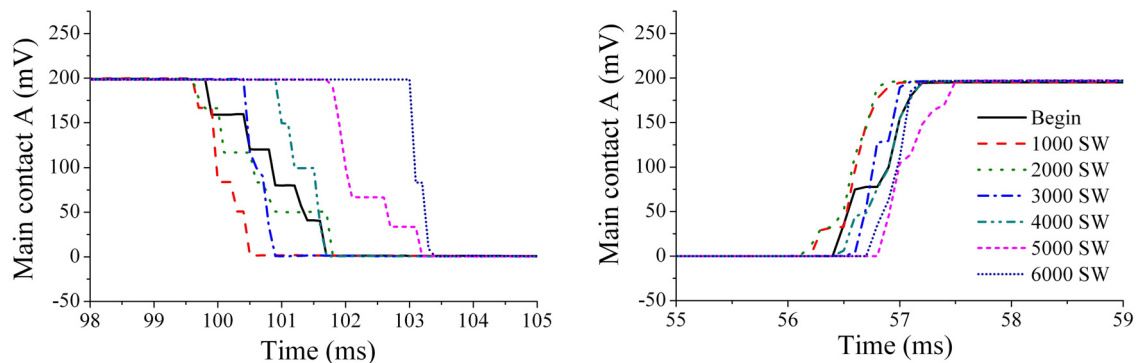


Figure 3.10: Closing (left) and opening time (right) of the first circuit breaker from the beginning to 6,000 switching operations

During the test period of CB1, the change in closing time is around 3ms and could be clearly seen after 5,000 switching operations. The sequence of pole according to faster in closing time is C, A and B respectively. There is no change in opening time (46-47ms). The sequence of pole according to faster in opening time is A, B and C respectively (A is the nearest pole to operating mechanism).

Dynamic contact resistance

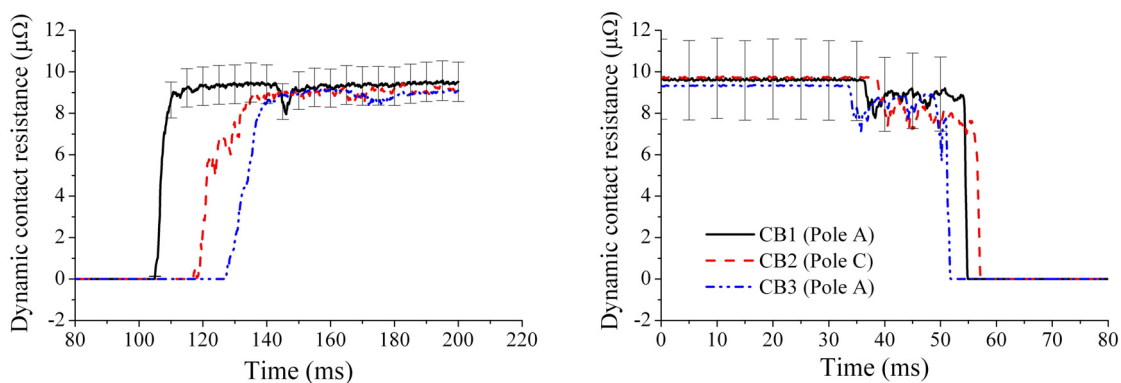


Figure 3.11: Closing (left) and opening dynamic contact resistance (right) of three circuit breakers at the beginning of the test (10% error bar of CB1 for closing and 20% for opening)

At the beginning of the test, closing time of CB3 was the slowest (120ms), CB1 was the fastest (97ms) and CB2 was in the between (110ms). The time between graphite nozzle and main contact separation, i.e. the time between event 3 and 4 in Figure

3.5, of CB1 was 40.8ms, but for CB2 and CB3 it could not be determined. Opening time of CB3 was fastest (41ms), while that of CB1 and CB2 was nearly the same (44.6-47ms). The time between graphite nozzle and main contact separation of CB3, 1 and 2 were 17.9, 18.1 and 18.4ms respectively.

At the end of the test, closing time of three circuit breakers were nearly the same around 100ms. The time between graphite nozzle and main contact separation of CB1 and CB3 were 40.4ms, but for CB2 it could not be determined. Opening time of three circuit breakers remained unchanged. The time between graphite nozzle and main contact separation of CB3, 1 and 2 were 18.2, 18.8 and 19.2 respectively.

The lower voltage drop across main contact of CB3 implies the lower main contact resistance when compared with the other two circuit breakers. During test period of CB3 (15 switching operations), the nozzle-contact time were 2ms faster for closing and 0.3ms longer for opening. The effect of maintenance to nozzle-contact timing during closing could not be determined, but caused 0.8ms longer for opening operation.

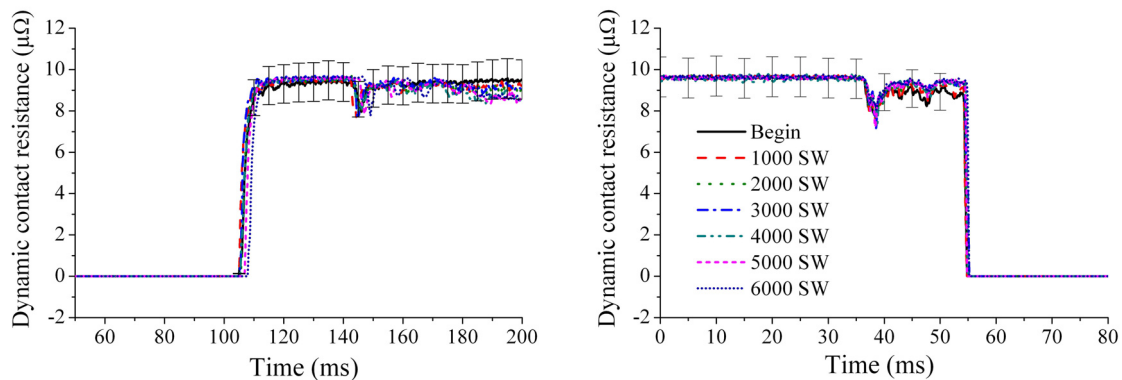


Figure 3.12: Closing (left) and opening dynamic contact resistance (right) at pole A of the first circuit breaker from the beginning to 6,000 switching operations (10% error bar of begin test)

During the test period of CB1, closing time was only slightly different (95 to 98ms). The time between graphite nozzle and main contact separation ranged from 38.6 to 41.1ms. Opening time was almost the same (54.6 to 55.4ms). The time between graphite nozzle and main contact separation was nearly the same (18.1 to 18.8ms). Therefore, the delay in time between graphite nozzle and main contact separation were 2.5ms for closing and 0.7ms for opening.

Vibration signature

In frequency-domain analysis, CB1 standing on flat surface had the highest frequency spectral density during closing at the following frequencies: 87, 97Hz for pole A, 87, 97 and 107Hz for pole B and C. The highest frequency spectral density during opening occurred at the frequencies of 4.9, 87, 112Hz for all 3 poles, which had the highest magnitude at 87Hz. These results corresponds to the theoretical calculation, which is approximately 97Hz, and the vibration result also obtained in low frequency for measurement with 420kV SF₆ circuit breaker [Man01].

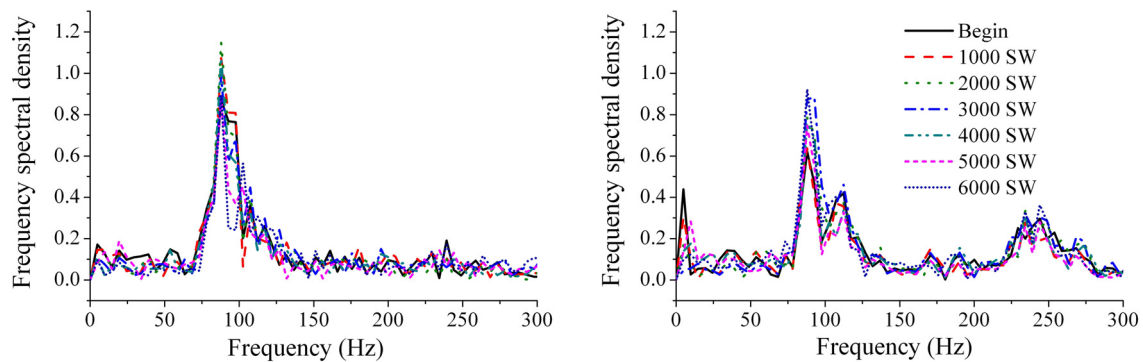


Figure 3.13: Frequency spectral density of pole A vibration for closing (left) and opening (right) of the first circuit breaker from the beginning to 6,000 switchings

CB2 installed on steel structure with conductors connected at terminal pads showed an almost equal vibration frequency spectrum signature of pole A and C when opening, but for pole B opening and three poles closing frequency spectrum signatures were very low in amplitude when compared with CB1.

Small delay in operation and maintenance effect did not affect frequency spectrum signature. Therefore, vibration method by using FFT of vibration signal cannot detect this problem.

The frequency spectrum signature of CB1 both for closing and opening operations did not change significantly throughout its test period.

During test period, the frequency spectrum signature of operating mechanism during closing and opening could not be clearly determined.

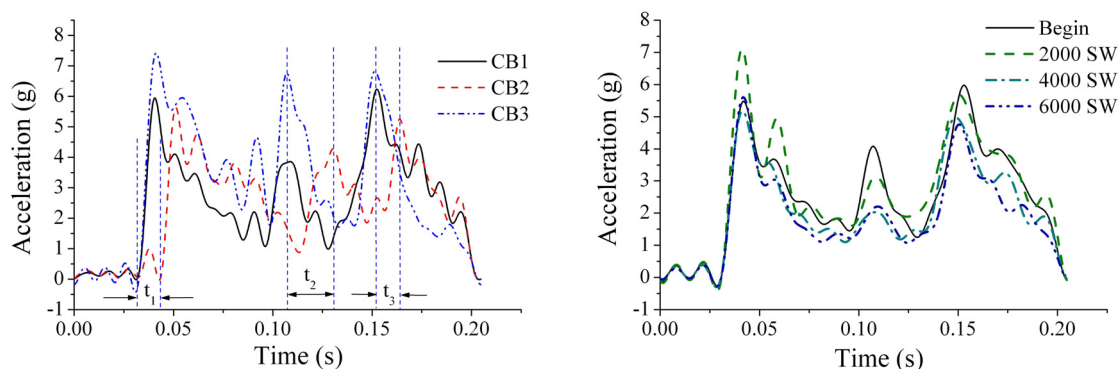


Figure 3.14: Signal envelope of pole A of three circuit breakers at the beginning of the test (left) and signal envelope of the first circuit breaker during test period (right) for closing operation

In time-domain analysis, the signal envelope of pole is mentioned because of better event extraction than the signal from operating mechanism. The signal envelope of three circuit breakers at the beginning of the test is shown in Figure 3.14 (left). The operating time of CB3 was identical to that of CB1 (90ms). The signal envelope of CB1 and CB3 shows that the important events, such as motion start, the arcing contact touches the fix contact and motion stop, occurs at the same time. The delay

in closing time of CB2 compared to CB1, when measured by contact timing and dynamic contact resistance, was 13ms. From signal envelope, the delay of motion start (t_1), the arcing contact touches the fix finger contact (t_2) and motion stop (t_3) events are 11.7ms, 23.7ms and 12ms respectively. The closing time from contact timing of CB2 pole A after maintenance was around 10ms faster than before maintenance. This faster closing time could be determined from signal envelope by faster in event occurrence of 6.6ms, 17.9ms and 6.9ms for t_1 , t_2 and t_3 respectively.

During test period of CB1, signal envelopes were almost identical. The amplitude was highest after 2,000 switching operations and then declined as shown in Figure 3.14 (right). The occurrence of three events was relatively identical, only 3.4ms and 4.8ms deviation for t_2 and t_3 respectively. The signal envelopes of operating mechanism were also nearly similar throughout the test period.

Pumping motor

After 6,000 switching operations, the pumping motor of CB1 still operates correctly. No changes in operating time (6.8s), peak starting current (45A), average running current (10.5A) and frequency spectrum occurs. The pumping motor currents of CB2 before and after maintenance look similar to each other. When compared with CB1, operating time is equal (7s), but different in values of running current (10.5A for CB1), peak starting current (45A for CB1) because CB2 uses 220Vdc supply voltage.

Result discussion

The measurement with three circuit breakers shows the good agreement of the results. However, the first measurement with CB2 and CB3, performed after a certain standing period, shows the slow operations, which can be observed from operating time, coil current, dynamic contact resistance measurement and from the vibration signal envelope. Therefore, it would be necessary to perform some switching operations after a certain period to keep the operating time within the acceptable limit. Even though the good agreement between the measurement and calculation is obtained, the vibration analysis in the frequency-domain is not recommended because the vibration frequency spectrum signature depends significantly on the circuit breaker installation methods. The vibration analysis in the time-domain is, however, very useful because the significant events can be extracted from the vibration signal envelopes. The occurrence of these events provides the helpful information about the cause of failures.

The maintenance of the second circuit breaker results in the 10ms faster in closing operations, which is clearly seen from the operating time measurement. Because of no-load switching operation, the mechanical degradation from 6,000 switching operations is relatively small and no significant changes can be determined. Thus, the variation of operating conditions and simulated defects, performed in the next section, is necessary to evaluate their effects on the monitored parameters.

3.2.2 Comparison of Various Operating Conditions and Artificial Defects

Coil current

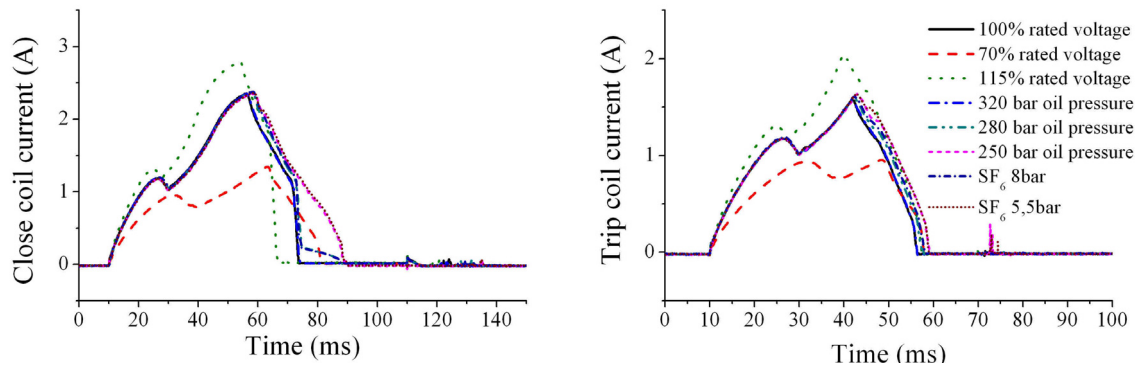


Figure 3.15: Close and trip coil current of the first circuit breaker under various operating conditions at the beginning of the test

The variation of control voltage causes changes in waveform of both coil currents. By decreasing control voltage to 70% of rated value, the first peak of close and trip coil current occurs 5.5ms slower and 19% decreases in amplitude; second peak occurred 7ms slower for both coil currents and 43% and 40% decreases in amplitude of close and trip coil current respectively. By increasing control voltage to 115% of rated value, first peak of close and trip coil current occurs 1ms faster and 15% and 10% increases in amplitude; second peak occurs 2ms faster for both coil currents and 18% and 30% increases in amplitude of close and trip coil current respectively.

By changing oil pressure 250, 280 and 320bar, the waveform of close coil do not change both in time and magnitude of first peak, but the second peak occurs faster at higher oil pressure due to the shorter current flow. Therefore, the second peak occurs 3ms and 4.5ms slower for 280bar and 250bar when compared with 320bar oil pressure. Oil pressure changes have no effect on trip coil current. At 250 and 280bar oil pressure, there are some spike of current occurred at 63ms because auxiliary contact is close or open completely, but higher in magnitude of spike at 250bar oil pressure. The changing SF₆ gas pressure from 6.5bar to 5.5 and 8bar has no effect on close and trip coil current

Operating time

By changing control voltage 70%, 100% and 115%, the operating time for both closing and opening of 70% control voltage is 7ms slower, but 115% control voltage causes 2ms faster when compared with 100% voltage (93ms for closing and 47ms for opening after receiving command). The relationship between main contact timing and supply voltage variation is shown in Figure 3.16.

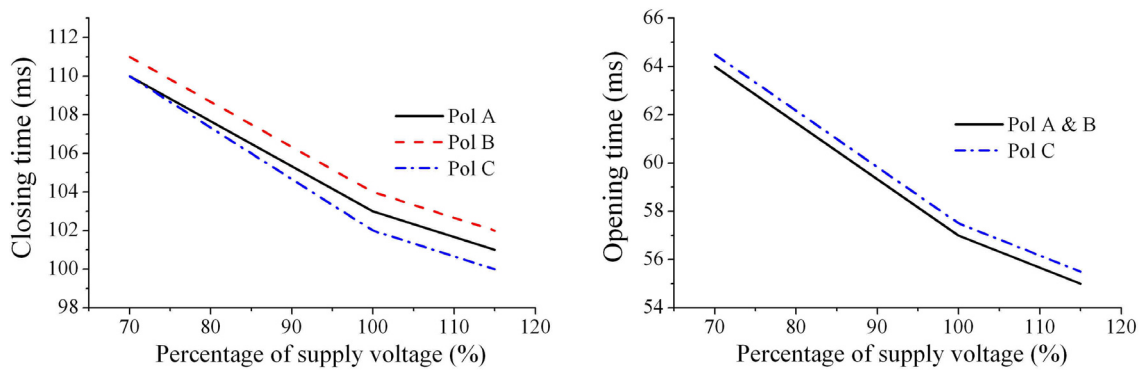


Figure 3.16: Closing and opening time of CB1 with variable supply voltage

By changing oil pressure 250, 280 and 320bar, the operating time with 250bar are 10ms and 4ms delayed for closing and opening, and the operating time with 280bar are 6ms and 2ms delayed for closing and opening when compared with 320bar rated oil pressure. The relationship between main contact timing and hydraulic oil pressure variation is shown in Figure 3.17.

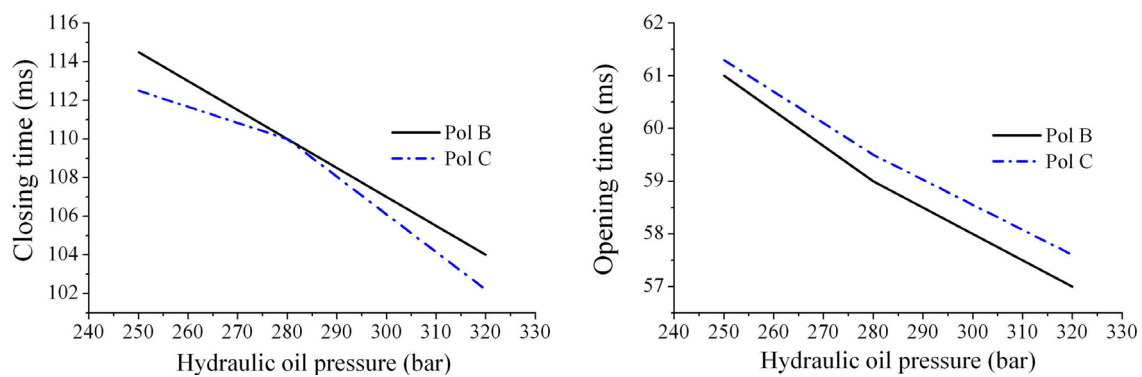


Figure 3.17: Closing and opening time of the first circuit breaker with variable hydraulic oil pressure

Changing of SF₆ pressure from 6.5 to 5.5bar has no effect on operating time, but changing of SF₆ from 6.5 to 8 bar causes 1.2-1.8ms delay in closing time and 0.5-1.0ms delay in opening time.

Dynamic resistance

The time between graphite nozzle and main contact separation is nearly constant at 40ms (range from 39.1 to 41.5ms) for closing operation and 18-19ms for opening operation. Therefore, it does not depend on control voltage variation. Only operating time is affected by control voltage variation.

The variation of oil pressure 250, 280 and 320bar causes the time between graphite nozzle and main contact separation with 250bar to be 5ms and 3ms delay for closing and opening, and the time between graphite nozzle and main contact separation with 280bar to be 3ms and 2.5ms delay for closing and opening when compared with 320bar rated oil pressure.

The change of SF₆ gas pressure has no effect on time between nozzle and main contact separation for both during closing and opening.

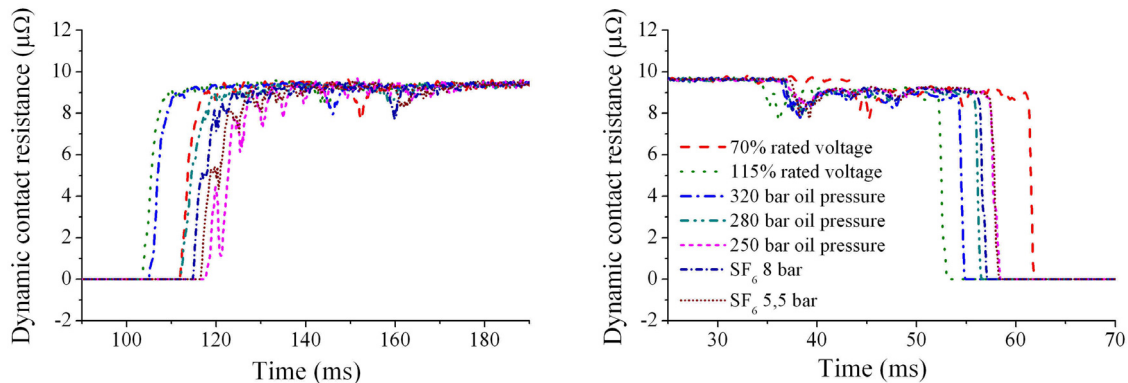


Figure 3.18: Closing (left) and opening dynamic contact resistance (right) from pole A of the first circuit breaker under various operating conditions

Vibration signature

Vibration method could not clearly detect changing of SF₆ from 6.5 to 5.5bar and variation of auxiliary supply voltage.

By changing of SF₆ from 6.5 to 8bar, the highest frequency spectrum density occurs at the frequency of 102Hz for all 3 poles instead of 107Hz during closing operation due to the increasing mass of the interrupting unit. During opening operation, the highest frequency spectrum density occurs at the frequency of 92Hz for pole A instead of 97 or 107Hz, and also occurs at 29Hz for pole C.

By changing oil pressure 250, 280, 320bar, the frequency spectrum of operating mechanism changed randomly and could not clearly determine.

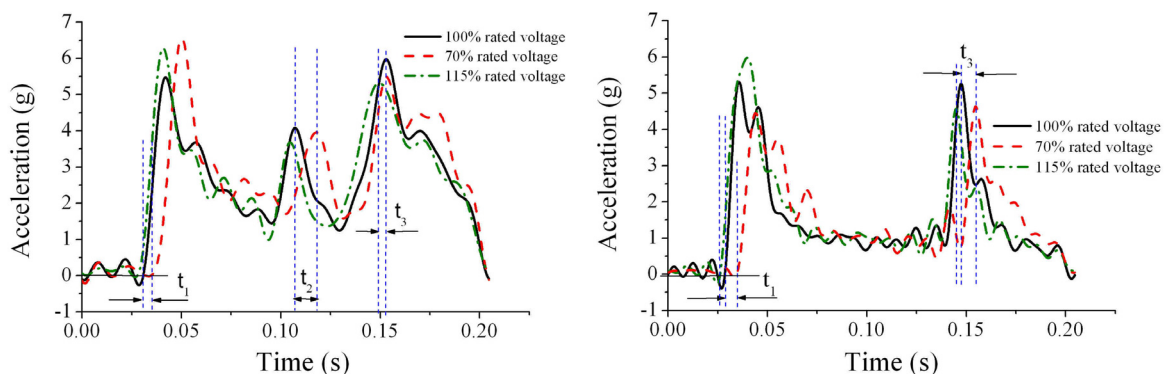


Figure 3.19: Signal envelope during closing of CB1 under variable supply voltage, left for pole A and right for operating mechanism

As mentioned in contact closing time measurement, the variation of supply voltage causes 2ms faster and 7ms slower for 115% and 70% rated voltage when compared with 100% rated voltage. Figure 3.19 (left) shows signal envelopes of pole A and right for that of operating mechanism under supply voltage variation. The event occurrences obtained from pole A envelope are 2.8ms, 3ms and 4.5ms faster for 115% rated voltage and 4.5ms, 11ms slower and no delay for 70% rated voltage for

t_1 , t_2 and t_3 events respectively. While the t_1 and t_3 events from operating mechanism envelope are 3.1ms and 2.5ms faster for 115% rated voltage, and 5.8ms and 7.6ms slower for 70% rated voltage.

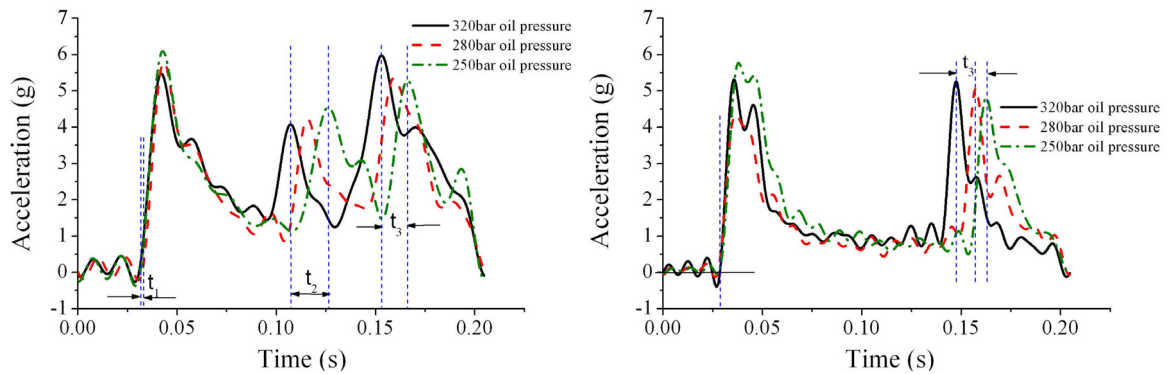


Figure 3.20: Signal envelope during closing of CB1 under variable hydraulic oil pressure, left for pole A and right for operating mechanism

The event occurrences from pole A envelope under hydraulic oil pressure variation, shown in Figure 3.20 (left), are 1.3ms, 8.3ms and 6.5ms delay for 280bar oil pressure and 1.3ms, 19ms and 13ms delay for 250bar oil pressure for t_1 , t_2 and t_3 events respectively. From operating mechanism signal envelope (right), the t_1 events occur at the same time. However, the t_3 events are 10ms and 15.5ms delay for 280bar and 250bar oil pressure.

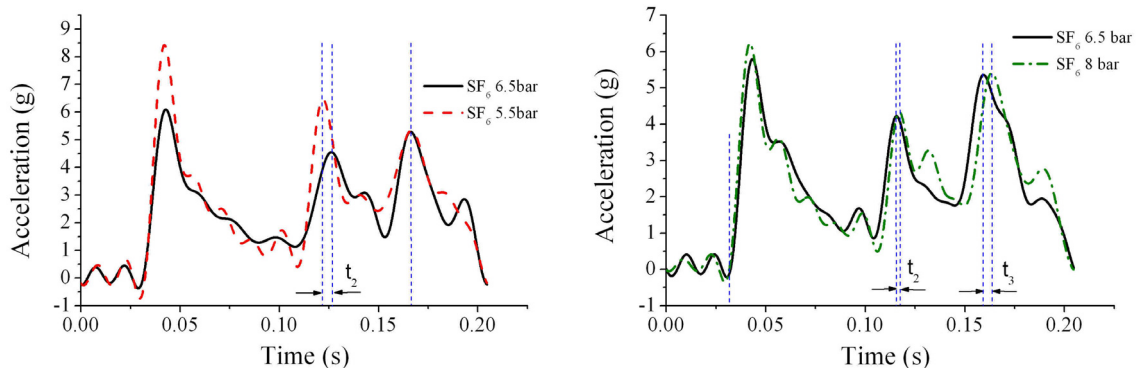


Figure 3.21: Signal envelope of pole A during closing of CB1 for SF₆ 5.5 bar (left) and SF₆ 8 bar (right)

For SF₆ pressure 5.5bar, signal envelope shows higher in amplitude for events t_1 and t_2 and only 5ms faster in event t_2 occurrence when compared to SF₆ 6.5bar with 250bar hydraulic oil pressure for both cases. The signal envelope of 8bar SF₆ pressure shows 1.7ms and 4.4ms delay for event t_2 and t_3 occurrences when compared to SF₆ 6.5bar with 280bar hydraulic oil pressure for both cases.

Pumping motor

From Figure 3.22, the variation of motor supply voltage to 70%, 100% and 115% of rated 110Vdc causes operating time to be 9.6s, 6.8s and 5.9s respectively and the peak starting current is changed to 26A, 45A and 52A respectively. But the average value of running current is nearly constant at 10.5A.

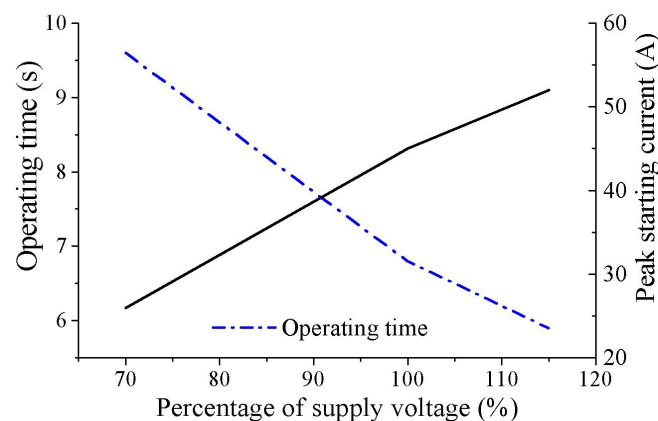


Figure 3.22: Motor operating time and peak starting current with voltage variation.

The frequency spectrum of pumping motor at 100% supply voltage has higher in magnitude (0.01-0.02) than at 70% and 115% supply voltage (0.005-0.01). This frequency spectrum at 100% supply voltage is nearly 2 times higher in amplitude than that at 70% and 115% of rated voltage because it operates at its full efficiency.

Artificial defect

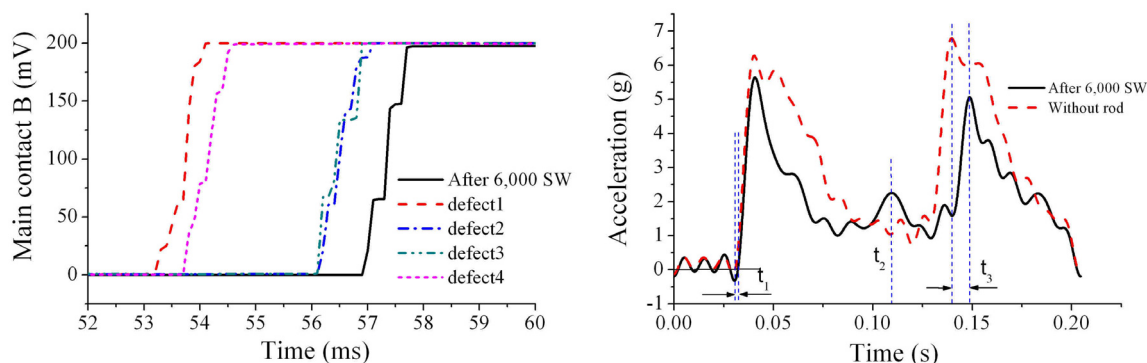


Figure 3.23: Contact opening time for incorporated defects and signal envelope for closing without connecting rod

Operation without connecting rod in pole A (Defect 1) causes small changes in close coil current waveform, contact closing time and higher amplitude of vibration signature, especially during opening. However from Figure 3.23 (left), contact opening time of pole B and C for the first and second measurements showed around 3.5ms faster in operation than the opening time measured before incorporating defect, which was after 6,000 no-load switching tests. The signal envelope, shown in Figure 3.23 (right), for pole A vibration shows that the event t_2 (arcing contact touched the fix finger contact) disappears and the occurrence of event t_3 is 8.6ms faster than normal operation.

Operation without bush in connecting rod causes only small deviation in closing time. Damaged fix contact B shows 3ms and 1ms faster in closing and opening time. However, the changes could not be clearly determined from the measurement. Operation until connecting rod was broken shows abnormal signal of main contact

timing since the third closing by some ripple and no voltage drop across the main contact at the third opening operation as shown in Figure 3.24.

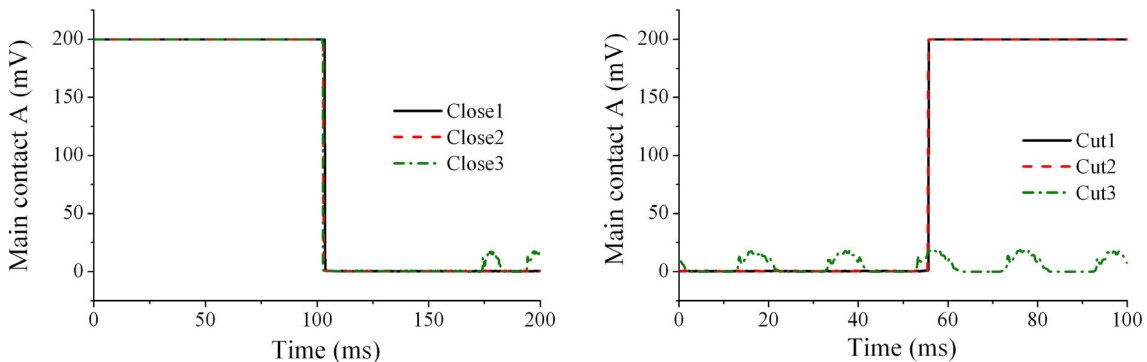


Figure 3.24: Contact A closing (left) and opening time (right) for cut connecting rod at pole A

Result discussion

The ability of the monitored parameters to detect significant changes due to the variation of operating conditions is summarized in Table 3.3. The variation of auxiliary supply voltage and hydraulic oil pressure is detectable, whereas the variation of SF₆ pressure causes only the slightly change in some monitored parameters. Vibration analysis in frequency-domain is not recommended, while this in time-domain analysis, operating time and dynamic contact resistance measurements are recommended as the useful parameters for circuit breaker diagnostics.

Variable operating condition	Coil current	Operating time	Dynamic resistance	Vibration analysis	
				frequency-	time-domain
Auxiliary supply voltage	yes	yes	yes	no	yes
Hydraulic oil pressure	no	yes	yes	no	yes
SF ₆ pressure	no	no	no	no	yes

Table 3.3: Summary of the detection of significant changes (yes = detectable)

In case of simulated defects, the operation without bush in connecting rod and damaged fix contact can not identified from the measurement. The operation with cut connecting rod and without operating rod is too severe and identifiable from the contact timing and vibration signal envelope.

3.3 Summary

The no-load mechanical test up to 6,000 switching operations does not cause any significant degradation in the operating mechanism. The circuit breaker still operates correctly. By the variation of auxiliary supply voltage and hydraulic oil pressure, the deviation of the monitored values from the reference normal condition can be determined, except for the case of SF₆ pressure variation. The maintenance of a circuit breaker causes faster in operating times. By the simulated defects, only the severe defects cause the significant changes in the observed parameters.

The conventional measurement alone is insufficient to provide the better information about the condition of the circuit breaker, e.g. the condition of contact is not identifiable only from the dynamic contact resistance measurement. However, by the evaluation of this measurement in combination with the vibration signal envelope, the significant events occurring inside the circuit breakers during closing operation can be realized from the external measurement, which is the benefit of this method. Therefore, the vibration measurement is recommended as a tool for circuit breaker diagnostics.

Even though, the analysis of the deviation from the reference base line of the observed parameters in combination provide the possibility to identify the cause of abnormalities, e.g. the change in coil current waveforms together with vibration signal envelopes and contact timing could be caused by the failure in the auxiliary supply voltage. This reverse procedure of using the measured parameters to identify the origin or the cause of failure needs the further development, such as the more field measurements, complex data base, parameter extraction methods, decision making procedures, etc.

4 Investigations on Current Interruption Using an SF₆ Circuit Breaker Model

The radiated heat from the high current interruptions leads to the contact erosion, nozzle ablation, geometry change and consequently the reduction in pressure build-up in the expansion volume, which is called an electrical degradation. The severity of the degradation depends on various parameters, such as the amplitude and arcing time of the interrupted current, circuit breaker configuration, voltage stress during the recovery period, etc. This degradation occurs after each current interruption and finally the circuit breaker cannot fulfil the switching requirement, which leads to the costly and unfavourable consequences. Hence, the investigation on the electrical degradation by focusing on the aging of nozzle and electrode under current interruption is performed in this chapter with a reduced-size SF₆ self-blast circuit breaker model and a synthetic test circuit, because of the extensive use of nozzle ablation, the possibility for parameters variation and the reduction of cost and time.

4.1 Experiment Set-up and Test Arrangement

The concept of experimental investigation using a reduced-size self-blast circuit breaker model and a synthetic test circuit, which has been performed for many years, are based on the following considerations:

1. The arc occurring inside the nozzle must be an ablation-controlled arc. The fictitious current density should be comparable to that in a real circuit breaker.
2. During the high current interval, the sinusoidal current waveform from the synthetic test circuit should provide a current density and steepness at current zero region comparable to the real condition and should generate a sufficient pressure build-up with reproducible gas flow phenomena in both nozzle region and expansion chamber.
3. At current zero region, the gas flow velocity, temperature and decomposition of the insulating gas should be comparable with the gas state in a real circuit breaker.
4. The current and voltage stresses applied during interaction interval should be continuous throughout the interval. Their waveforms should have acceptable deviation from prospective values. The switching of the auxiliary circuit breaker should not affect the switching phenomena of the test circuit breaker. Furthermore, the impedance of the test circuit should be low enough to permit reignition or restrike during high voltage interval, if they occur.

The experiment set-up and arrangement provide the possibility for crucial parameters variations, such as nozzle diameter, expansion chamber volume, current amplitude and recovery voltage amplitude. To gain the understanding on the electrical degradation of a circuit breaker model, the following parameters have been varied:

1. Current amplitude by the variation of the charging voltage in high current circuit from 1kV, 1.3kV and 1.5kV.
2. Nozzle bore diameter 5mm and 8mm to change the radiation flux density on the nozzle surface along the arcing column and the cross sectional area for the hot gas to escape to the surroundings.
3. Expansion chamber of circuit breaker model 0.5Litre and 1Litre.
4. Using one or two ignition wires in parallel for the different arcing time.
5. Different charging voltage of high voltage circuit with identical rate of rise.
6. Filling pressure of SF₆ in test vessel is fixed at 5bar (0.5MPa) absolute.

In each test, the voltage drop across the nozzles and across the electrodes, the current flowing through the circuit breaker and the pressure rise in the expansion chamber were recorded. Furthermore, the mass losses of nozzles and electrodes and change in nozzle geometry after each interruption were determined. The number of successive tests, performing on one nozzle pair under each test condition until thermal failure occurred, and the number of current zero at the moment of interruption failure were also recorded.

4.1.1 Circuit Breaker Model

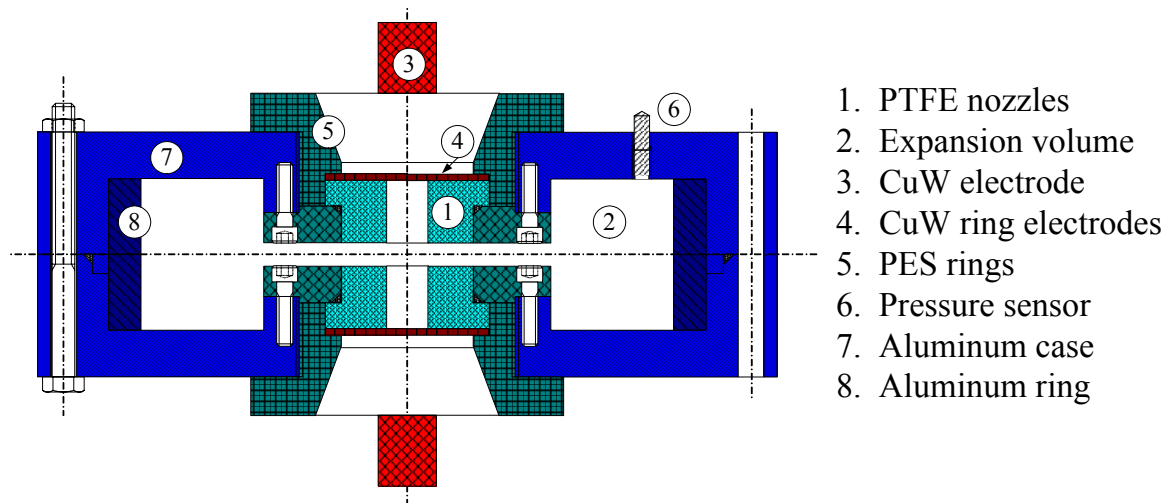


Figure 4.1: Cross section of circuit breaker model

The rotational symmetric self-blast circuit breaker model as shown in Figure 4.1 was used throughout the test. Its construction is made on the basis of easy for installation and dismantling of two cylindrical PTFE nozzles (1) with variable diameter, adjustable expansion volume (2), various electrode forms (3), adjustable distance between both electrodes and durability for mechanical and thermal stresses. The nozzle wall should be thick enough to provide ablated material for several successive tests. The two Cu-W ring electrodes (4), aligned on the top of both PTFE nozzles by screwed PES (Polyethersulphone) rings (5) for the easy of mounting and dismantling, are used to measure the voltage drop across the two nozzles. The pressure build-up inside the expansion chamber is measured by a pressure sensor

(6). Inside the two aluminium half bowls (7), used as a case or housing of the expansion chamber, an aluminum ring (8) is inserted to adjust the volume of expansion chamber from 1Litre to 0.5Litre.

The circuit breaker model is installed on the retaining flange, supported by two epoxy resin insulators, in a GIS 5 flange die-cast pressure container called test vessel. The high voltage electrode is movable to provide the space for the installation of the circuit breaker model and the flexibility of setting the desired electrode distance. The distance between the two electrodes is 10 cm. SF₆ up to 5bar absolute is filled in the 70Litre volume test vessel with a pressure release valve on the top cover as safety device. The back cover contains the leading bushing for the high voltage electrode, bushings for measurement purposes and the connector to the SF₆ filling unit for evacuation, filling and draining of SF₆ to the gas storage system. The access to the inner parts is only possible by opening the aluminium front cover.

4.1.2 Synthetic Test Circuit and Measurement Techniques

Due to the fact that the thermal and dielectric phases as the current and voltage stresses to circuit breakers occur in separate time with only short overlapping interval, the synthetic test circuit with current injection method using parallel current injection circuit [Dom05], [Kah05], was used throughout the experiment. The required stresses are produced from 2 separate test circuits. The high current circuit, consisting of C_H, L_H, DS and HS, supplies a 53.17Hz sinusoidal positive half wave current with variable amplitude through the circuit breaker during the high current interval. This current should be high enough to cause the arc gap at the end of the high current interval to be in the state of ionization, temperature rise, pressure build-up, gas flow, electrode heating, etc. After that, it is followed by the voltage stress from the high voltage circuit, consisting of C_S, L_S, R_P, C_P, R_E, and the triggering spark gaps ZFS and FS. C_S and L_S perform as a 956Hz oscillating voltage source with variable voltage by variation of charging voltage up to 54kV on C_S. C_P, R_P and R_E work together as a TRV shaping circuit.

During the experiment, the interrupting current was measured by using a Manganin-tube shunt with 840 $\mu\Omega$ resistance and 720ns rise time. The voltages were reduced to a measurable value by using Tektronix high voltage test probes (T) with a divider ratio 1,000:1 for both voltage measurements. The rise time of these voltage probes is 4ns and the input capacitance is less than 3pF. The pressure in the expansion chamber was measured by a piezoelectric pressure sensor, installed in an adapter and fitted into the aluminium housing of the expansion chamber. The transmission of above-mentioned electrical signals to two oscilloscopes was performed by optical transmission between an optical sender (S) in the testing room and a receiver (R) in the control room. Before and after each test, the weight of two nozzles and two electrodes were measured with 1mg measurement uncertainty to determine the mass losses of nozzles and electrodes. Furthermore, the expanded diameters in four positions in nozzle bore were measured to obtain the geometry change after each interruption. To obtain more exact geometry changes, the nozzles after the successive tests were cut, scanned and evaluated by using a digitizer software.

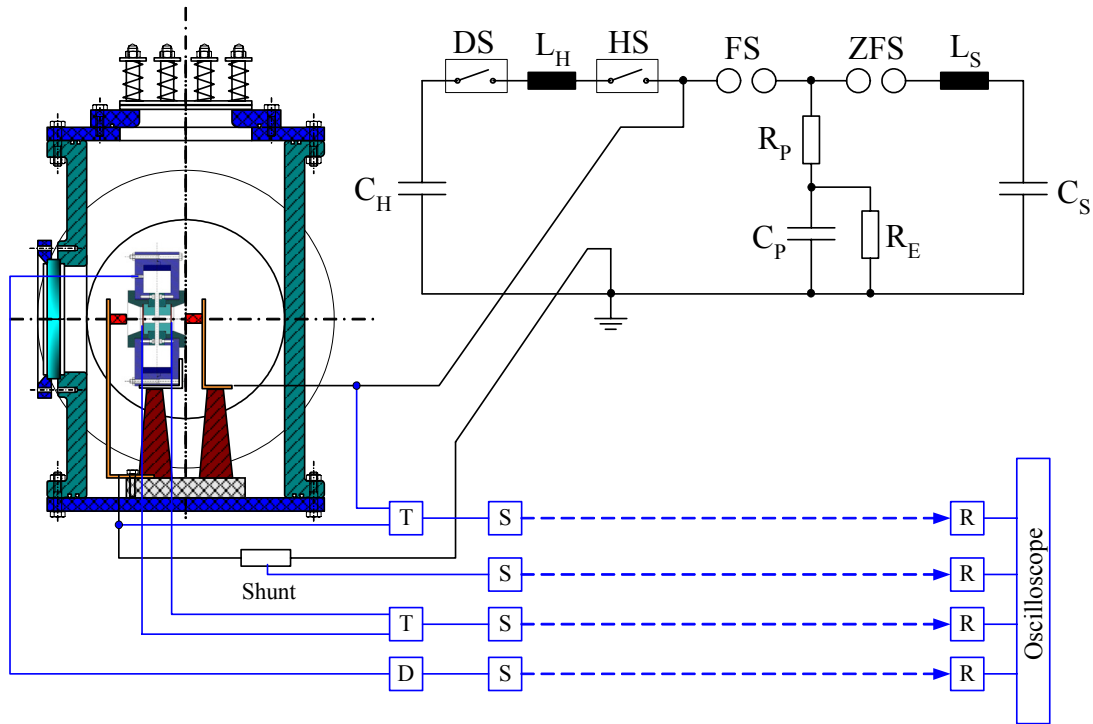


Figure 4.2: Synthetic test circuit and measurement system [Kah05]

4.1.3 Example of the Measured Result and the Gas Flow Observation

The measured waveforms of the current, voltage and pressure in the expansion chamber for 8mm nozzle with the interruption failure are shown in Figure 4.3 and Figure 4.4 as an example. After the arc initiation, the current is now in sinusoidal waveform and the voltages across the nozzles and across the electrode (not shown) are constant during this high current period. This high current reaches the peak at point 1 in Figure 4.4 and causes the pressure to rise up linearly. The current falls down and the pressure reaches the maximum (P_{\max}) at point 2 due to the time delay of the gas flow to the monitored point. At point 3 the current is now zero and a drop in pressure occurs, which indicates the back flow of the stored gas.

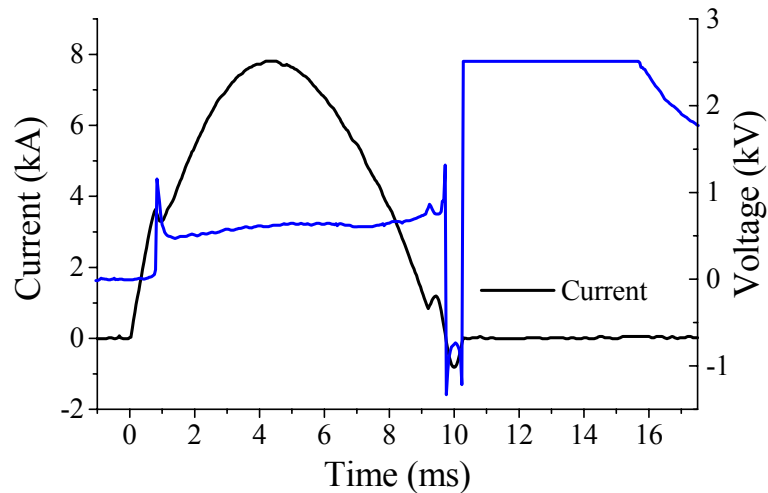


Figure 4.3: Measured waveforms of current and voltage over 8mm nozzle

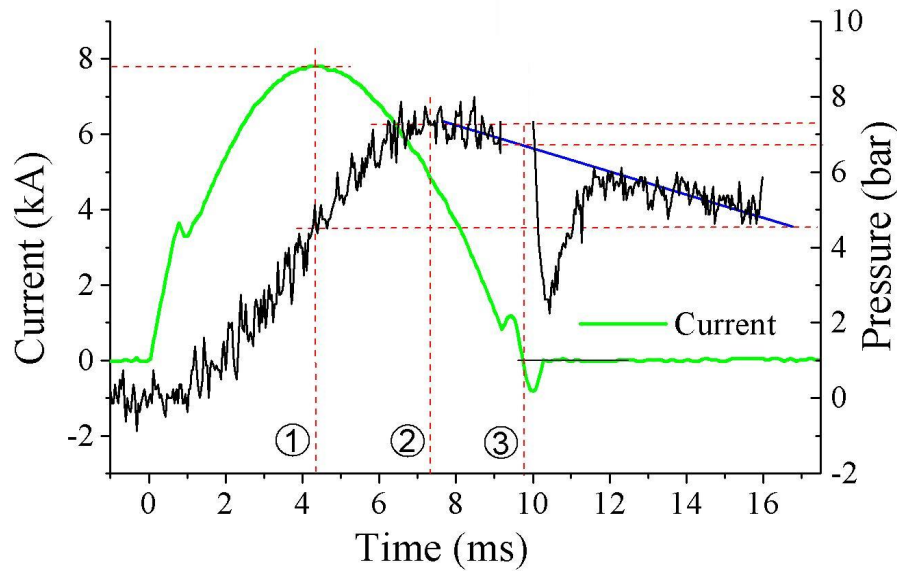


Figure 4.4: Measured waveforms of current and pressure for 8mm nozzle in case of interruption failure

In Figure 4.4, the gas flow observation from the comparison between the pressure rise in the expansion chamber and the current waveform of each interruption is presented. The amplitude of current peak, time to peak current and pressure rise at this time are measured as shown at point (1). Then, the peak value of the pressure rise and time to reach are also measured at point (2). Finally, the pressure at the first current zero and time to the first current zero at point (3) are determined. The time after current peak (1) to pressure peak (2) can be easily derived from those measured values.

Because the current does not cease to flow after the first current zero, the thermal failure occurs. Hence, the tests were performed successively on one pair of nozzle until the thermal failure occurred.

4.1.4 Experiment Methods

Effect of arc energy on ablated mass

The mass loss of the nozzle material or the electrode depends on the transferred energy into the material. The energy across nozzle is defined as

$$w_{noz}(t) = \int_0^t u_{noz}(t) i(t) dt \quad (4.1)$$

The energy over electrode was determined in the same way as

$$w_{elec}(t) = \int_0^t u_{elec}(t) i(t) dt = \hat{\text{arcing energy}} \quad (4.2)$$

where $w_{noz}(t)$ and $w_{elec}(t)$ are the energy across the nozzle and across the electrode
 $u_{noz}(t)$ and $u_{elec}(t)$ are the voltage across the nozzle and across the electrode

The charge generated by an arcing current $i(t)$ is defined as

$$q(t) = \int_0^t i(t) dt \quad (4.3)$$

The accumulated arc heating can be calculated by

$$h_{arc}(t) = \int_0^t i^2(t) dt \quad (4.4)$$

The current density (j) inside nozzle can be written as

$$j(t) = \frac{i(t)}{\pi r_0^2} \quad (4.5)$$

where r_0 is the radius of nozzle at the beginning of each test. The ablation factor of the nozzles and the electrodes M [mg/kJ] is determined by dividing mass loss Δm of the nozzle or the electrode by its corresponding energy as shown in equation 4.6 for nozzle.

$$M = \frac{\Delta m}{W_{noz}} \quad (4.6)$$

Ablated nozzle observation

In the experiment, the mass losses (Δm) of the nozzles and the electrodes were measured before and after each current interruption until a thermal failure occurred. The geometry changes of the nozzle were determined by measurement of the enlarged diameter of the nozzle at four positions around the nozzle edge, where the gas flow between cylindrical arcing column along nozzle bore and expansion chamber occurs, as shown in Figure 4.5. Nozzle 1 and electrode 1 were on the left hand side when installed in test vessel shown in Figure 4.2, and nozzle 2 and electrode 2 or Anode were on the right hand side. Hence, nozzle 1 and electrode 1 or Cathode were located closer to the tank than the other side because of space required for high voltage leading cable.

The geometry of new nozzles is drawn in Figure 4.5 (a). The right-angle edge of nozzle bore marked by circles was investigated. Before inserting them into the circuit breaker model, D_{in} at the middle of the nozzle bore was exactly measured and recorded with 0.01mm uncertainty. After current interruption, the diameter of nozzle bore was measured at four positions as shown in Figure 4.5 (b). After current interruption, the edge of nozzle becomes round and the bore diameter becomes larger. This change influences the gas flow phenomena and the limit interrupting capability of the next interruption.

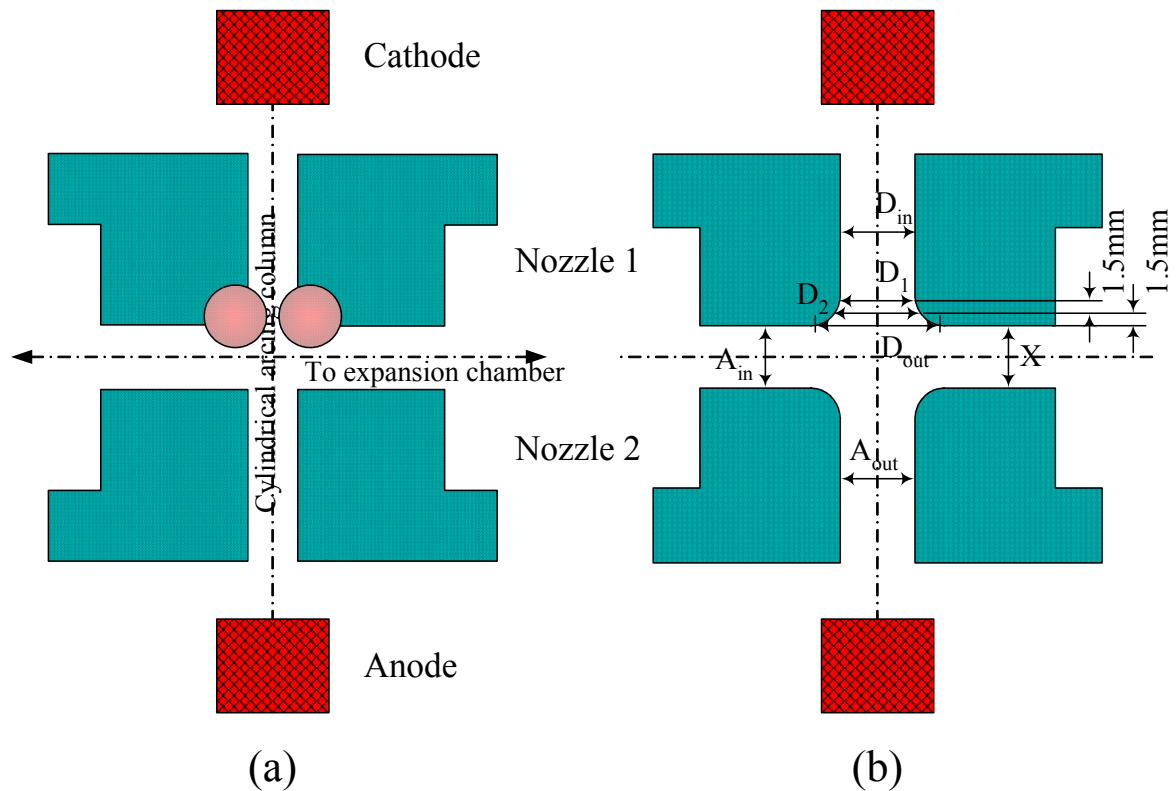


Figure 4.5: Measured positions of nozzle geometry (a) new nozzles, (b) after current interruptions

For more precise evaluation of the changes in nozzle contour, a digitizer software² was used. At first, the centre-cut nozzle cross sectional area must be scanned and then imported to the software. After that, the scale bar should be set according to nozzle dimension and followed by the setting of measurement points along the nozzle contour as shown in Figure 4.6.

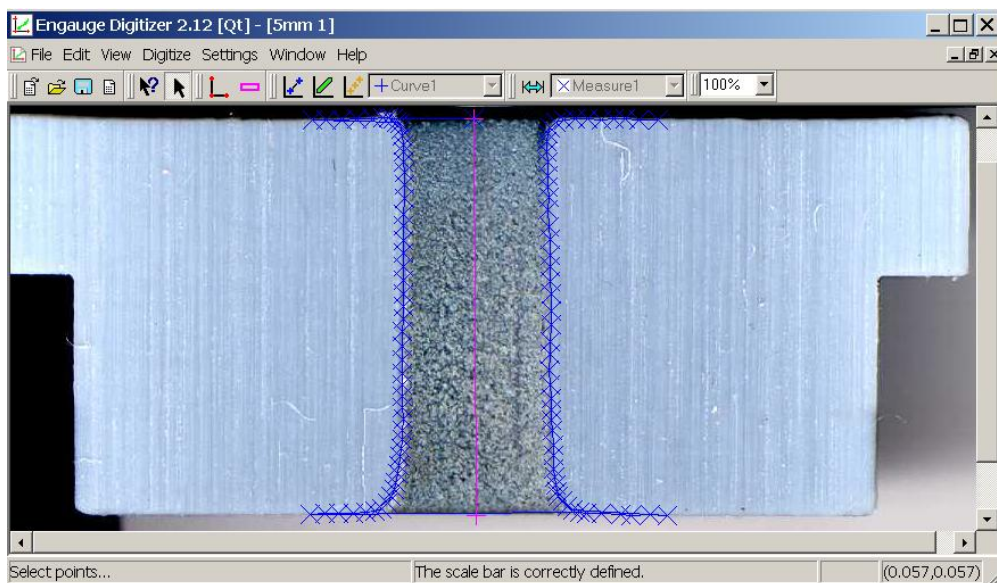


Figure 4.6: Measurement points along the nozzle contour

² The Engauge Digitizer freeware version 2.12

The position of each measured points was recorded in the table, which can be exported for further calculation. Therefore, the result from nozzle contour changes can be further derived to determine the ablated volume loss and mass loss of nozzle as follows:

$$\text{Volume Loss} = \sum_{n=1}^m \pi r_n^2 \Delta x_n - \pi r_0^2 L \quad (4.7)$$

And the ablated mass loss is

$$\text{Mass Loss (m)} = \text{Volume Loss } \rho \quad (4.8)$$

where

- m is number of measured points
- r_n is radius at each measured points [mm]
- Δx_n is distance between two measured points [mm]
- r_0 is radius before test or like-new condition [mm]
- L is nozzle length [mm]
- ρ is PTFE density 2.18 [mg/mm³]

The measurement uncertainty can be calculated by knowing the dimension of a scanned picture, which is 864x470 pixels. Therefore, one pixel error (Δr) represents the length of 0.056mm. The maximum volume loss error per pixel along nozzle length $\Delta V = \pi((r_0 + \Delta r)^2 - r_0^2)L = 17.79\text{mm}^3$ or 38.78mg.

Effect of the nozzle geometry on the pressure build-up

According to Figure 4.5 (b), the cross-sectional area of the channel to the expansion chamber is considered as A_{in} , while the cross-section of the opening exit along the nozzle column at both ends is A_{out} . The relationship of those areas is defined as

$$\frac{A_{in}}{A_{out}} = \frac{2\pi R_{avg} X}{2\left(\frac{\pi D_{in}^2}{4}\right)} = 4 \frac{R_{avg} X}{D_{in}^2} = \frac{K}{D_{in}^2} \quad (4.9)$$

where

- R_{avg} is 10mm from the rotational axis to the middle of nozzle thickness
- X is the gap distance between two nozzle ends = 7mm
- K is constant = 280mm²
- D_{in} is the average diameter at the middle of nozzle column

Since a lot of nozzle ablation appears along the arcing column, but not in the channel to the expansion chamber, A_{in} can be considered as constant, whereas A_{out} increases significantly after each interruption. The reduction of this area ratio after each interruption due to nozzle widening results in the reduction of pressure build-up in the expansion chamber because of the larger area for the hot gas to escape to the surrounding space.

4.2 Measured Parameters and Characteristics of Synthetic Test Circuit

The amplitude of the arcing current has been varied by variation of the charging voltage in the high current circuit. For a 5mm nozzle, the charging voltages 1kV, 1.3kV and 1.5kV were used for the high current circuit, while the charging voltage of the high voltage circuit was fixed at 23kV. To gain the proper statistical results, the performed tests under equally controlled testing environment were repeated four times of six consecutive current interruptions for 1kV, four and five times of testing until a thermal failure occurred for 1.3kV and 1.5kV charging voltage respectively. In case of the 8mm nozzle, the five successive interruption tests were repeated three times for 1kV, 1.1kV and 1.3kV, and four times for 1.5kV charging voltage.

The average values from repetitive tests calculated from the recorded waveforms of arcing current, pressure inside expansion volume and voltage across the nozzles and across the electrodes are plotted in Figure 4.7 and 4.8 as solid line for 5mm and dot line for 8mm nozzle testing. The average values of the first and the fifth interruption, mean vales of five successive interruptions and percentage of increment are shown in Appendix B, Table 1.

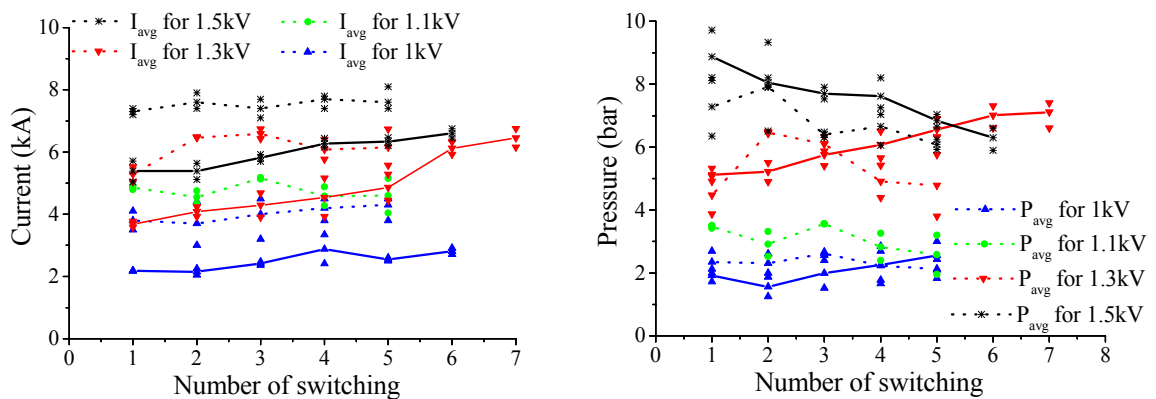


Figure 4.7: Measured peak current and pressure at each interruption

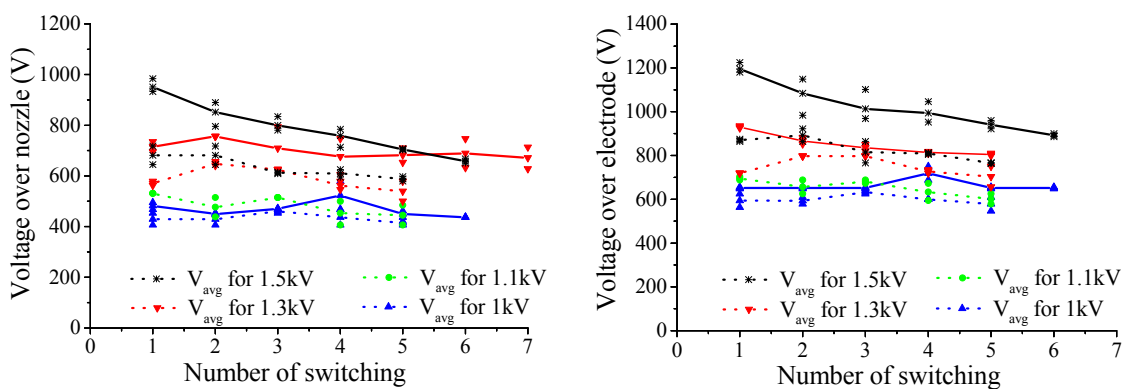


Figure 4.8: Measured voltage over nozzle and electrode at each interruption

When comparing the results, the peak currents of 8mm nozzle are higher than that of 5mm nozzle in every charging voltage because the arc is confined in the

narrower cylindrical nozzle in case of 5mm nozzle. This causes the voltages across nozzles and the electrodes in case of a 8mm nozzle to be lower than those of a 5mm nozzle due to the exponential V-I characteristics of the arc. The pressures inside the expansion volume are nearly equal for the 1kV case, but for 1.3kV and 1.5kV the pressures generated by a 5mm nozzle are higher than by a 8mm nozzle since the reduced cross-section forces the hot gas to flow more intensively to the pressure chamber. This means that in case of a low current density, the thermal energy may not be sufficient to generate a sufficient pressure in the expansion volume.

The measured pressures for the 1.5kV case decrease gradually, whereas these increase steadily for the 1.3kV case. This results from the larger nozzle diameter expansion in case of 1.5kV, which allows more hot gas to escape to the surroundings. The reduction in the pressure build-up due to the larger nozzle diameter expansion will be discussed in the next section.

The mean values of average energy over the nozzles and over the electrodes, calculated from equation 4.1 and 4.2 respectively, are almost constant for each interruption test and shown in Table 4.1. Therefore, the cumulative energy increases linearly with the number of interruptions. The cumulative energy over the nozzles and the electrodes is shown in Figure 4.9.

Charging Voltage	Energy over nozzle [kJ]		Energy over Electrode [kJ]	
	5mm	8mm	5mm	8mm
1kV	8.6	11.4	12.6	15.7
1.1kV		13.4		18.7
1.3kV	18.8	21.2	22.4	28.7
1.5kV	29	27.9	37.7	37.3

Table 4.1: Average energy over nozzle and over electrode for each interruption

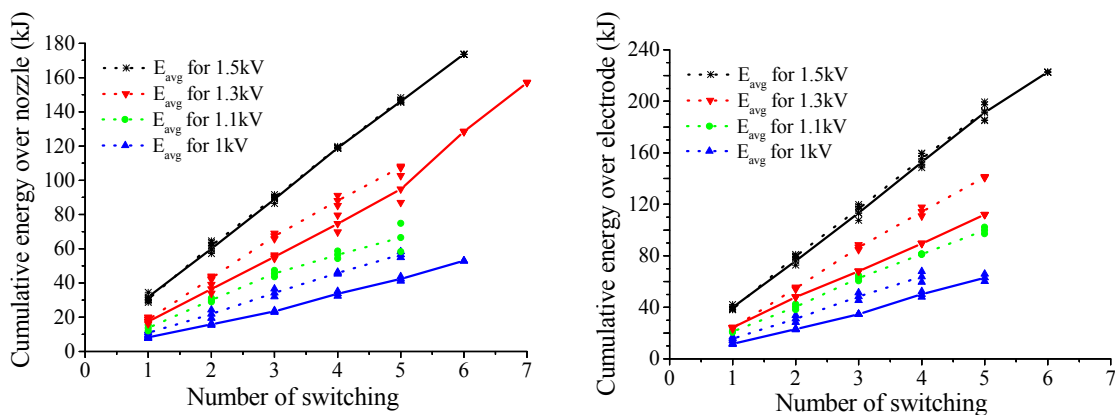


Figure 4.9: Cumulative energy over nozzle and over electrode for successive interruption

Because of the linear increase of the cumulative energy over the nozzles and the electrodes with respect to the number of interruptions, the linear regression curve

fitting, in term of $Y = A + BX$, could be suitably used to describe the relationship between the cumulative energy (Y) and the number of interruptions (X). The coefficient from curve fitting is shown in Appendix B, Table 2.

The average values of the charge ($\int i dt$) and the heat ($\int i^2 dt$) generated by an arcing current, calculated from equation 4.3 and 4.4, are listed in Appendix B, Table 3. They are nearly constant from the first to the fifth interruptions for a 8mm nozzle, while they increase gradually when using 5mm nozzle, especially with 1.3kV charging voltage, due to the increase in the current amplitude. Therefore, the relationship between the cumulative charge or heat (Y) and the number of current interruption (X) can be described by the linear regression curve fitting and by the polynomial regression curve fitting, in term of $Y = A + B_1X + B_2X^2$ as listed in Appendix B, Table 4.

The average values of the nozzle current density (A/mm^2) calculated from equation 4.5 are shown in Table 4.2. The current density of nozzle is nearly constant around the average value at each interruption for most of the test, except for that of a 5mm nozzle with 1.5kV charging voltage, which decreased steadily after each interruption. This is because the increasing current causes the larger nozzle diameter expansion after each interruption.

Charging Voltage	Current density [A/mm^2]	
	5mm	8mm
1kV	120	80
1.1kV		90
1.3kV	184	113.5
1.5kV	226	138

Table 4.2: Average values of the nozzle current density

For this variable high current test, the circuit breaker model can successfully interrupt the current up to four and six interruptions for 1.5kV and 1.3kV charging voltage with 5mm nozzle testing. For 1kV charging voltage, there was no sign of interruption failure for 5mm and 8mm nozzle. However, for 1.3kV and 1.5kV charging voltage with 8mm nozzle, the circuit breaker model failed to interrupt since the first interruption due to high stress for contact gap.

4.3 Circuit Breaker Model Degradation

The investigation on the degradation of a circuit breaker model due to the variation of the current amplitude is focused primarily on the electrode and the nozzle by measurement of its mass loss after each interruption, ablation factor, expansion of nozzle diameter D_{in} or D_1 , D_2 and D_{out} and nozzle geometry change. Subsequently, its degradation effects on pressure build-up reduction and gas flow characteristics are presented in this section.

4.3.1 Determination of Mass Loss and Ablation Factor

The average mass losses of the nozzles and the electrode after each interruption are summarized in Table 4.3. The current in a 8mm nozzle increases approximately 26% more than that in a 5mm nozzle, but it merely causes slightly increase in the mass loss of nozzles due to the less radiation flux density at the nozzle wall. This higher current causes more significant mass loss of the electrodes, which depends mainly on the current amplitude and the arcing time.

Charging Voltage	Mass loss of nozzle 1 [mg]		Mass loss of nozzle 2 [mg]		Mass loss of electrode 1 [mg]		Mass loss of electrode 2 [mg]	
	5mm	8mm	5mm	8mm	5mm	8mm	5mm	8mm
1kV	78.2	102.2	82.8	99.7	24.2	57.2	37	58.2
1.1kV		121.6		127.8		84.1		75
1.3kV	183.7	183	161.8	179.8	137.8	165.1	137.6	170.1
1.5kV	220.8	220.1	224.3	248	207.7	207.5	202	247.2

Table 4.3: The average mass loss of the nozzles and the electrodes after each interruption

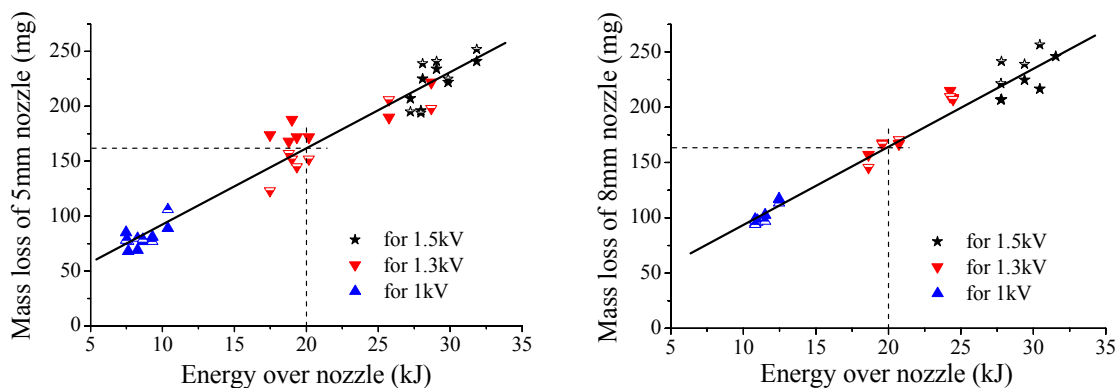


Figure 4.10: Relationship between mass loss of each nozzle and energy over nozzle pair

The mass losses of the nozzles or the electrodes depend primarily on the energy across them. Hence, this linear relationship under three different energy stresses is

presented in Figure 4.10 for nozzle and in Figure 4.11 for electrode. The symbol with fully filled colour represents for nozzle 1 or electrode 1, while the half-filled with white colour symbol represents for nozzle 2 or electrode 2. The average energy of each stress shown on the x-axis of Figure 4.10 and 4-11 is corresponding to Table 4.1. The ablation factor or mass loss per energy derived from both graphs, by assuming that a half of the energy is used to ablate each nozzle or electrode, are approximately 16mg/kJ for 5mm and 8mm nozzles, and 10mg/kJ and 10.8mg/kJ for electrodes when testing with 5mm and 8mm nozzle respectively.

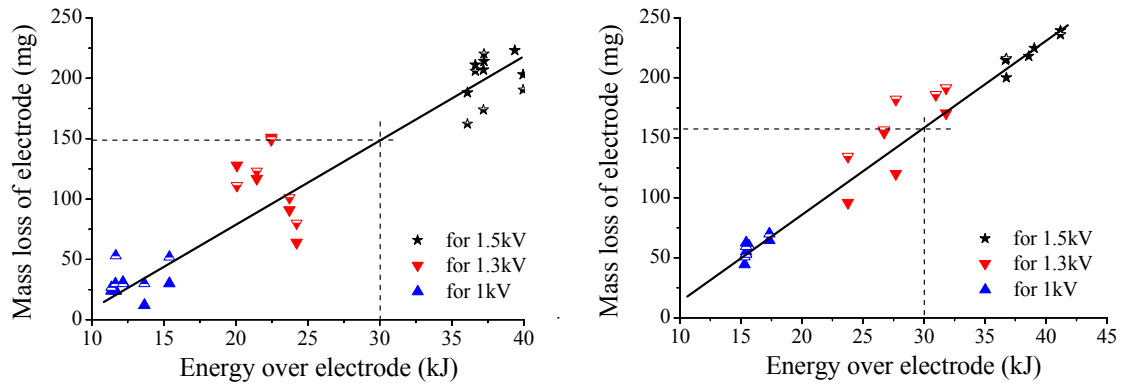


Figure 4.11: Relationship between mass loss of each electrode and energy over electrode (left) for 5mm nozzle and (right) for 8mm nozzle testing

The cumulative mass losses of 5mm and 8mm nozzle are plotted in Figure 4.12. Since the mass losses of nozzle are almost constant after each interruption, the linear regression curve fitting could be used to determine the relationship between cumulative mass losses of nozzle and number of interruption as shown in Appendix B, Table 5.

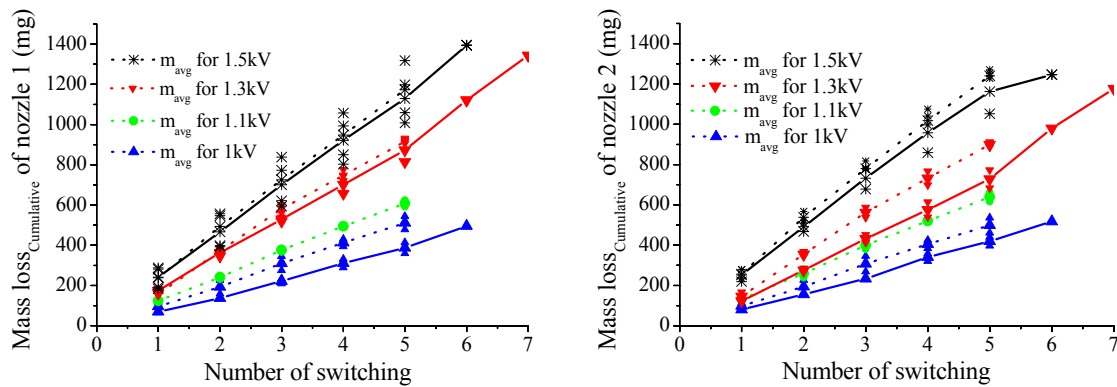


Figure 4.12: Cumulative mass loss of nozzles in function of number of switching

In Figure 4.13, the cumulative mass loss of nozzle in function of the cumulative energy over nozzle for 5mm nozzle is shown. Since the circuit breaker model can successfully interrupt the current up to six and four switching operations for 1.3kV and 1.5kV charging voltage respectively, then the limit of successful interruption can be drawn as shown and the expected number of allowable interruptions according to different stresses can be determined.

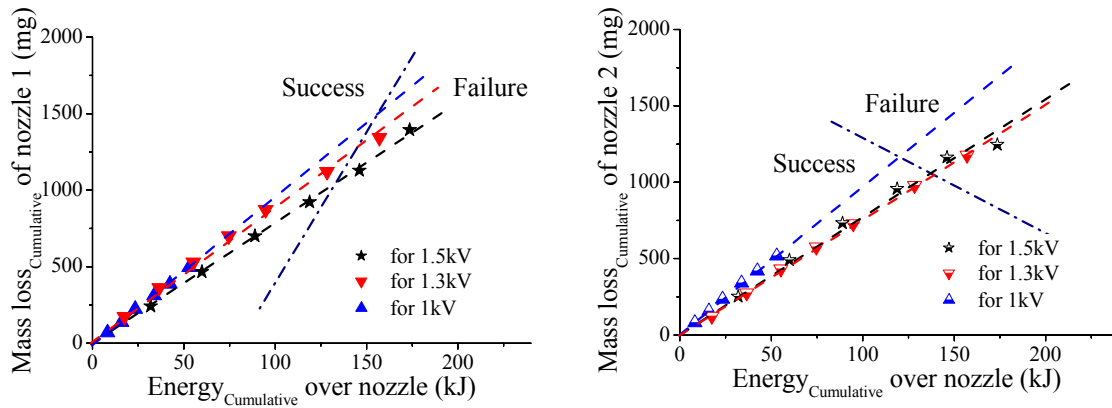


Figure 4.13: Relationship between cumulative mass losses of nozzle and cumulative energy over 5mm nozzle pair

The mean values of average ablation factor or mass loss per energy (mg/kJ) of nozzle and electrode calculated from equation 4.6 for each voltage stress are summarized in Table 4.4.

Charging Voltage	5mm nozzle [mg/kJ]		8mm nozzle [mg/kJ]		5mm nozzle [mg/kJ]		8mm nozzle [mg/kJ]	
	Nozzle1	Nozzle2	Nozzle1	Nozzle2	Electrode 1	Electrode 2	Electrode 1	Electrode 2
1kV	18.3	19.2	18	17.5	4	5.6	7.4	7.5
1.1kV			17	17.7			8.2	7.5
1.3kV	17.6	15.3	17	16.6	9.74	9.59	11.6	11.8
1.5kV	15.2	15.4	15	14.8	10.9	10.6	10.9	11.7

Table 4.4: Ablation factor of nozzle and electrode

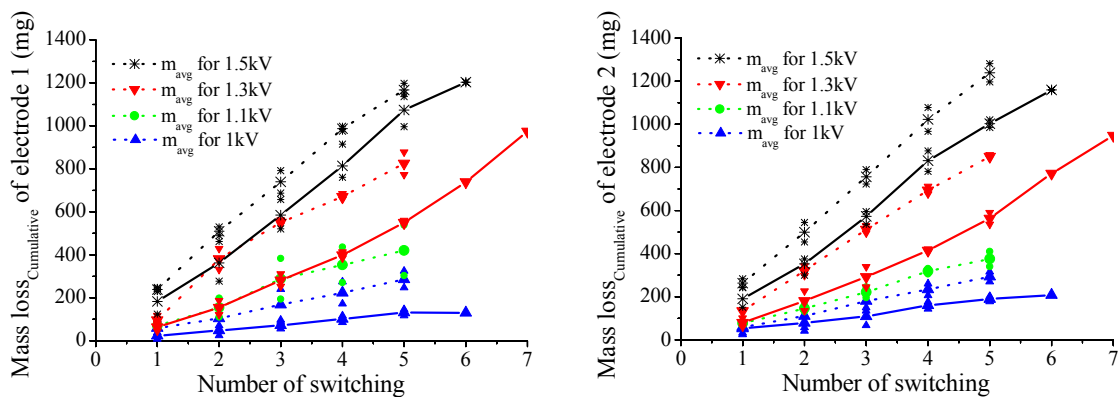


Figure 4.14: Cumulative mass loss of electrodes in function of number of switching

The cumulative mass losses of electrodes for 5mm and 8mm nozzle testing are presented in Figure 4.14. Because the mass losses of electrodes are almost constant after each interruption for most of the test, the linear regression curve fitting could be used to determine the relationship between the cumulative mass losses of

electrode and the number of interruption, except for 1.3kV charging voltage test with 5mm nozzle which required the polynomial regression curve fitting. The coefficients from curve fitting are shown in Appendix B, Table 6.

4.3.2 Determination of Nozzle Geometry Change

The relationship between expanded diameters, D_{in} or D_1 , D_2 and D_{out} according to Figure 4.5, for both 5mm and 8mm nozzles and number of current interruption are summarized in Appendix B, Table 7 and Table 8. Figure 4.15 is an example plot of measured inside diameters after each interruption of 5mm and 8mm nozzle respectively.

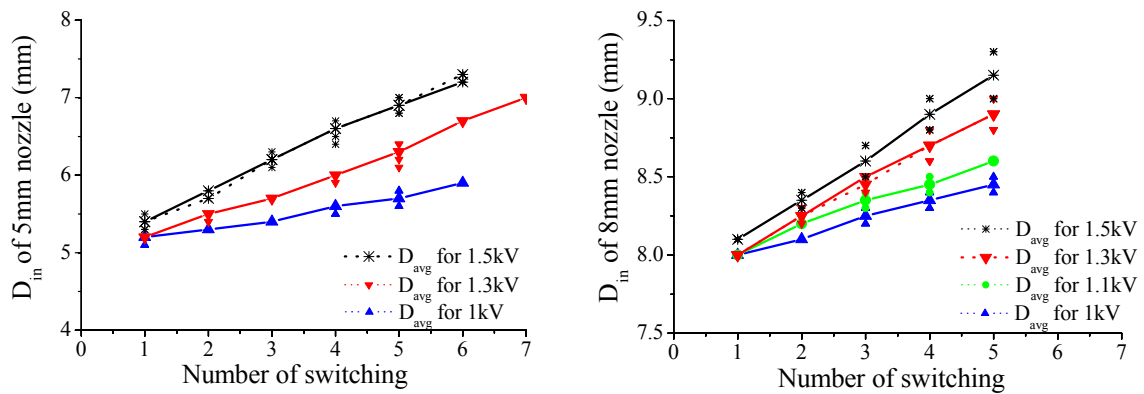


Figure 4.15: Inside diameter (D_1) of 5mm and 8mm nozzle after each current interruption (solid line for nozzle 1 and dot line for nozzle 2)

From Appendix B, Table 7 for a 5mm nozzle with 1kV charging voltage, the diameters of nozzle 1 and nozzle 2 increased 0.14mm equally along the cylindrical column after each interruption, without roundness in the focus area. In case of 1.3kV and 1.5kV charging voltage, the roundness at the nozzle edge occurred as indicated by unequally expanded diameters.

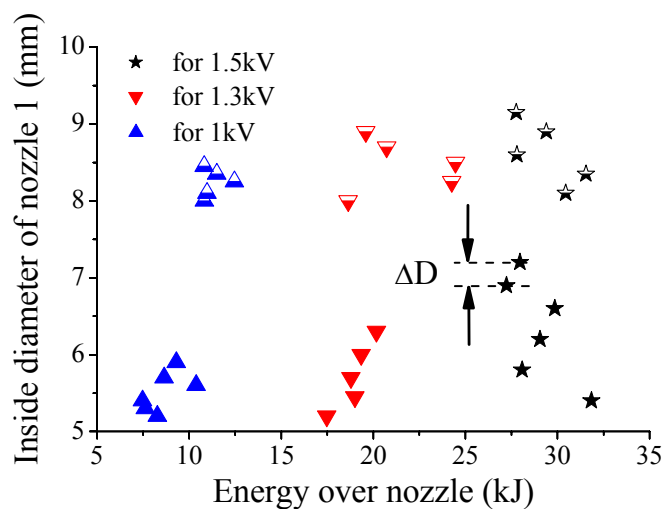


Figure 4.16: Relationship between inside diameter and energy over nozzle pair for 5mm and 8mm nozzle

In Appendix B, Table 8 for 8mm nozzle, the three measured diameters increased unequally due to the roundness around nozzle edge. The relationship between the nozzle diameter and the energy over nozzle pair of 5mm (fully filled symbols) and 8mm nozzle (half-filled with white symbols) is partly shown in Figure 4.16 only for inside diameter. The increment of the nozzle diameters (ΔD) per energy over nozzle pair in mm/kJ increased steadily for most cases, except for testing of a 5mm nozzle with 1kV charging voltage having constant increment per energy.

The geometry changes along a 5mm nozzle bore after 5 interruptions is shown below and compared with that before testing. The roughness of the surface due to ablated mass caused by arc heating and the enlarged diameter together with the roundness around nozzle edge can be clearly seen.

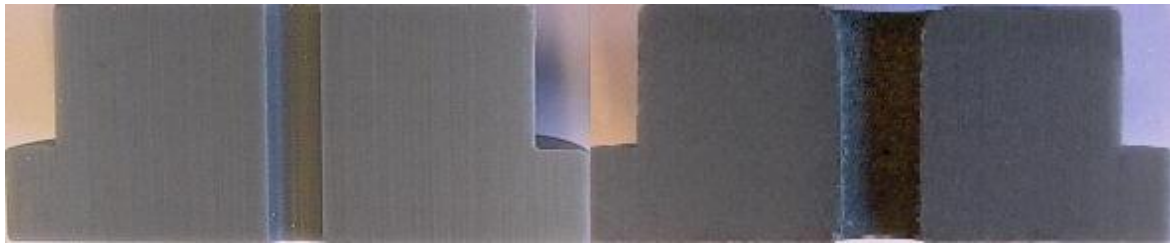


Figure 4.17: Cross section of 5mm nozzle before testing (left) and after 5 interruptions (right)

The exact changes in nozzle contour obtained from the Digitizer software are presented in Figure 4.18 (left) for a 5mm nozzle after five and six interruptions and in Figure 4.18 (right) for 8mm nozzle after five interruptions under variable voltage stresses. For 5mm nozzle, the cross symbols represented the geometry before test. After current interruptions the rounded nozzle edge between the arcing column and the expansion chamber, which is on the top of the picture, and the enlarged diameter along nozzle bore could be seen. Furthermore by comparing the geometry after five and six interruptions, the change of nozzle geometry caused by one interruption can be seen. In case of 8mm nozzle, the higher stress also caused more rounded edge and enlarged diameter. With this method, the nozzle geometry changes, especially in the focus area, can be exactly determined.

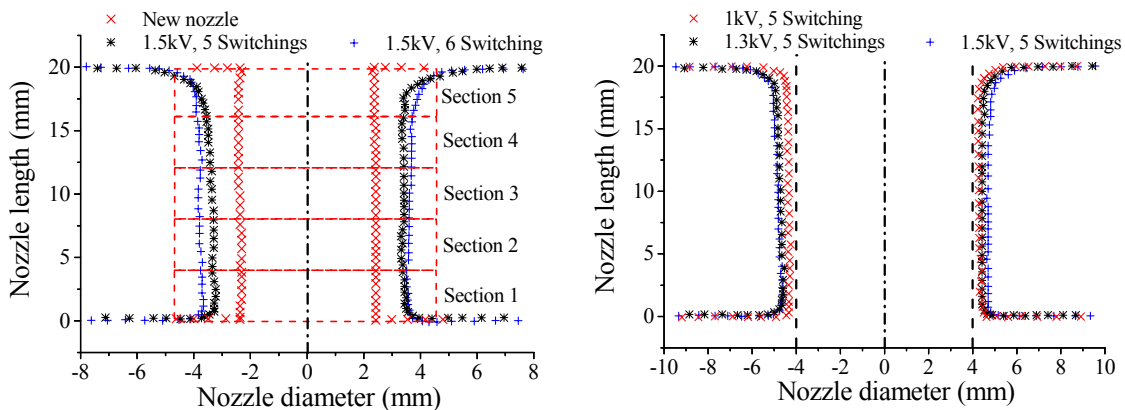


Figure 4.18: Changes in nozzle contour after current interruption for 5mm (left) and 8mm nozzle (right)

After the determination of nozzle geometry, the volume loss and mass loss could be defined according to equation 4.7 and 4.8. The mass loss determined by this method agrees well with the result from measurement as shown in Table 4.5.

Test condition	Volume loss [mm ³]	Calculated mass loss [mg]	Measured mass loss [mg]
5mm, 1.5kV stress, 5 interruptions	461	1017	1052
5mm, 1.5kV stress, 6 interruptions	651	1431	1398
8mm, 1kV stress, 5 interruptions	257	564	536
8mm, 1.3kV stress, 5 interruptions	474	986	924
8mm, 1.5kV stress, 5 interruptions	572	1246	1252

Table 4.5: Volume loss and mass loss of nozzle derived from geometry change

From Figure 4.18 (left) the nozzle was divided along its length into 5 sections with 4mm long in each section. Section 1 was the lowest part, where the hot gas flows out to the surrounding space, while section 5 was located on the top, where the influence of a gas flow between the arcing column and the expansion chamber dominated. The mass loss of each section was calculated from the obtained geometry under various conditions and shown in Figure 4.19.

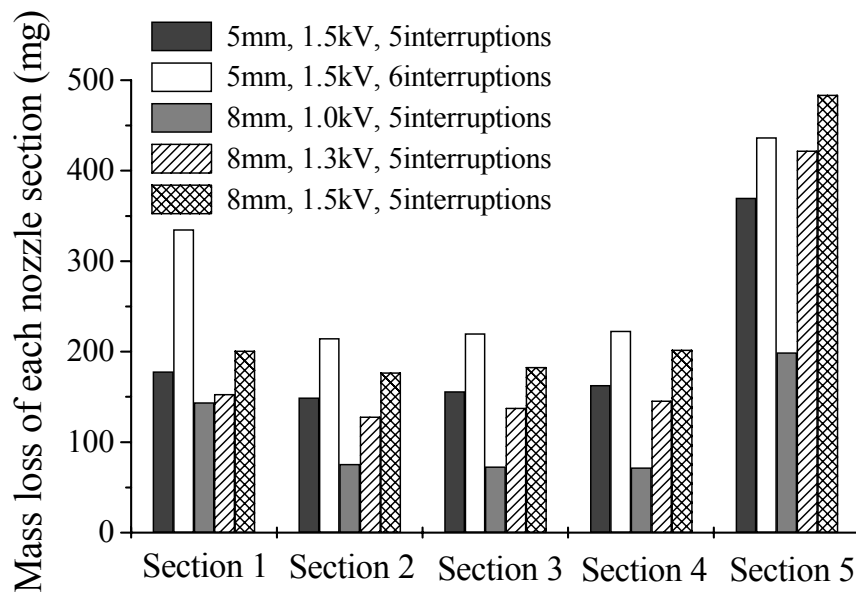


Figure 4-19: Mass loss of each nozzle section under variable test conditions

For a 5mm nozzle after 5 and 6 switching tests with 1.5kV stress the mass loss in section 2, 3 and 4 were nearly equal and had the lowest value at approximately 15%, while section 5 and section 1 had the higher mass loss approximately 30% and 20% respectively. The percentage of ablated mass in section 1 increased for the sixth interruption because the larger nozzle cross-section allows more hot gas to flow out, which causes the higher percent of ablation in section 1.

In case of a 8mm nozzle after 5 switching tests with variable voltage stress the lowest ablated mass also occurred in section 2, 3 and 4 respectively, while the majority of ablated mass approximately 40% took place in section 5 for 1.3kV and 1.5kV stresses. The percentage of ablated mass in section 1 was of greater extent when testing with 1kV stress owing to less clogging effect and more out-flow gas.

The ablated mass loss of each nozzle section and its percentage under various test conditions are summarized again in Table 4.6.

Test condition	Mass loss of each nozzle section									
	Section 1		Section 2		Section 3		Section 4		Section 5	
	[mg]	[%]	[mg]	[%]	[mg]	[%]	[mg]	[%]	[mg]	[%]
5mm, 1.5kV, 5 interruptions	178	17.5	149	14.7	156	15.4	163	16.0	370	36.4
5mm, 1.5kV, 6 interruptions	335	23.4	215	15.1	220	15.4	223	15.6	437	30.6
8mm, 1kV, 5 interruptions	144	25.6	76	13.4	73	13.0	72	12.8	199	35.2
8mm, 1.3kV, 5 interruptions	153	15.5	128	13.0	138	14.0	146	14.8	422	42.8
8mm, 1.5kV, 5 interruptions	201	16.1	177	14.2	183	14.7	202	16.2	484	38.8

Table 4.6: Mass loss of each nozzle section and its percentage under variable test conditions

4.3.3 Influence of Nozzle Widening on the Pressure Build-up and Gas Flow

To compare the pressure of each interruption, the pressure build-up should be normalized by the peak current because the current increases steadily after each successive interruption due to nozzle expansion. Hence, the reduction of normalized pressure waveforms after each interruption could be seen in Figure 4.20 for a 5mm nozzle testing with 1.5kV charging voltage.

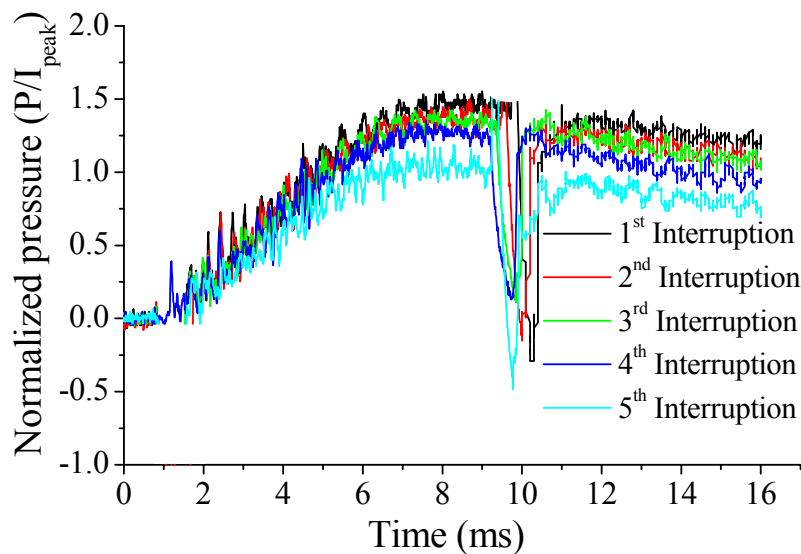


Figure 4.20: Plot of normalized pressure waveform at each interruption

The relationship between the normalized P_{\max} , $P_{\text{at } I_{\max}}$ or P_1 , and $P_{\text{current zero}}$ or P_2 and the number of interruption for 5mm nozzle test is shown in Figure 4.21. Those three normalized pressures were nearly constant at each interruption for most cases, except for P_{\max} and P_2 of 1.5kV charging voltage test, which decreased steadily after each interruption. In 1.3kV charging voltage test, the three normalized pressures also decreased after the fifth interruption and later on the interruption failure occurred at the seventh interruption. This result agrees well with [Kno95] that the number of interruptions influences the drop in pressure and interruption performance due to a slight geometry change of the nozzles from test to test.

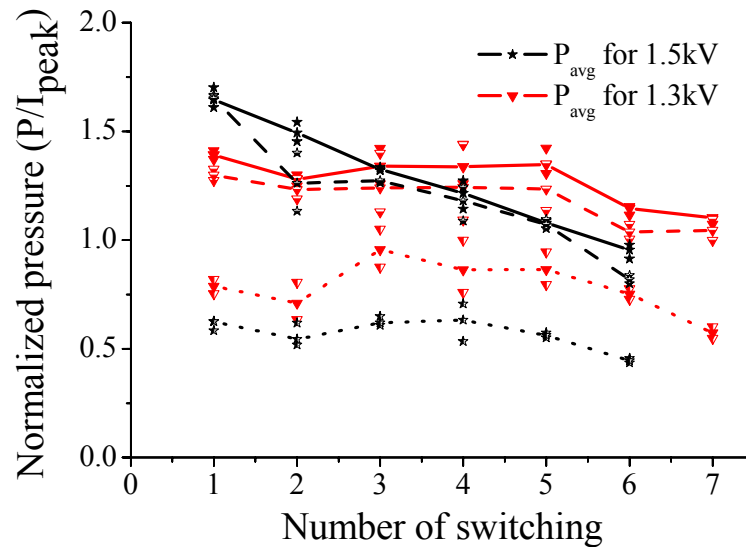


Figure 4.21: Pressure values of each interruption (solid line for P_{\max} , dot line for $P_{\text{at } I_{\max}}$ and dash line for $P_{\text{current zero}}$)

In Figure 4.22 (left), the relationship between P_{\max} and I_{peak} is shown for 5mm (fully filled symbol) and 8mm nozzle (half-filled with white symbol). The interruption failure is on the right hand side of the separating line because of insufficient pressure build-up. For successful interruption, the higher-pressure build-up at each current could be clearly seen. In Figure 4.22 (right), the linear relationship between the normalized P_{\max} and the current density is determined.

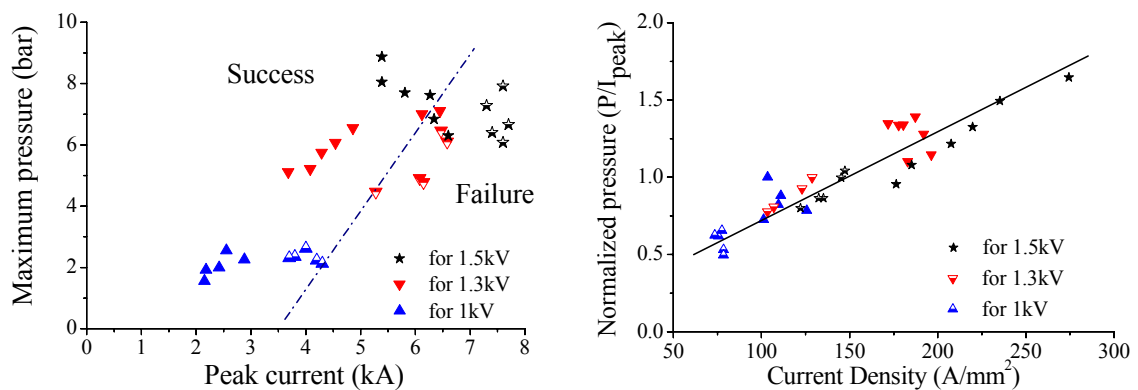


Figure 4.22: Relationship of maximum pressure to peak current and current density for 5mm and 8mm nozzle

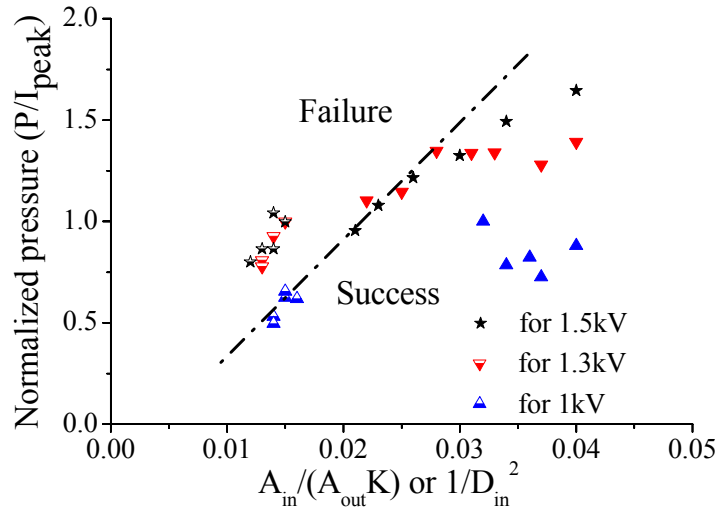


Figure 4.23: Relationship between normalized pressure and area ratio

The influence of the nozzle widening on the switching performance is defined in term of the reduction of the normalized maximum pressure as shown in Figure 4.23. The change in nozzle diameters due to current interruption causes the large gas escaping area (A_{out}). Thus, after each current interruption, each point moves to the left. In case of a 5mm nozzle (fully filled symbol) with 1.5kV charging voltage, the significant reduction in the normalized pressure (P_{max}) and the large increase of the gas escaping area can be determined. In case of 1.3kV, there is no reduction of the normalized pressure up to the fifth interruption and the smaller increase of the gas escaping area compared with the 1.5kV case. For 1kV test, the normalized pressure is nearly constant with the smaller increase of the escaping area. In case of the 8mm nozzle testings, only the relatively small increase of A_{out} occurs due to the less radiation flux density on the nozzle wall, whereas the larger A_{out} causes the lower and insufficient normalized pressure, which leads to the thermal failure.

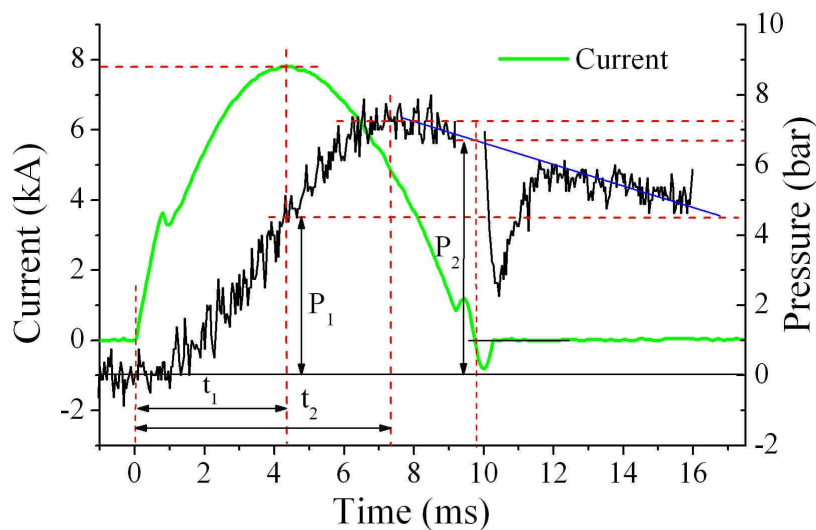


Figure 4.24: Time to maximum current, time to maximum pressure and three measured pressures

The influence of the change in nozzle contour on the gas flow can be realized from the pressure waveform as shown in Figure 4.24. The time to maximum current or t_1 and the time to maximum pressure or t_2 and the delay time between the maximum current and the maximum pressure ($t_2 - t_1$) are listed in Appendix B, Table 9.

The faster time needed for maximum pressure build-up for each successive interruption can be determined because the roundness at the nozzle edge facilitates the flow of hot gas into the expansion chamber. Furthermore, the increase in a volume along the nozzle column owing to nozzle widening leads to the reduction of pressure in that area as well as the larger escaping area, which results in the faster gas back-flow from the expansion chamber. Even though, an empirical understanding of the impact from nozzle widening on the switching performance based on the pressure change is determined, the exact detail of gas flow pattern, the shape of the arc, the temperature and conductivity of the hot gas need further investigations to determine the interrupting limit

4.4 Impact from the Other Parameters on the Degradation

The main investigation on the influence of current amplitude on the electrical degradation was carried out in the last section. However, from the test setup it is possible to vary some impact parameters. Therefore, the further investigations on the influence of the expansion volume, recovery voltage and arcing time on the degradation is performed in this section. The reference test has the following test condition; 1.5kV and 23kV charging voltage on the high current and high voltage circuits; 5bar filling pressure, 1l expansion chamber and one ignition wire.

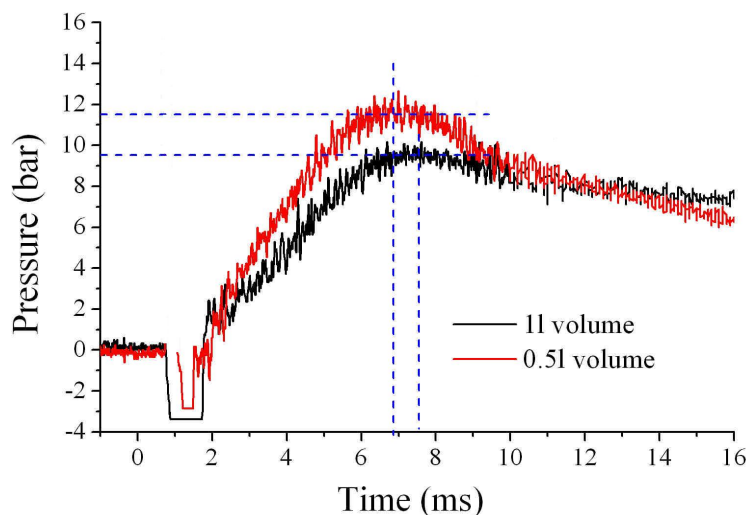


Figure 4.25: Comparison of measured pressure in 1l and 0.5l expansion volume

The reduction of an expansion volume to 0.5l caused the pressure to increase 25% from the mean value measured with 1l volume. The measured pressure waveforms are compared in Figure 4.25, from which it shows that the pressure inside 0.5l volume has the higher pressure gradient for both rising and falling of pressure, which corresponds to the result from [Wen93]. The mean value of the time to the first current zero was changed from approximately 9.6ms in the 1l volume test to 9.29ms due to the faster gas back-flow. Hence, the larger expansion volume would cause the insufficient pressure built-up generated by the arc heating. While the smaller volume would result in a too high gas temperature and an insufficient gas flow duration to cover a half cycle arcing period, which reduces the breaking capability. Therefore, the size and geometry of the expansion volume have a significant effect on the gas pressure built-up and the average gas temperature. The suitable shape ensures the desired gas temperature for back-flow when reaching the arc extinction area. Due to the faster cooling of back-flow gas, the mass loss of nozzle 1 and nozzle 2 decreases 9% and 12.5% respectively. The mass loss of electrode 1 and electrode 2 is reduced 7% and 16% respectively.

By increasing the charging voltage on the high voltage circuit from 23kV to 33kV, this voltage stress is higher than the withstand capability of a contact gap. Thus, it shows an interruption failure since the first interruption with 9 current zero crossing. This higher voltage stress during recovery period causes the mass loss of

5mm nozzle 1 and nozzle 2 to increase 6% and 3.6% respectively, whereas the mass loss of both electrodes increases 4%.

By using two ignition wires, the 0.50ms shorter arcing time is obtained. The mass losses of nozzle 1 and nozzle 2 were reduced 14.5% and 15.2% for 5mm nozzle testing, and 15.7% and 11% for 8mm nozzle testing. The mass losses of both electrodes were significantly reduced around 35% for both 5mm and 8mm nozzle testing.

The ablation factors under variable test conditions are shown in Table 4.7 for the nozzles and in Table 4.8 and for the electrodes. The ablation factor of a 5mm nozzle is nearly constant around 15mg/kJ for every test condition, but for a 8mm nozzle there is less ablation factor in case of using two ignition wires (shorter arcing time) and using 0.5l expansion volume (faster gas back-flow). The less ablation factor of a 8mm nozzle than that of a 5mm nozzle results from the more hot gas flowing out through the larger escaping area. The ablation factor of the electrodes decreases significantly due to the shorter arcing time.

Test conditions	Ablation factor of nozzle [mg/kJ]			
	5mm nozzle		8mm nozzle	
	Nozzle 1	Nozzle 2	Nozzle 1	Nozzle 2
Reference test	15.2	15.4	15	14.9
Two ignition wires	15	15	12.8	12.7
33kV on HV circuit	14.8	14.9	-	-
0.5L Expansion volume	-	-	13.5	12.9

Table 4.7: Ablation factor of 5mm and 8mm nozzles under variable test conditions

Test conditions	Ablation factor of electrode [mg/kJ]			
	5mm nozzle		8mm nozzle	
	Electrode 1	Electrode 2	Electrode 1	Electrode 2
Reference test	10.9	10.6	10.9	11.7
Two ignition wires	7.5	7.7	6.7	8.5
33kV on HV circuit	10.6	10.3	-	-
0.5L Expansion volume	-	-	10.7	10.4

Table 4.8: Ablation factor of electrodes for 5mm and 8mm nozzles testing under variable conditions

The mean values of the expanded diameters, D_{in} , D_2 and D_{out} , under various test condition are listed in Appendix B, Table 10 and Table 11 for testing with 5mm

nozzle and 8mm nozzle. When compared with the reference test, the shorter arcing time causing less ablation results in the smaller increase in the nozzle diameters, while in case of using 33kV voltage stress caused the larger increase in the nozzle diameters owing to more mass loss during recovery period.

The mean value of the measured pressures at a current maximum (P_1) and pressure at the first current zero (P_2) for both 5mm and 8mm nozzles under variable test conditions are summarized in Table 4.9. Since some energy of the arc is needed to melt the additional wire, the pressure P_1 and P_2 are lower in case of using two ignition wires in 5mm nozzle testing due to the lower in current amplitude leading to less radiation heat. However, in a 8mm nozzle the current is relatively high and the energy needed to melt the wires is only a small portion the total arcing energy. Thus, only a slightly decrease in P_2 can be observed. These pressures are higher when using 0.5l expansion volume. The time to maximum pressure, t_2 in Figure 4.24, for the test with 0.5l expansion volume is 6.9ms, which is faster than the reference test (7.5ms) due to the higher pressure gradient.

Test conditions	Measured pressure at current maximum (P_1) and pressure at first current zero (P_2)			
	5mm nozzle		8mm nozzle	
	P_1	P_2	P_1	P_2
Reference test	3.4	7.1	3.9	6.4
Two ignition wires	2.9	6.5	3.9	6.2
33kV on HV circuit	3.4	7.0	-	-
0.5L Expansion volume	-	-	6.3	7.8

Table 4.9: Measured pressure under variable test conditions for both 5mm and 8mm nozzles

4.5 Summary and Outlook

In this chapter the investigation on the electrical degradation is performed with the variation of the current amplitude as a primary concern. The degradation is determined in term of the mass loss of the nozzles and the electrodes, geometry change of nozzle and its impact on the pressure build-up and gas flow. After that some parameters, which also have an impact on the degradation, are investigated in the same way, such as the arcing time, expansion volume and the recovery voltage.

Because of the simple configuration of the test setup, it is difficult to use this result with the real circuit breaker. However, the result from this investigation can be used to verify the arc model, ablation model of the nozzle and the electrode, and the results from CFD simulation performed at The Institute for High Voltage Technology, RWTH-Aachen University. The measured current, nozzle radius and its length, filling pressure and ablation factors are used as the input parameters for the simulation. The simulation results, which are the arcing voltage, pressure at the monitored point, the increased nozzle radius and the total mass loss of the nozzles and the electrodes, can be compared with the experimental result to verify the accuracy of the simulation tools.

The determination of the geometry change of nozzle and the mass loss in each nozzle section along the column in section 4.3.2 also provide the more accurate comparison with the locally ablated mass result from the incorporated ablation model, which considers the divergence of radiation flux density on the nozzle wall together with the vaporization enthalpy, the sublimation energy etc. By using the simulation as a tool to predict the electrical degradation, the number of expensive and time-consuming power tests can be reduced. The integration into the circuit breaker performance evaluation scheme is shown in Figure 4.26.

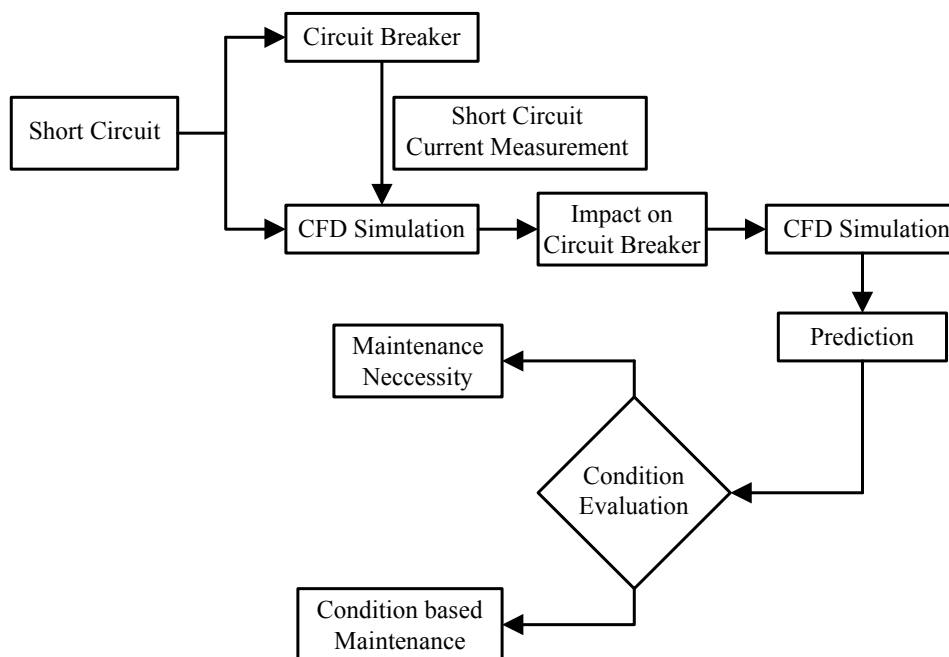


Figure 4.26: Overview of circuit breaker condition evaluation process

5 Withstand Capability of Circuit Breaker Model to Breaking Current

Because circuit breakers have to interrupt fault current repeatedly during their service life, their degradation occurs due to thermal and mechanical stresses on the interrupter parts, which are primarily nozzle and the arcing contact. Therefore, the electrical endurance, the extent to which the circuit breaker can cope with this electrical arcing stress [Sme05], should be concerned. Test programs, as in IEC technical report (TR) 62271-310, or new approaches, as proposed to TF A3.01 by [Sme05], are needed to express the equivalent degradation caused by interrupting a number of fault currents with distributed magnitude during a given time of 25 years, a period without interrupter chamber maintenance, in a smaller number of larger current test series in laboratory. To derive a representative test program, the comprehensive information is needed, such as fault and system parameter statistics, an estimate of the actual fault current etc. However, the complete information is hardly to obtain. From [Sme05] the number of fault current interruptions at rated short circuit breaking current, which is equivalent to electrical arcing stress in a 25-year period for 110-220kV circuit breakers, is around 4.4 times. This number is approximately half of the recommended test number proposed in IEC TR 62271-310.

To judge the electrical endurance of a circuit breaker, the accumulative wear of nozzle or electrode is employed as a criterion. According to the experiment, the permitted total electrical erosion is generally defined by two parameters: the rated short circuit current ($I_{SC(max)}$) and the permitted number of interruption at rated short circuit current ($N_{allow(max)}$). This permitted erosion will be further used to derive the allowable number of interruption at any breaking current. The degradation or relative electrical erosion corresponding to any breaking current is the inverse relationship of the allowable number of interruptions.

5.1 Method to Determine the Allowable Number of Interruptions and the Remaining Lifetime of Circuit Breaker

Generally, the electrical erosion depends on various parameters and the other random factors [Wal92] as shown in Figure 5.1. With the limited present knowledge and a mix of varying parameters during operation in service it is, therefore, difficult to apply theoretical considerations regarding nozzle and contact ablation to estimate the lifetime of circuit breakers. Thus, the experimental study [Fuj98] is of practical importance to obtain the erosion characteristics. In this work, the methods to estimate the remaining lifetime of a circuit breaker based on the interrupting current magnitude are presented. Furthermore, the test data have been processed to see some dependencies of nozzle and contact mass losses on the interrupting current in term of $\int i dt$ and $\int i^2 dt$.

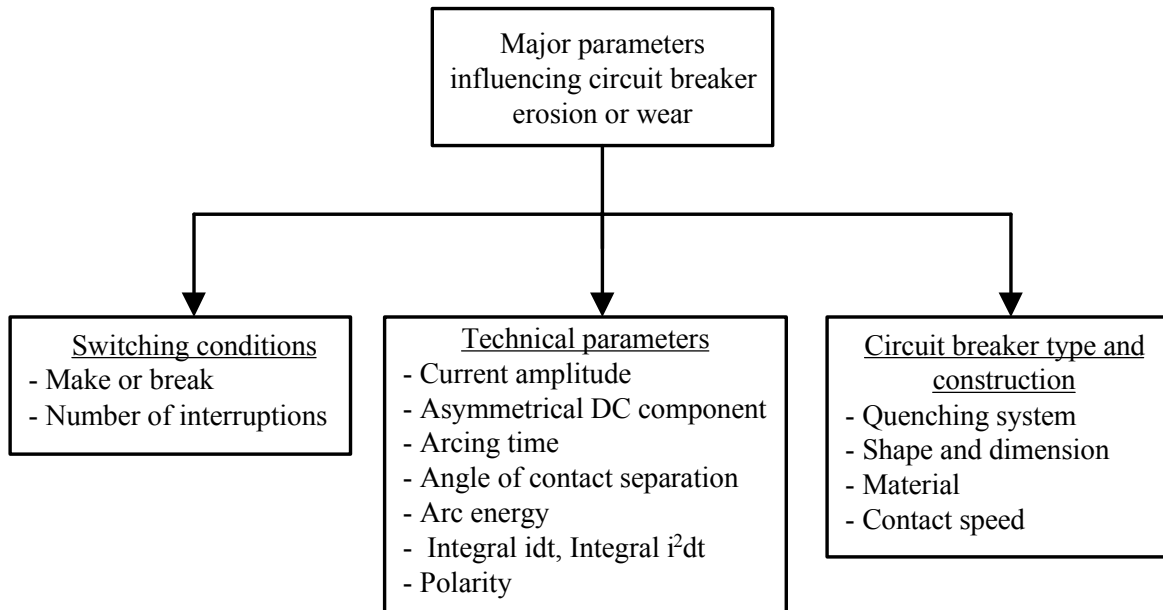


Figure 5.1: Major parameters influencing circuit breaker erosion or wear

5.1.1 Interrupting Current Consideration

Simplified linear extrapolation

Usually, current interruptions take place at different current ratings. Therefore, in order to estimate the interruption life the lower current interruptions are simply extrapolated into full rating [Sto00] as shown in Table 5.1.

Percentage of rated fault current	Number of interruptions	Equivalent interruptions at 100% fault current
100%	1	1
75%	1	0.75
50%	2	1
25%	2	0.5
Total	6	3.25

Table 5.1: Linear extrapolation to equivalent interruptions at 100% fault current [Sto00]

When the allowable number of interruptions at any percentage of rated short-circuit current is known, the remaining lifetime can be determined. Equation 5.1 is written by assuming that the allowable number of interruptions at 100% rated short-circuit current is known.

$$\text{Remaining lifetime (\%)} = \left[1 - \sum_{i=1}^n \frac{N_i I_{SCi}}{N_{allow(max)} I_{SC(max)}} \right] \times 100 \quad (5.1)$$

where I_{SCi} is any interrupted current

N_i is the number of interruptions at current I_{SCi}

$I_{SC(max)}$ is rated short-circuit current

$N_{allow(max)}$ is the allowable number of interruption at $I_{SC(max)}$

Exponential decay function

The allowable number of breaking operations ($N_{allow(i)}$) as a function of any breaking current for an SF₆ circuit breaker is usually provided by the manufacturer or can be obtained from electrical endurance test by a series of test with different breaking currents. The allowable number of breaking operations at any breaking current (I_{SCi}) is usually described by an exponential decay function [Pon93], [Fuj98], [Bec01] as

$$N_{allow(i)} = a \left(\frac{I_{SCi}}{I_{SC(max)}} \right)^{-b} \quad (5.2)$$

where a and b are constant depending on circuit breaker type

Then, the remaining lifetime can be written as

$$\text{Remaining lifetime (\%)} = \left[1 - \frac{1}{a} \sum_{i=1}^n N_i \left(\frac{I_{SCi}}{I_{SC(max)}} \right)^b \right] \times 100 \quad (5.3)$$

Comparison of both methods

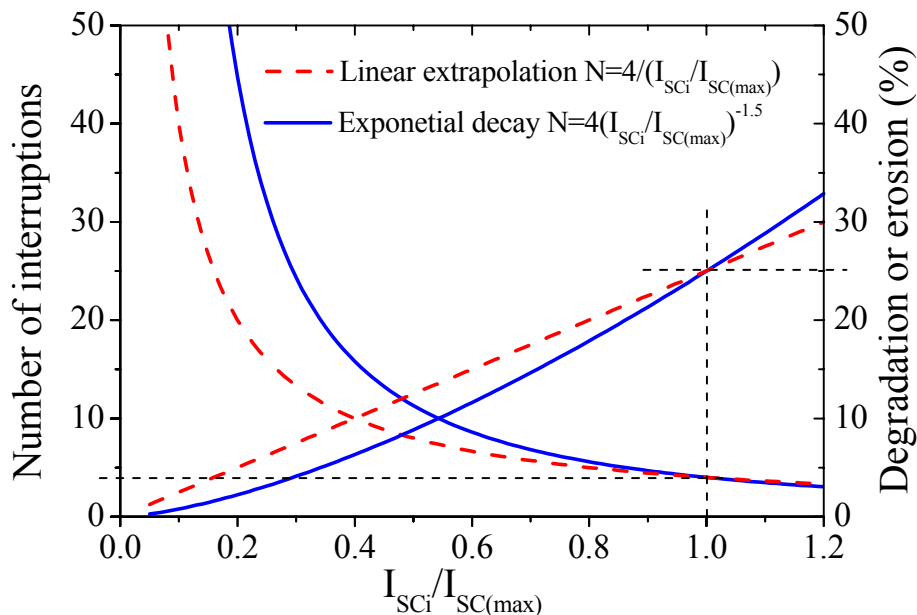


Figure 5.2: Allowable number of interruptions and degradation caused by single interruption as a function of breaking current ratio

Figure 5.2 shows the comparison of both methods by assuming that the circuit breaker can interrupt up to four times at its 100% rated short-circuit current. This

means that for one interruption at rated short-circuit current causes 25% degradation or equivalent erosion. By exponential decay function assuming that a and b parameters are 4 and 1.5 respectively, the approximation result is more reasonable than that by linear extrapolation because the degradation or erosion caused by smaller current is lower, which results in larger number of allowable interruptions. For example, if the mentioned circuit breaker interrupted the current as stated in two columns on the left of Table 5.2, its remaining lifetime determined from equation 5.3 by exponential decay method is 52.8%, which is higher than 25% remaining lifetime by using equation 5.1 for linear extrapolation.

Percentage of I_f/I_{SC}	Number of Interruption	Linear extrapolation		Exponential decay	
		Equivalent to 100% fault current interruption	Relative erosion (%)	Allowable number of interruption	Relative erosion (%)
10	5	0.5	12.5	126	4.0
25	3	0.75	18.8	32	9.4
50	2	1	25.0	11	17.7
75	1	0.75	18.8	6	16.2
Total		3	75.0		47.2
Remaining lifetime (%)			25.0		52.8

Table 5.2: Comparison of relative erosion and remaining lifetime calculated by both methods

During recording of the interrupted current, the problem of current transformer's saturation exists, which depends on the magnitude of the short-circuit current. This results in the distortion of recorded secondary current waveform. The reconstruction of distorted secondary current, which should be comparable with the undistorted primary current, is necessary in order to obtain the reasonable data for evaluation.

5.1.2 $\int i dt$ and $\int i^2 dt$ Consideration

The general expression of $\int i dt$ for a sinusoidal current can be written as

$$\int i(t) dt = \int_{t_s}^{t_s+t_a} \hat{I} \sin(\omega t) = \frac{\hat{I}}{\omega} [\cos(\omega t_s) - \cos(\omega(t_s + t_a))] \quad (5.4)$$

where t_s is the time at moment of contact separation
 t_a is the arcing time

Owing to the ablation-controlled arc in narrow cylindrical nozzle and small frequency deviation (53Hz), the $\int i dt$ of a positive half-wave sinusoidal current supplied from synthetic test circuit was deviated from the theoretical 50Hz current, represented as straight line in Figure 5.3 (left). This deviation was large for 5mm nozzle as well as for current less than 5kA, but the linear relationship between current and $\int i dt$ could be determined, which could be written according to equation

5.4 for theoretical 50Hz current as $\int i dt [As] = 6.3662 \times I_{peak} [A]$. Since the investigated mass losses of nozzle and electrode show a linear dependence on the interrupting current as shown in Figure 5.3 (right), only the scale of the x-axis changes when considering mass losses of nozzle and electrode in function of $\int i dt$.

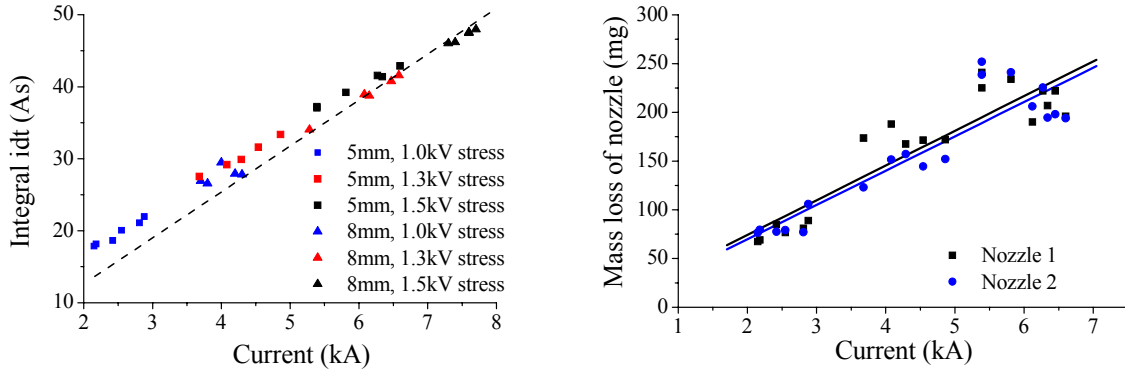


Figure 5.3: Comparison of measured $\int i dt$ to theoretical 50Hz current (left) and the relationship between mass loss of nozzle and interrupting current (right)

Since a positive half-wave sinusoidal current was used throughout the experiment, this made it difficult to analyse the influence of arcing time on the mass loss of nozzle and electrode. However by using two ignition wires connected in parallel between electrodes, the time, at the moment that the arc started to burn, is delayed. This results in shorter arcing time as well as slightly lower current magnitude due to more energy needed to burn the wires. The smaller mass loss of nozzle and electrode is, therefore, expected in case of using two wires test, if the linear relationship is still applicable. The linear relationship between mass loss and $\int i dt$ from two-ignition wires test is shown and compared with the reference test in Figure 5.4. The equal amount of $\int i dt$ from both test conditions caused nearly the same ablated mass of nozzle and electrode. Small discrepancy in electrode mass losses maybe caused by small inaccuracy during test, such as electrode distance, wires attachment position etc.

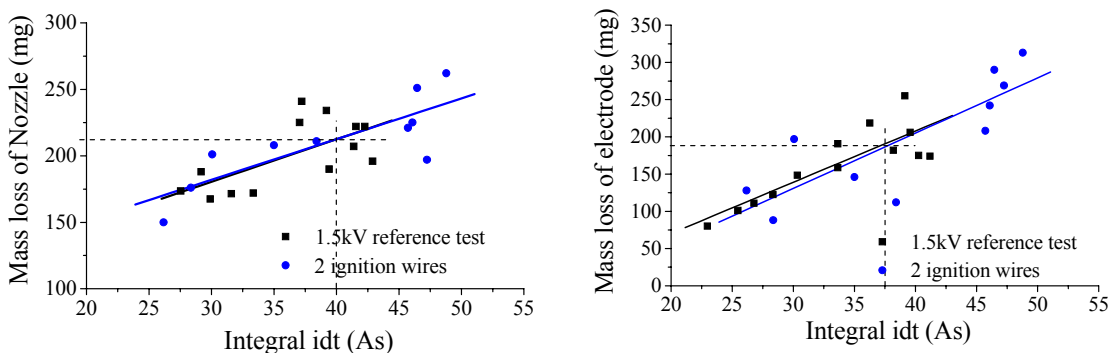


Figure 5.4: Mass loss in function of $\int i dt$ for testing with and without delay ignition time, (left) for nozzle and (right) for electrode

Because of this linear relationship, the mass loss Δm per ampere-seconds of the arc is defined as

$$M' = \frac{\Delta m}{q(t)} \tag{5.5}$$

From Figure 5.4, the nozzle ablation is 5.3mg/As and the contact erosion is 5.06mg/As. Thus, only the measurement of the short circuit current and time can be derived to find the mass loss of the nozzles and the electrodes.

For $\int i^2 dt$ consideration the deviation of measurement result from theoretical 50Hz sinusoidal current, presented by solid line, also exists, but the relationship between $\int i^2 dt$ and interrupting current is a parabolic function as shown in Figure 5.5.

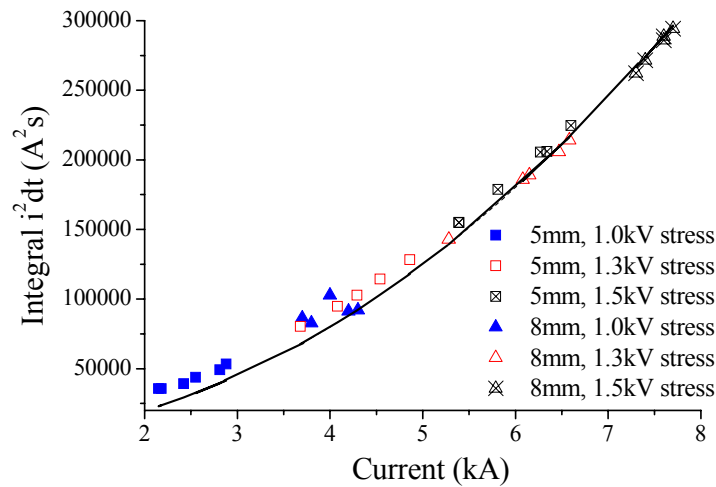


Figure 5.5: Comparison of $\int i^2 dt$ to theoretical 50Hz current

The measured mass loss of nozzle and electrode in function of $\int i^2 dt$ is presented in Figure 5.6. Like $\int i dt$ consideration the mass loss of nozzle 1 is larger than that of nozzle 2, whereas the mass loss of electrode 1 (cathode) is higher than that of electrode 2 (anode) only for $\int i^2 dt$ larger than 130000A²s.

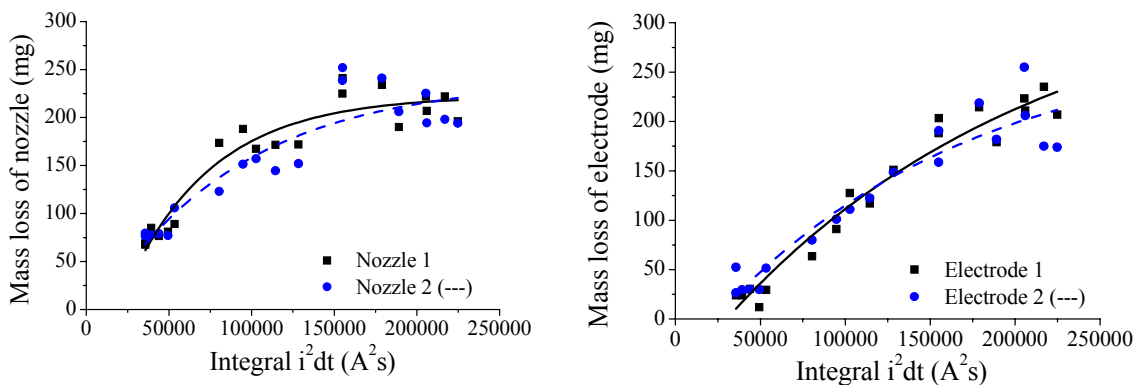


Figure 5.6: Mass loss of nozzle and electrode in function of $\int i^2 dt$

The relationship between measured mass loss (y) and $\int i^2 dt$ (x), as shown in Figure 5.6, can be mathematically expressed by using a first order exponential decay function as

$$y = y_0 + Ae^{-(x-x_0)/t} \quad (5.6)$$

The parameters from a first order exponential decay curve fitting for nozzles and electrodes are summarized in Table 5.3.

	Y offset (y_0)	Exponential amplitude (A)	X offset (X_0)	Decay constant (t)
Nozzle 1	222.68	-161.1	35671	52514.7
Nozzle 2	239.54	-171.41	35671	86206.9
Electrode 1	353.12	-342.57	35671	184563.5
Electrode 2	287.36	-263.49	35671	151475.2

Table 5.3: Curve fitting parameters for nozzles and electrodes

Because the non-linear relationship between the mass loss and $\int i^2 dt$, the $\int i dt$ method is preferred. However, this method is only applicable for a circuit breaker model. For the real circuit breaker the data during development and type test should reveal the linear relationship between the mass losses and $\int i^x dt$.

5.2 Result from Measurement with Circuit Breaker Model

From the measurement, the result of 5mm nozzle testing showed that the thermal failure occurred after the fourth interruption with 1.5kV charging voltage, which was the highest stress used in the tests. In order to find the number of interruption that the circuit breaker model can withstand as a function of breaking current, the wear equivalent law [Pon93], [Jea02] has been applied. Thus, the mass loss limit or wear limit of nozzle had to be determined first. Then, the number of interruptions, which must be performed to cause a level of mass loss comparable to the mass loss limit, in a function of the interrupted current would be further computed.

To find the mass loss limit, the linearized equations of mass loss of nozzle 1 and nozzle 2 should be used. By using the coefficients from Table 5 in Appendix B for both nozzles, the equations could be written as follows:

$$\text{Mass loss}_{\text{nozzle1}} = 11.06667 + 227.88571 * N \quad (5.7)$$

and

$$\text{Mass loss}_{\text{nozzle2}} = 85.86667 + 205.94286 * N \quad (5.8)$$

Equation 5.7 and 5.8 were used to determine cumulative mass loss of nozzle 1 and nozzle 2 as a function of number of interruption (N) respectively. By substituting $N = 4$ into both equations, the mass loss limits of nozzle 1 and nozzle 2 are 922.6mg and 909.6mg.

From the measurement result, the average of current at each successive interruption for three charging voltage stresses and the averages of mass losses of nozzle caused

by that current were known. The wear equivalent law defined that wear limit or mass loss limit is equal to number of allowable interruption, which must be performed to reach wear or mass loss limit, times wear or mass loss caused by one single interruption at that corresponding breaking current. This could be written as shown in equation 5.9.

$$\text{Mass loss limit} = N_{\text{allowable}} * \text{Mass loss}_{I_{\text{breaking}}} \quad (5.9)$$

Because the mass loss of nozzle at any breaking current was measured during the experiment, this could be further derived with the aid of equation 5.9 to determine the allowable number of interruption as a function of breaking current.

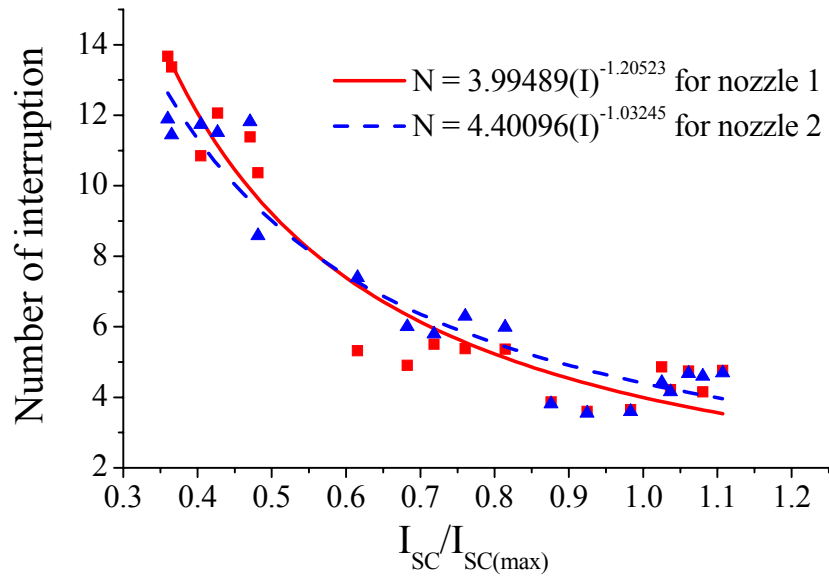


Figure 5.7: Allowable number of interruption as a function of breaking current ratio for nozzle consideration

Figure 5.7 represents the relationship between allowable number of interruption and the ratio of breaking current to rated short-circuit current ($I_{SC(max)}$), which is the mean value of current (5.97kA) at 1.5kV charging voltage. The square and triangle symbols are the result from measurement, while the solid and dash lines are the result obtained from non-linear curve fitting for nozzle 1 and nozzle 2 respectively.

Hence, the allowable number of interruption ($N_{\text{allowable}}$) in function of breaking current ratio ($I_{SC}/I_{SC(max)}$) could be written as follows:

$$N_{\text{allowable}1} = 3.99489 \left(\frac{I_{SC}}{I_{SC(max)}} \right)^{-1.20523} \quad (5.10)$$

and

$$N_{\text{allowable}2} = 4.40096 \left(\frac{I_{SC}}{I_{SC(max)}} \right)^{-1.03245} \quad (5.11)$$

Equation 5.10 and 5.11 obtained by considering nozzle 1 and nozzle 2 as a limiting component respectively.

The configuration of circuit breaker model in the laboratory does not allow finding the limit of using electrode. In case of assuming that four interruptions with 1.5kV charging voltage is a limit value for both electrodes as for nozzle, with the coefficients from Table 6 in Appendix B the linearized equations between mass loss of both electrodes and number of switching could be written as follows:

$$\text{Mass loss}_{\text{electrode 1}} = -42.4833 + 213.15 * N \quad (5.12)$$

and

$$\text{Mass loss}_{\text{electrode 2}} = -20.15 + 201.436 * N \quad (5.13)$$

By substituting $N = 4$ in in Equation 5.12 and 5.13, the mass loss limit is 810.12mg and 785.6mg for electrode 1 and electrode 2 respectively. Now following the same procedure as for nozzle, the relationship of allowable number of interruption ($N_{\text{allowable}}$) as a function of breaking current ratio ($I_{\text{SC}}/I_{\text{SC(max)}}$) for both electrodes could be expressed as follows:

$$N_{\text{allowable elk1}} = 4.73796 \left(\frac{I_{\text{SC}}}{I_{\text{SC(max)}}} \right)^{-2.03275} \quad (5.14)$$

and

$$N_{\text{allowable elk2}} = 4.76917 \left(\frac{I_{\text{SC}}}{I_{\text{SC(max)}}} \right)^{-1.91703} \quad (5.15)$$

Equation 5.14 and 5.15 obtained by considering electrode 1 and electrode 2 as a limiting component respectively.

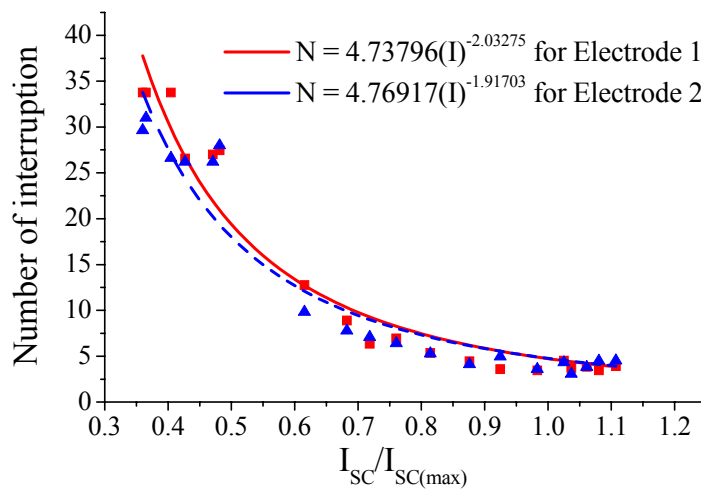


Figure 5.8: Number of interruption as a function of breaking current ratio for electrode consideration

The allowable number of interruptions in function of interrupting current ratio for electrode consideration is presented in Figure 5.8. The square and triangle symbols are the result from measurement, while the solid and dash lines are the result obtained from non-linear curve fitting for electrode 1 and electrode 2 respectively.

Although the cumulative mass loss of electrode 2 is less than that of electrode 1, the allowable number of interruption is limited by electrode 2 as seen from Figure 5.8 because it depends not only on mass loss limit, but on mass loss at any breaking current as well. The result from circuit breaker model shows that its nozzle is the limit component for successful current interruption. The coefficient a and b from non-linear curve fittings for each consideration are summarized in Table 5.4.

Constant	Non-linear curve fitting by considering			
	Nozzle 1	Nozzle 2	Electrode 1	Electrode 2
a	3.99489	4.40096	4.73796	4.76917
b	1.20523	1.03245	2.03275	1.91703

Table 5.4: Coefficient a and b from non-linear curve fitting for each consideration

6 Conclusions

The no-load mechanical endurance of an industrial type circuit breaker and the electrical degradation of a circuit breaker model under short circuit condition were studied and reported in this work. The objective is to find a non-invasive method to access the internal mechanical condition of the circuit breaker without opening the major parts, to investigate the electrical degradation due to the current interruptions, and to find a method to predict the erosion and the remaining lifetime of the circuit breaker.

For the no-load mechanical endurance investigation, a 110kV industrial type SF₆ puffer circuit breaker with a hydraulic operating mechanism served as a reference in the laboratory test environment. At first, the comparison of the measurement results from three circuit breakers of the same type showed a good agreement and verified the reliability of results. The maintenance effects were also observed from the on-site measurement with the second circuit breaker. Then, the no-load switching test up to 6,000 switching operations and the subsequently simulated defects, such as the operation without bush in the connecting rod, fix contact B manipulated to a damage, operation without the connecting rod between the mechanism and the interrupter, and operation until the cut connecting rod is broken, were executed with this reference circuit breaker.

Both conventional and vibration measurements were applied. The vibration analysis was done in both frequency and time domain using signal envelope for event timing extraction. From the analysis of the measured signals, the significant events occurring during circuit breaker operation, e.g. armature movement, latch release, auxiliary contact movement, arcing contact and fix contact touching and motion stop, can be determined.

The mechanical degradation during 6,000 switching operations was relatively small and no significant changes could be determined. After testing, the circuit breaker still operates correctly. By means of the variation of operating conditions, the variation of the auxiliary supply voltage and hydraulic oil pressure are detectable, whereas the significant changes cannot be determined from the variation of SF₆ pressure. Simulated defects, the operation without bush in the connecting rod and a damaged fix contact cannot be distinguished by measurement. More severe defects as the operation with a partly cut connecting rod or without connecting rod show significant changes in the contact timing and vibration signal envelope.

Even though, the good agreement between the measurement and the theoretical calculation was verified, the vibration analysis in the frequency-domain is not recommended owing to its sensitivity to the circuit breaker's installation method. The vibration signal envelope, operating time, coil current and dynamic contact resistance measurements are recommended as a tool for circuit breaker diagnostics because of their sensitivity to detect the changes in operating conditions and the possibility to access the internal mechanical events from the outside measurement.

The analysis of the deviation from the reference base line to evaluate the circuit breaker conditions needs further development, such as data collection from the field measurement, parameter extraction methods and the expert system for determining the final conclusions. The economical initial- and operating-costs as well as the simplicity in application, installation and result interpretation should be considered when applying the monitoring and diagnostic techniques.

The electrical degradation of the interrupting unit of industrial type circuit breakers is difficult to access. Hence, the investigation on the electrical degradation by focusing on the nozzles and the electrodes under current interruption was performed with a reduced-size SF₆ self-blast circuit breaker model and a synthetic test circuit, because of the extensive use of nozzle ablation, the possibility for parameter variation and the reduction of cost and time. The impact of the interrupted current amplitude (from 2kA to 7.5kA) on the degradation was the primary investigation, while the influence of the pressure volume, arcing time and recovery voltage on the electrical degradation was subsequently determined. The electrical degradation after each current interruption was determined in term of the total mass losses of the nozzles and the electrodes; geometry changes of the nozzle; ablation factor or the mass loss per energy; mass losses along the nozzle column; and the impact of nozzle widening on the pressure build-up and the gas flow.

The investigation with variable current amplitudes was performed with the consecutive tests on one pair of nozzle until thermal failure occurred. For 4.9kA current (1.3kV charging voltage) the circuit breaker model can withstand up to six interruptions and four interruptions for 6kA current (1.5kV charging voltage). A linear relationship between the mass losses of the nozzles as well as the electrodes and the current amplitude can be determined. The current in a 8mm nozzle is approximately 26% higher than that in a 5mm nozzle, but it only causes a slight increase in the mass loss of the nozzles due to less radiation flux density at the nozzle wall. This higher current causes more significant mass loss of the electrodes, which depends primarily on the current amplitude and the arcing time. The ablation factor is approximately 16mg/kJ for nozzle, whereas it is 10mg/kJ and 10.8mg/kJ for electrode when testing with 5mm and 8mm nozzle respectively. From the linear relationship between the cumulative mass loss of the nozzle and the cumulative energy, the number of successful interruptions for 2.5kA current (1kV charging voltage) can be estimated (see Figure 4.21).

Furthermore, the nozzle geometry changes were determined by measuring three diameters around the nozzle edge after each switching operation. The cross section profile of the nozzle after five switching operations shows the roughness of the surface, enlarged diameter and roundness around the edge. With the aid of a digitizer software the exact geometry changes can be obtained and the volume loss and mass loss calculated from the obtained geometry agrees well with the measured mass loss. The determination of the mass losses of each section along a nozzle column provides a better understanding of the locally ablated mass.

The influence of nozzle widening on the pressure build-up and gas flow was examined. After each switching operation, the normalized pressure build-up is

reduced and its maximum is reached faster. From the relationship between normalized pressure and the number of switching operations, the drop in pressure before an interruption failure occurs can be seen.

The impact of a shorter arcing time and a smaller expansion volume causes the reduction in the mass loss of the nozzles and the electrodes, the smaller increment of nozzle diameter as well as a lower ablation factor. When using 0.5l pressure volume, a higher pressure and a higher pressure gradient occur and the arcing time is reduced. The higher recovery voltage causes nearly no significant change on the electrical erosion because of the lower energy.

In order to estimate the allowable number of interruptions and the remaining lifetime, the exponential decay function is more reasonable than the simplified linear extrapolation. From the linear relationship between the mass losses and $\int i dt$, the nozzle ablation (5.3mg/As) and the contact erosion (5.06mg/As) per ampere-seconds can be determined. Thus, only the measurement of the short circuit current and time implies the mass losses of the nozzles and the electrodes. This method is only applicable for the circuit breaker model but it can be adapted to real circuit breakers by using $\int i^x dt$. Applying the wear equivalent law, the allowable number of interruptions as a function of the breaking current to rated short-circuit current ratio can be determined. The constants a and b of this relationship are calculated from experimental results and are in good agreement with other experimental studies.

Further investigations to improve and verify the accuracy of the nozzle ablation and contact erosion models in the CFD simulation need to be performed in order to use the simulation as a powerful tool to evaluate the interrupter condition and to minimize the demand on performing expensive experimental tests.

7 Zusammenfassung

Die mechanische Leerlauf-Dauerprüfung eines industriell gefertigten Leistungsschalters und die elektrische Abnutzung eines Selbstblasschalter-Modells bei Lichtbogenbeanspruchungen wurden in dieser Arbeit untersucht. Das Ziel ist, eine Methode zur Bestimmung des inneren mechanischen Zustandes eines Leistungsschalters ohne Öffnung des druckdichten Gehäuses herauszufinden, die elektrische Abnutzung durch die Lichtbogenbeanspruchung experimentell zu ermitteln und eine Methode zur Abschätzung des Isolierstoffdüsen- und Elektrodenabbrands und der Restnutzungsdauer des Leistungsschalters zu entwickeln.

Für die Untersuchung der mechanischen Leerlauf-Dauerprüfung wurde ein 110kV-Blaskolben-Leistungsschalter mit hydraulischem Antrieb als Referenz unter Laborbedingungen genutzt. Zunächst zeigte der Vergleich der Messergebnisse von drei gleichen Leistungsschaltern eine gute Übereinstimmung und verifizierte die Zuverlässigkeit der Ergebnisse. Die Instandhaltungseffekte wurden ebenfalls aus der Vor-Ort-Messung beim zweiten Leistungsschalter beobachtet. Danach wurden die mechanische Leerlauf-Dauerprüfung bis zu 6.000 Schalthandlungen und die anschließend simulierten Defekte, z. B. Schaltungen ohne Gleitlager an der Verbindung zwischen Antrieb und Koppelstange, Schaltungen mit künstlich herbeigeführten Defekten auf dem Festkontakt B, Schaltungen mit angesägter Koppelstange und ohne Koppelstange zwischen Antrieb und Unterbrechereinheit, mit dem Referenzschalter durchgeführt.

Konventionelle Messungen sowie Vibrationsmessungen wurden verwendet, wobei die Vibrationsanalyse im Frequenz- und Zeit-Bereich mittels Hüllkurve zur zeitlichen Zuordnung der Ereignisse durchgeführt worden ist. Durch die Auswertung der Vibrationssignale können die während der Schalthandlung auftretenden signifikanten Ereignisse, z. B. die Betätigung des Einschaltmagnets, die Bewegung des Hilfskontakts, die Hauptkontaktberührung und das Bewegungsende, ermittelt werden.

Die mechanische Abnutzung während 6.000 Schalthandlungen war relativ gering und es konnten keine signifikanten Änderungen bestimmt werden. Nach der Prüfung funktioniert der Leistungsschalter noch einwandfrei. Durch die variablen Betriebsbedingungen kann die Variation der Versorgungsspannung und des Hydraulikdruckes detektiert werden, wobei signifikante Änderungen bei der Variation des SF₆-Druckes nicht zu bemerken sind. Simulierte Defekte, Schaltungen ohne Gleitlager oder mit künstlich herbeigeführten Defekten auf dem Festkontakt sind durch Messungen nicht zu unterscheiden. Auf der anderen Seite zeigen sich die stärkeren Defekte wie Schaltungen mit angesägter Koppelstange bzw. ohne Koppelstange in signifikanten Änderungen in der Schaltzeit und der Vibrationssignalhüllkurve.

Trotz der guten Übereinstimmung zwischen Messung und theoretischer Berechnung ist die Vibrationsanalyse im Frequenzbereich wegen ihrer Empfindlichkeit

gegenüber der Installationsmethode des Leistungsschalters nicht empfehlenswert. In diesem Fall sind die Vibrationssignalhüllkurve, die Schaltzeit, der Spulenstrom und der dynamische Kontaktwiderstand aufgrund ihrer Empfindlichkeit zur Erkennung der Änderungen in Betriebsbedingungen und der Möglichkeit zur Erfassung der inneren mechanischen Ereignisse aus der äußeren Messung für Leistungsschalterdiagnosen zu empfehlen.

Die Analyse der Abweichung von der Referenzkennlinie zur Bewertung des Leistungsschalterzustandes verlangt die weitere Entwicklung, z.B. die Datensammlung aus der Messung bei in Betrieb befindlichen Leistungsschaltern, die Parameter-Extraktions-Methoden und ein Expertensystem zur Bestimmung endgültiger Schlussfolgerungen. Die ökonomischen Anschaffungs- und Betriebskosten sowie die Vereinfachung in Anwendung, Installation und Ergebnisauswertung sollen berücksichtigt werden, wenn die Monitoring- und Diagnostikstechnik angewendet werden.

Da die elektrische Abnutzung der Unterbrechungseinheit bei industriell gefertigten Leistungsschaltern schwer zu bestimmen ist, wurde die experimentelle Bestimmung der Abnutzung der Düsen und der Elektroden bei Lichtbogenbeanspruchungen mit einem SF₆-Selbstblasschalter-Modell und einem synthetischen Prüfkreis untersucht. Dabei konnten Parametervariationen schnell und kostengünstig vorgenommen werden. Die Auswirkung der zu schaltenden Stromstärke (von 2kA bis 7,5kA) auf die Abnutzung war die primäre Untersuchung, wobei zusätzlich der Einfluss des Druckkammervolumens, der Lichtbogenzeit und der Wiederkehrspannung auf die elektrische Abnutzung bestimmt wurden. Die elektrische Abnutzung nach jeder Stromunterbrechung wurde in Bezug auf die Massenverluste der Düsen und Elektroden, die Düsengeometrieänderung, den Abbrandfaktor (Massenverlust pro Energie), die Massenverluste entlang des Düsenkanals und den Einfluss des Düsenaufbrandes auf den Druckaufbau untersucht.

Die Untersuchung mit variablen Stromstärken wurde in aufeinanderfolgenden Versuchen bei einem Düsenpaar so lange durchgeführt, bis ein thermischer Schaltversager auftrat. Das Schaltermodell konnte für bis zu sechs erfolgreiche Abschaltungen bei 4,9kA (1,3kV-Ladespannung) bzw. bis zu vier erfolgreiche Abschaltungen bei 6kA (1,5kV-Ladespannung) eingesetzt werden. Daraus kann ein lineares Verhältnis zwischen Massenverlust der Düsen sowie Elektroden und Stromstärke ermittelt werden. Der Strom in einer 8mm-Düse ist annähernd 26% größer als der in einer 5mm-Düse. Allerdings verursacht er eine nur geringe Erhöhung der Massenverluste der Düsen wegen der niedrigen Strahlungsflussdichte an der Düsenwand. Dieser hohe Strom verursacht erhebliche Massenverluste der Elektroden, die überwiegend von der Stromstärke und Lichtbogenzeit abhängen. Der Abbrandfaktor beträgt etwa 16mg/kJ für die Düse. Andererseits beträgt er etwa 10mg/kJ bzw. 10,8mg/kJ für die CuW-Elektrode, wenn es bei einer 5mm- bzw. 8mm-Düse getestet wird. Aus dem linearen Verhältnis zwischen kumulativen Massenverlusten und Energien können die zulässige Schaltanzahl der erfolgreichen Abschaltungen bei 2,5kA (1kV-Ladespannung) abgeschätzt werden (Siehe Abbildung 4.21).

Weiterhin wurden die Düsengeometrieänderungen durch die Messung von drei Durchmessern im Bereich der Düsenkante nach jeder Schalthandlung bestimmt. Ein Längsschnitt durch die Düse nach fünf Schaltungen stellt die Rauigkeit der Oberfläche, den vergrößerten Durchmesser und die Rundung der Kante dar. Mit Hilfe eines Software-Tools können die exakten Geometrieänderungen bestimmt werden. Die aus den Geometrieänderungen berechnete Massenverluste stimmen gut mit den gemessenen überein.

Die Einflüsse der Düsenaufweitung auf den Druckaufbau und die Gasströmung wurden durch die Reduzierung des normierten Druckaufbaus nach jeder Schaltung und die kürzere Zeit bis zum Druckmaximum ermittelt. Aus dem Verhältnis zwischen normiertem Druck und Schaltanzahl kann der Druckabfall vor einem Schaltversagen erkannt werden.

Die Auswirkung einer kürzeren Lichtbogenzeit und einer kleineren Druckkammer verursacht die Verringerung der Massenverluste der Düsen und Elektroden, die kleinere Erhöhung der erweiterten Durchmessern sowie geringeren Abbrandfaktor. Bei 0,5l-Volumen ergibt sich ein höherer Druck, ein steilerer Druckgradient und eine kürzere Lichtbogenzeit. Die höhere Wiederkehrspannung hat keinen Einfluss auf die elektrische Abnutzung.

Zur Abschätzung der zulässigen Schaltanzahl und der Restnutzungsdauer ist eine abklingende e-Funktion sinnvoller als die vereinfachte lineare Extrapolation. Aus dem linearen Verhältnis zwischen Massenverlusten und $\int i^x dt$ können der Düsenabbrand (5,3mg/As) und die Kontakterosion (5,06mg/As) pro Ampere-Sekunde bestimmt werden. Daher implizieren nur die Messungen des Kurzschlussstromes und der Lichtbogenzeit die Massenverluste der Düsen und Elektroden. Diese Methode ist nur für das Schaltermodell anwendbar, kann aber durch Verwendung von $\int i^x dt$ auf reale Leistungsschalter übertragen werden. Durch die Anwendung des Abnutzungsäquivalent-Gesetzes kann die zulässige Schaltanzahl als Funktion des Verhältnisses vom zu schaltenden Strom zu Nennkurzschlussstrom bestimmt werden. Die aus den experimentellen Untersuchungen ermittelten Konstanten a und b für das Schaltermodell stimmen gut mit anderen Untersuchungen überein.

Weitere Untersuchungen müssen durchgeführt werden, um die Düsen- und Elektrodenabbrandmodelle in CFD-Simulationen zu verifizieren, so das diese Simulationen zu einem leistungsfähigen Werkzeug zur Zustandsbewertung von Leistungsschaltern weiter entwickelt und die erforderlichen experimentellen Untersuchungen reduziert werden können.

8 References

- [Ada03] M. Adam, A. Baraboi, C. Pancu, "*About the monitoring and diagnostic of the circuit breakers*", XIIIth International Symposium on High Voltage Engineering, Netherlands, 2003
- [Air76] D. R. Airey, R. E. Kinsinger, P. H. Richards, J. D. Swift, "*Electrode vapour effects in high current gas blast switchgear arcs*", IEEE Transactions on power apparatus and systems, Vol PAS-95, No.1, 1976, page 1-13
- [Ana99] S. Ananthkrishnan and K. P. Guruprasad, "*Transient recovery voltage and circuit breaker*", Tata McGraw-Hill, New Delhi, 1999
- [ANS81] ANSI/IEEE C37.081-1981, "*IEEE guide for synthetic fault testing of AC high-voltage circuit breakers rated on a symmetrical current basis*", 1981
- [Ari90] H. Arita, K. Natsui, M. Tsukushi, Y. Kurosawa, K. Hirasawa, "*Interruption ability of a self extinguishing type gas circuit breaker*", IEEE Transactions on power delivery, Vol. 5, No.3, July 1990, page 1362-1369
- [Aub94] V. Aubrecht and B. Gross, "*Net emission coefficient of radiation in SF₆ arc plasmas*", J. Phys. D: Appl. Phys. 27, 1994, page 95-100
- [Aub02] V. Aubrecht and M. Bartlova, "*Radiation in SF₆ + PTFE arc plasmas*", XIV International conference on gas discharge and their applications, 2002, Liverpool, England, page 47-50
- [Bae02] C. Y. Bae, J. Y. Lee, K. Y. Cho, H. K. Jung, "*Numerical analysis of arc-flow interaction in SF₆ gas circuit breaker*", XIV International conference on gas discharge and their applications, 2002, Liverpool, England, page 71-74
- [Bal98] G. Balzer, M. Brandl, A. Strand, A. Schnettler, M. Mathis, "*Rechnergestützte Instandhaltungsoptimierung im Netzbereich: Anwendung und praktische Erfahrung bei EVS*", Elektrizitätswirtschaft Jg. 97 (1998), Heft 12, page 26-32
- [Bar88] P. Barken, J. A. Deni, A. K. McCabe, J. G. Reckleff, H. N. Jr. Scherer, R. C. Woodward, "*Methodology for monitoring the condition of high voltage circuit breakers*", Cigre' Session Paper Ref. 13-04, Published: 1988
- [Bar97] Milada Bartlova, "*Reaction rate constants of electron-ion recombination in SF₆ arc plasma*", 8th international conference on switching arc phenomena, 1997, Poland, page 109-110
- [Bec01] Jörg Becker, "*Schaltbeanspruchungen von Hochspannungs-Leistungsschaltern im Netzbetrieb*" Fachbereich Elektrotechnik und Informationstechnik, Technische Universität Darmstadt, Dissertation 2001

- [Biz97] M. Bizjak and M. Drobnic, "*Characteristics of arc in a long narrow rectangular channel with ablative walls*", Eight international conference on switching arc phenomena, 1997, Poland, page 71-76
- [Blu97] R. E. Blundell and M. T. C. Fang, "*The similarity and scaling of radiating arcs burning in a turbulent, axially accelerating gas flow*", J. Phys. D: Appl. Phys. 30, 1997, page 628-635
- [Bou96] M. Bouaziz, G. Raynal, M. Razafinimanana, A. Gleizes, "*An experimental and theoretical study of the absorption of SF₆ arc plasma radiation by cold SF₆ gas*", J. Phys. D: Appl. Phys. 29, 1996, page 2885-2891
- [Bra82] K. P. Brand, W. Egli, L. Niemeyer, K. Ragaller, "*Dielectric recovery of an axially blown SF₆-arc after current zero: partIII-Comparison of experiment and theory*", IEEE Transactions on plasma science, Vol. 10, No.3, 1982, page 162-172
- [Bro84] T. E. Browne, "*Circuit Interruption*", Marcel Dekker, New York, 1984
- [Cam89] L. C. Campbell, "*HV circuit breaker contacts*", IEE colloquium on electrical contacts, 4 Apr. 1989, page 8/1-8/3
- [Cao91] L. C. Cao and A. D. Stokes., "*Ablation arc:III. Time constants of ablation-stabilized arcs in PTFE and ice*", J. Phys. D: Appl. Phys. 24, 1991, page 1557-1562
- [Cig00a] Cigre' working group 37.27, "*Aging of the system impact on planning*", Cigre', published: 2000
- [Cig00b] Cigre' working group 23.02, task force 01, "*Guide for SF₆ gas mixtures (Application and handling in electrical power equipment)*", Cigre', published: 2000
- [Cla97a] Max Claessens and Martin Kriegel, "*Experimental and theoretical investigations of an experimental self-blast circuit-breaker*", Eight international conference on switching arc phenomena, 1997, Poland, page 87-91
- [Cla97b] Max Claessens, Roland von Starck and H.G. Thiel, "*Simulation of gas flow phenomena in high-voltage self-blast circuit breakers at heavy fault current interruption*", IEEE Transactions on plasma science, Vol. 25, No.5, October 1997, page 1001-1007
- [Cla97c] Max Claessens, "*Simulation von Gasströmungen in SF₆-Selbstblässchaltern bei Kurzschlussabschaltungen*", Institut für Allgemeine Elektrotechnik und Hochspannungstechnik, RWTH Aachen, Dissertation, 1997
- [Cle96] Barry Clegg, Graeme Ewart, Frank Brankin, "*Advances in circuit breaker testing and condition monitoring*", IEE Colloquium on monitors and condition assessment equipment, 5 December 1996, page 7/1-7/21

- [Col94] E. Colombo, E. Emolumento, E. Paganini, L. Placentino, G. Tondello, "*Application of an optical monitoring system for the assessment of internal conditions of an HV circuit breaker*", Cigre' Session Paper Ref. 13-205, Published: 1994
- [Cou98] O. Coufal, "*Composition and thermodynamic properties of SF₆-C-(C₂F₄)_n-CaF₂-Cu-W reacting mixtures*", J. Phys. D: Appl. Phys. 31, 1998, page 2025-2039
- [deG96] Martin H. B de Grijp, Joost S. Bedet, Richard A Hopkins, John E Greyling, "*Condition monitoring of high voltage circuit breakers*", IEEE AFRICON 4th, Volume 2, 24-27 Sept 1996, page 880-885
- [deH01] Markus de Hesselle, "*Modellierung der Strahlung und der Gasströmung in SF₆ Selbstblasleistungsschaltern*", Institut für Hochspannungstechnik, RWTH Aachen, Dissertation, 2001
- [deH03] Markus de Hesselle, Jean-Yves Trepanier, "*Comparison of CFD tools for SF₆ self-blast circuit breaker development*", IEEE Transactions on power delivery, Vol. 18, No.2, April 2003, page 468-474
- [Dem92] V. Demjanenko, et al., "*A non-invasive diagnostic instrument for power circuit breakers*", IEEE Transactions on power delivery, Vol. 7, No.2, April 1992, page 656-663
- [Dom05] R. Dommerque, M.-C Tang, M. Schwinne, C. Kahlen, A. Schnettler, "*Influence of the electrode vapour contamination on the interrupting limit of SF₆ self-blast-circuit breakers*", XVIth symposium on physics of switching arc, 5-9 Sep 2005, Brno, Czech Republic, Vol.1, page 55-58
- [Fan86] M. T. C. Fang and J. F. Zhang, "*The dynamic behavior of nozzle arcs*", IEEE Transactions on plasma science, Vol PS-14, No.4, 1986, page 350-356
- [Faw78] C. A. Fawdrey, "*The application of development and diagnostic techniques to circuit breaker reliability*", Cigre' Session Paper Ref. 13-02, published: 1978
- [FGH01] Technical report, "*Zustandsmodell für die Instandhaltungsplanung für einen 123-kV-Leistungsschalter*", Forschungsgemeinschaft für Elektrische Anlagen und Stromwirtschaft e.V., 2001
- [Flu77] C. H. Flurscheim, "*Power circuit breaker theory and design*", Peter Peregrinus LTD., 1977
- [Fuj98] Sun Fujie, Qin Hongsan, "*Diagnosis techniques on contact electrical endurance of high voltage circuit breaker*", Proceedings POWERCON'98, International conference on power system technology, 18-21 August 1998, Vol. 1, page 105-109
- [Gaj98] Z. Gajic, "*Experience with puffer interrupter having full self-compensation of resulting gas pressure force generated by the electrical arc*", Cigre' Session Paper Ref. 13-103, published: 1998

- [Gar76a] R. D. Garzon, "*Rate of change of voltage and current as functions of pressure and nozzle area in breaker using SF₆ in the gas and liquid phases*", IEEE Transactions on power apparatus and systems, Vol PAS-95, No.5, 1976, page 1681-1688
- [Gar76b] R. D. Garzon, "*The effect of SF₆-N₂ mixture upon the recovery voltage capability of a synchronous interrupter*", IEEE Transactions on power apparatus and systems, Vol PAS-95, No.1, 1976, page 140-146
- [Gar97] R. D. Garzon, "*High voltage circuit breakers design and applications*", Marcel Dekker Inc., 1997
- [Gle88a] A. Gleizes, A. M. Rahal, H. Delacroix, P. V. Doan, "*Study of a circuit-breaker arc with self-generated flow: part I - Energy transfer in the high current phase*", IEEE Transactions on plasma science, Vol PS-16, No.6, 1988, page 606-614
- [Gle88b] A. Gleizes, A. M. Rahal, S. Papadopoulos, S. Vacquie, "*Study of a circuit-breaker arc with self-generated flow: part II - the flow phase*", IEEE Transactions on plasma science, Vol PS-16, No.6, 1988, page 615-622
- [Gon96] J. J. Gonzalez, J. B. Belhaouari, A. Gleizes, "*Influence of demixing effect on the temperature in wall-stabilized SF₆ arcs*", J. Phys. D: Appl. Phys. 29, 1996, page 1520-1524
- [Gre91] Allan N. Greenwood, and Anthony D. Stokes, "*Electric power switches*", IEEE Transactions on plasma science, Vol 19, No.6, 1991, page 1132-1142
- [Hei94] C. R. Heising, et al., "*Final report on high voltage circuit breaker reliability data for use in substation and system studies*", Cigre' Session Paper Ref. 13-201, published: 1994
- [Her77] W. Hermann, K. Ragaller, "*Theoretical description of the current interruption in HV gas blast breakers*", IEEE Transactions on power apparatus and systems, Vol PAS-96, No.5, 1977, page 1546-1555
- [Hes92] D. P. Hess, et al., "*Noninvasive condition assessment and event timing for power circuit breakers*", IEEE Transactions on power delivery, Vol 7, No.1, January 1992, page 353-360
- [Hof92] P. Hoff, A. Holm, O. Karlen, U. Lager, U. Akesson, "*Condition monitoring of SF₆ circuit breakers*", Cigre' Session Paper Ref. 13-104, Published: 1992
- [Hoi99] H. K. Hoidalén, M. Runde, O. Haugland, G. Ottesen, M. Öhlen, "*Continuous monitoring of circuit-breakers using vibration analysis*", 11th international symposium on high voltage engineering, 23-27 August 1999, Conference publication No. 467, Vol 1
- [Hua03] Y. Huang, Y. Guan, G. Xu, J. Qian, "*Mechanical condition monitoring of high voltage circuit breakers*" XIIIth International Symposium on High Voltage Engineering, Netherlands, 2003

- [IEC04] IEC 62271-310, "*High-voltage switchgear and control gear*", part 310 Electrical endurance testing for circuit-breakers of rated voltage 72.5kV and above, 2004
- [IEEE81] ANSI/IEEE C37.081-1981, "*IEEE guide for synthetic fault testing of AC high-voltage circuit breakers rated on a symmetrical current basis*"
- [IEEE95] IEEE Std. C37.10-1995, "*IEEE Guide for diagnosis and failure investigation of power circuit breakers*"
- [IEEE97] IEEE Std. 493-1997, "*IEEE recommended practice for the design of reliable industrial and commercial power systems*"
- [IEEE00] IEEE Std. C37.10.1-2000, "*IEEE Guide for the selection of monitoring for circuit breakers*"
- [Ike84] H. Ikeda, T. Ueda, A. Kobayashi, M. Yamamoto, S. Yanaba, "*Development of large-capacity, SF₆ gas interruption chamber and its application to GIS*", IEEE Transactions on power apparatus and systems, Vol PAS-103, No.10, 1984, page 3038-3043
- [Jai99] H. S. Jain, S. N. Saxena and M. S. Agarwal, "*Studies on effects of metal vapour in an experimental self-blast interrupter*", IEEE Transactions on power delivery, Vol 14, No.4, 1999, page 1327-1332
- [Jai01] H. S. Jain and Rao M. Mohana, "*Estimation of energy transport in expansion-volume of a self-blast interrupter using CFD techniques*" XII International Symposium on High Voltage Engineering, India, 2001
- [Jan92] A. L. J. Janssen, et al., "*Application of diagnostic techniques for high voltage circuit breakers*", Cigre' Session Paper Ref. 13-101, published: 1992
- [Jan94] A. L. J. Janssen, et al., "*A summary of the final results and conclusions of the second international enquiry on the reliability of high voltage circuit breakers*", Cigre' Session Paper Ref. 13-202, published: 1994
- [Jan96] A. L. J. Janssen, J. H. Brunke, Ch. R. Heising, W. Lanz, "*Cigre WG 13.06 studies on the reliability of single pressure SF₆-Gas high voltage circuit breakers*", IEEE Transactions on power delivery, Vol 11, No.1, January 1996, page 274-281
- [Jea88] R. Jeanjean, M. Landry, A. Chenier, D. Demissy, "*Electronic system for controlling and monitoring the mechanical and electrical integrity of HV circuit-breakers*", Cigre' Session Paper Ref. 13-11, Published: 1988
- [Jea02] R. Jeanjean, C. Salzard, P. Migaud, "*Electrical endurance tests for HV circuit-breakers: EDF experience*", IEEE Power engineering society winter meeting, Vol 1, 27-31 Jan 2002, page 294-298

- [Jon86] G. R. Jones, N. Y. Shammass, A. N. Prasad, "*Radiatively induced nozzle ablation in high-power circuit interrupters*", IEEE Transactions on plasma science, Vol PS-14, No.4, 1986, page 413-422
- [Jon88a] G. R. Jones, H. Weilin, S. M. El-Kholy, "*A spectroscopic investigation of electrode material entrained into the extinguishing arc of an SF₆ circuit breaker*", J. Phys. D: Appl. Phys. 21, 1988, page 1414-1420
- [Jon88b] G. R. Jones, S. M. G. Ali, T. Irwin, D. Parr, "*Circuit breaker monitoring using optical fiber based systems*", Cigre' Session Paper Ref. 13-09, Published: 1988
- [Jon94] C. J. Jones, W. B. Hall, G. R. Jones, M. T. C. Fang, S. S. Wiseall, "*Recent development in theoretical modeling and monitoring techniques for high voltage circuit breakers*", Cigre' Session Paper Ref. 13-109, Published: 1994
- [Kah05] C. Kahlen, R. Dommerque, M. Schwinne, M.-C Tang, A. Schnettler, "*Application of a new measuring system for investigations of the interruption behaviour of a SF₆-selfblast circuit breaker model*", XVIth symposium on physics of switching arc, 5-9 Sep 2005, Brno, Czech Republic, Vol.1, page 109-112
- [Kez02] M. Kezunovic, et al., "*Automated circuit breaker monitoring and analysis*", Power engineering society summer meeting 2002, IEEE Vol. 1, 21-25 July 2002, page 559 - 564
- [Kie93] A. Kieliszek, et al., "*Experimental investigations and numerical simulation of arcing phenomena in an SF₆ autopuffer circuit breaker*", Seventh international conference on switching arc phenomena, 1993, Poland, page 117-120
- [Kim02] H. K. Kim, et al., "*Numerical analysis of hot gas flow in SF₆ GCB using the method of partial characteristics and FVFLIC method*", XIV International conference on gas discharge and their applications, 2002, Liverpool, England, page 75-78
- [Kir98] B. N. Kishore and R. V. Agashe, "*Dynamic mechanical stress in HV circuit breakers development of estimation method*", Cigre' Session Paper Ref. 13-201, published: 1998
- [Kno95] H. Knobloch, "*Relation between gas flow and arc extinguishing capability of SF₆ circuit breaker*" IEE Colloquium on physics of power interruption, 31 Oct 1995, page 7/1-7/6
- [Kno99] H. Knobloch and U. Habedank, "*Arc resistance at current zero: A tool to describe the breaking capacity of SF₆ circuit breakers at short-line faults*" XI International Symposium on High Voltage Engineering, England, 1999, page 205-208
- [Kol00] Prof. Dr. Josef Kolerus, "*Zustandsüberwachung von Maschinen*", Expert Verlag, 2000

- [Kom97] M. Komarek, K. Filakovsky, J. Bartl, Z. Vavra, V. Aubrecht, "*Pressure and velocity fields in the model of an SF₆ self-blast extinguishing chamber*", Eight international conference on switching arc phenomena, 1997, Poland, page 111-114
- [Kov84] P. Kovitya and J. J. Lowke, "*Theoretical predictions of ablation-stabilized arcs confined in cylindrical tubes*", J. Phys. D: Appl. Phys. 17, 1984, page 1197-1212
- [Kri99] M. Kriegel, "*Einfluss des Düsenmaterials auf das Ausschaltverhalten von SF₆-Selbstblusschaltern*", Institut für Allgemeine Elektrotechnik und Hochspannungstechnik, RWTH Aachen, Dissertation, 1999
- [Lai88] M. L. Lai, et al., "*Mechanical failure detection of circuit breakers*", IEEE Transactions on power delivery, Vol 3, No.4, October 1988, page 1724-1731
- [Lee75] T. H. Lee, "*Physics and engineering of high power switching devices*", The Massachusetts Institute of Technology, 1975
- [Loo02] H. M. Looe, K. J. Brazier, Y. Huang, P. F. Coventry, G. R. Jones, "*Arc induced high frequency effects in high voltage SF₆ puffer circuit breakers*", XIV International conference on gas discharge and their applications, 2002, Liverpool, England, page 35-38
- [Man01] I. Manea, C. Chiciu, F. Balasiu, N. Tulici, "*Complex method to diagnose the technical state of the medium and high voltage circuit breaker after short-circuit events*", CIRED 16th International conference and exhibition on electricity distribution (IEE Conf. Publ. No. 482), Part 1, Volume 1, 18-21 June 2001
- [Mei86] R. Meier, F. K. Kneubühl, R. Coccioni, H. Wyss, E. Fischer, H. J. Schötzau, "*Investigations of nozzle materials in SF₆ circuit breakers*", IEEE Transactions on plasma science, Vol PS-14, No.4, 1986, page 390-394
- [Men92] H. H. Mensing, "*Life extension of circuit-breakers*", Cigre' Session Paper Panel 1-03, published: 1992
- [Mit86] R. R. Mitchell, "*Theoretical analysis of dielectric recovery in SF₆ gas-blast arcs*", IEEE Transactions on plasma science, Vol PS-14, No.4, 1986, page 384-389
- [Mou97] John Moubray, "*Reliability-centered Maintenance*", second edition, Butterworth-Heinemann, 1997
- [Mül88] L. Müller, "*Untersuchungen zum Abbrandverhalten von PTFE unter SF₆ bei der Einwirkung von Hochstromlichtbögen*", Institut für Allgemeine Elektrotechnik und Hochspannungstechnik, RWTH Aachen, Diplomarbeit, 1988
- [Mül93a] L. Müller, "*Modeling of an ablation controlled arc*", J. Phys. D: Appl. Phys. 26, 1993, page 1253-1259

- [Mül93b] L. Müller, "*Ablation controlled arcs in nozzles of polymeric insulating materials*", Seventh international conference on switching arc phenomena, 1993, Poland, page 126-130
- [Mül94] L. H. Müller, "*Untersuchung und Modellierung des Abbrandverhaltens von Isolierstoffdüsen in SF₆-Leistungsschaltern*", Institut für Allgemeine Elektrotechnik und Hochspannungstechnik, RWTH Aachen, Dissertation, 1994
- [Nie78] L. Niemeyer, "*Evaporation dominated high current arcs in narrow channels*", IEEE Transactions on power apparatus and systems, Vol PAS-97, No.3, 1978, page 950-958
- [Nel01] Jeffrey H. Nelson, "*Electric utility considerations for circuit breaker monitoring*", IEEE/PES, Transmission and distribution conference and exposition, Vol 2, 28 Oct – 2 Nov. 2001, page 1094-1097
- [Neu90] C. Neumann, W. Degen, H. Karrenbauer, G. Moritz, "*Economic monitoring and maintenance of modern HV-switchgear and – switching equipment with regard to service experiences*", Cigre' Session Paper Ref. 23-104, Published: 1990
- [Neu04] Claus Neumann and Norbert Lambrecht, "*Automatisierte, benutzergeführte und Datenbank gestützte Inspektion und Diagnose von Leistungsschaltern*", ETG-Fachbericht 97, Diagnostik elektrischer Betriebsmittel, VDE Verlag GmbH, Berlin 2004
- [Noa88] F. Noack, J. Gärtner, T. Heider, J. Schwarz, "*Computer-aided diagnostic system for high voltage circuit breakers*", Cigre' Session Paper Ref. 13-10, Published: 1988
- [Nor89] M. P. Norton, "*Fundamentals of noise and vibration analysis for engineers*", Cambridge university press, 1989
- [Nos77] H. O. Noeske, "*Investigation of dynamic nozzle parameters for various nozzle geometries and test conditions of an experimental half-size SF₆ puffer breaker*", IEEE Transactions on power apparatus and systems, Vol PAS-96, No.3, 1977, page 896-906
- [Ohs89] Y. Ohshita, A. Hashimoto, Y. Kurosawa, "*A diagnostic technique to detect abnormal conditions of contacts measuring vibrations in metal enclosures of gas insulated switchgear*", IEEE transaction on power delivery, Vol 4, No.4, October 1989, page 2090-2094
- [Osa03] N. Osawa and Y. Yoshioka, "*Analysis of nozzle ablation characteristics of gas circuit breaker*", IEEE PES, Transmission and distribution conference and exposition, Vol 2, 7-12 Sept 2003, page 810-815
- [Pau97] K. C. Paul, T. Sakuta, T. Takashima, M. Ishikawa, "*The dynamic behavior of wall-stabilized SF₆ arcs contaminated by Cu and PTFE vapours*", J. Phys. D: Appl. Phys. 30, 1997, page 103-112

- [Per72a] John F. Perkins and Leslie S. Frost, "*Dielectric recovery and predicted AC performance of blown SF₆ arc*", IEEE Transactions on power apparatus and systems, Vol PAS-91, 1972, page 368-375
- [Per72b] John F. Perkins and Leslie S. Frost, "*Magnetic pumping effect on dielectric recovery of blown SF₆ arcs*", IEEE Transactions on power apparatus and systems, Vol PAS-91, 1972, page 376-380
- [Per78] John F. Perkins, "*Scaling criteria for interruption performance in gas-blast circuit-breaker*", IEEE Transactions on power apparatus and systems, Vol PAS-97, No.1, 1978, page 232-241
- [Pfl78] M. Pflaum, et al., "*New aspects of the reliability of high voltage circuit breakers*", Cigre' Session Paper Ref.13-07, published: 1978
- [Pol95] A. A. Polycarpou, A. Soom, V. Swarnakar, J. W. Porter, "*Event timing and shape analysis of vibration bursts from power circuit breakers*", IEEE Transactions on power delivery, Vol. 11, No.2, April 1995, page 848-857
- [Pon93] A. Pons, A. Sabot, G. Babusci, "*Electrical endurance and reliability of circuit-breakers*", IEEE Transactions on power delivery, Vol. 8, No.1, January 1993, page 168-174
- [Puf01] Ralf Puffer, "*Experimentelle Untersuchung der Heißgasströmung in einem SF₆-Selbstblasschaltermodell mittels Particle Image Velocimetry (PIV) zur Verifikation von Simulationsmodellen*", Institut für Hochspannungstechnik, RWTH Aachen, Dissertation, 2001
- [Rag77] K. Ragaller, et al., "*Current interruption in high current networks*", Plenum Press, New York, London, 1977
- [Ray95] G. Raynal, P. J. Vergne, A. Gleizes, "*Radiative transfer in SF₆ and SF₆-Cu arcs*", J. Phys. D: Appl. Phys. 28, 1995, page 508-515
- [Ruc86] C. B. Ruchti and L. Niemeyer, "*Ablation controlled arcs*", IEEE Transactions on plasma science, Vol PS-14, No.4, 1986, page 423-434
- [Run92] M. Runde, T. Aurud, L. E. Lundgaard, G. E. Ottessen, K. Faugstad, "*Acoustic diagnosis of high voltage circuit breakers*", IEEE transaction on power delivery, Vol 7, No.3, July 1992, page 1306-1315
- [Run96] M. Runde, G. E. Ottesen, B. Skyberg, M. Ohlen, "*Vibration analysis for diagnostic testing of circuit breakers*", IEEE transaction on power delivery, Vol 11, No.4, October 1996, page 1816-1823
- [Run99] M. Runde, B. Skyberg, M. Öhlen, "*Vibration analysis for periodic diagnostic testing of circuit breakers*", 11th international symposium on high voltage engineering, 23-27 August 1999, Conference publication No. 467, Vol 1
- [Rya89] H. M. Ryan and G. R. Jones, "*SF₆ Switchgear*", Peter Peregrinus Ltd., 1989

- [Sca92] P. Scarpa, B. Dauby, J. M. Defise, M. Barrault, G. Bernard, S. Rowe, "*SF₆ Auto-expansion circuit breaker design: numerical and experimental investigation of arc-gas interactions*", IEEE Transactions on power delivery, Vol. 7, No.1, January 1992, page 339-345
- [Sch02] P. H. Schavemaker, L. van der Sluis, "*Quantification of the interrupting performance of high-voltage circuit breakers*", IEE Proceeding on science measurement technology, Vol. 149, No.4, July 2002, page 153-157
- [Sed03] J. Sedlacek, Z. Vostracky, H. Knobloch, H. Schramm, C. Wiesinger, "*Optimization of high-voltage self-blast interrupters by gas flow and electric field computations*", IEEE Transactions on power delivery, Vol. 18, No.4, October 2003, page 1228-1235
- [Sme05] R. P. P. Smeets, et al., "*Statistical analysis of electrical stresses on high-voltage circuit-breaker in service*", TF A3.01 report, Electra No 220, June 2005, page 24-29
- [Smi93] A. M. Smith, "*Reliability-centered Maintenance*", New York, McGraw-Hill, 1993
- [Son02] W. P. Song, D. I. Yang, Y. H. Chung, D. S. Kim, H. S. Koh, "*A study of large current interrupting capability of SF₆/N₂ mixtures*", XIV International conference on gas discharge and their applications, 2002, Liverpool, England, page 39-42
- [Sto88] A. D. Stokes, L. Timbs, "*Circuit breaker diagnostics*", Cigre Session Paper Ref. 13-03, Published: 1988
- [Sto00] Paul N. Stoving and John F. Baranowski, "*Interruption life of vacuum circuit breakers*", XIX International symposium on discharges and electrical insulation in vacuum, 2000, Volume 2, 18-22 Sept 2000, page 388-391
- [Suw03] T. Suwanasri, A. Schnettler, D. Fricke, A. Noack, "*Non-invasive condition monitoring of a high voltage circuit breaker*", XIIIth International Symposium on High Voltage Engineering, Netherlands, 2003
- [Suw04] T. Suwanasri, A. Schnettler, D. Fricke, A. Noack, "*Untersuchung zur Zustandsüberwachung an Hochspannungsleistungsschaltern*", ETG-Fachbericht 97-Diagnostik elektrischer Betriebsmittel, VDE Verlag GmbH, Berlin, 2004
- [Suz82] T. Suzuki, H. Yoshida, A. Koyama, S. Tomimuro, "*Degradation process of grease due to SF₆ gas dissociation products*", IEEE Transactions on power apparatus and systems, Vol PAS-101, No.8, 1982, page 2805-2809
- [Suz92] K. Suzuki, H. Toda, A. Aoyagi, H. Ikeda, A. Kobayashi, I. Ohshima, S. Yanaba, "*Development of 550kV 1-break GCG (part I) investigation of interrupting chamber performance*", IEEE

- Transactions on power delivery, Vol. 8, No.3, July 1992, page 1184-1191
- [Swa77] B. W. Swanson, "*Nozzle arc interruption in supersonic flow*", IEEE Transactions on power apparatus and systems, Vol PAS-96, No.5, 1977, page 1697-1706
- [Swe02] C. Sweetser, et al., "*Strategies for selecting monitoring of circuit breakers*", IEEE Transactions on power delivery, Vol17, No. 3, July 2002, page 472-476
- [Tel02] D. J. Telfer, J. Humphries, J. W. Spencer, G. R. Jones, "*Influence of PTFE on arc quenching in an experimental self-pressurized circuit breaker*", XIV International conference on gas discharge and their applications, 2002, Liverpool, England, page 91-94
- [Van02] Theo G. M. van Rijn, et al., "*Diagnostics for condition assessment of HV switchgear*", ETG-Fachbericht 87, Diagnostik elektrischer Betriebsmittel, Vorträge der ETG-Fachtagung 26-27 Feb 2002, Berlin
- [Vou94] P. R. Voumard, "*A simple approach to condition monitoring of circuit breakers*", Cigre' Session Paper Ref. 13-203, Published: 1994
- [Wal92] E. Walczuk, "*Arc erosion of high current contacts in the aspect of CAD of switching devices*", Proceedings of the Thirty-Eighth IEEE Holm Conference on Electrical Contacts, 18-21 Oct. 1992, Page 1-16
- [Wen93] Guo Wenyuan, Guo Bin, Xia Guoyi, Hu Liang, "*The pressure calculation during its storage in arc chamber with self-energy quenching arc*", 7th international conference on switching arc phenomena, 1993, Poland, page 103-106
- [Xin02] Lin Xi and Zhong Jianying, "*Numerical calculation of gas flow in the nozzle of a self-extinguished SF₆ circuit breaker*", XIV International conference on gas discharge and their applications, 2002, Liverpool, England, page 143-146
- [Yan99a] J. D Yan. and M. T. C. Fang, "*Visualization of arcing process in an auto-expansion circuit breaker*", IEEE Transactions on plasma science, Vol. 27, No.1, February 1999, page 40-41
- [Yan99b] J. D. Yan, M. T. C. Fang, W. Hall, "*The development of PC based CAD tools for auto-expansion circuit breaker design*", IEEE Transactions on power delivery, Vol. 14, No.1, January 1999, page 176-181
- [Yan01] J. D. Yan, M. T. C. Fang, Q. S. Lui, "*Dielectric recovery of a residual SF₆ plasma between two parallel plane electrodes*", IEEE Transactions on dielectrics and electrical insulation, Vol. 8, No.1, February 2001, page 129-136
- [Yos02] D. Yoshida, H. Ito, H. Kohyama, T. Sawada, K. Kamei, M. Hidaka, "*Evaluation of current interrupting capability of SF₆ gas blast circuit*

-
- breakers*", XIV International conference on gas discharge and their applications, 2002, Liverpool, England, page 11-14
- [Zha00] J. L. Zhang, J. D. Yan, M. T. C. Fang, "*Investigation of the effects of pressure ratios on arc behavior in a supersonic nozzle*", IEEE Transactions on plasma science, Vol. 28, No.5, October 2000, page 1725-1734
- [Zha02a] J. L. Zhang, J. D. Yan, A. B. Murphy, W. Hall, M. T. C. Fang, "*Computational investigation of arc behavior in an auto-expansion circuit breaker contaminated by ablated nozzle vapor*", IEEE Transactions on plasma science, Vol. 30, No.2, April 2002, page 706-719
- [Zha02b] J. L. Zhang, J. D. Yan, M. T. C. Fang, "*Prediction of arc behaviour during the current zero period in an auto-expansion circuit breaker*", XIV International conference on gas discharge and their applications, 2002, Liverpool, England, page 131-134

9 List of Abbreviations and Symbols

Abbreviations

BIL	Basic lightning impulse Insulation Level
CB	Circuit Breaker
CFD	Computational Fluid Dynamics
CT	Current Transformer
DES	Discrete Envelope Statistics
DFT	Discrete Fourier Transform
FFI	Failure Findind Interval
FFT	Fast Fourier Transform
MPC	Method of Partial Characteristics
MTBF	Mean Time Between Failures
PES	PolyEtherSulphone
PTFE	PolyTetraFluoroEthylene
RCM	Reliability Centred Maintenance
RRRV	Rate of Rise of the Recovery Voltage
SIL	Switching impulse Insulation Level
SLF	Short Line Fault
TF	Terminal Fault
TRV	Transient Recovery Voltage

Variable and Symbols

c	Sound velocity
C_H	Capacitor for high current circuit
C_P	Specific heat capacity
C_P	Parallel capacitor
C_S	Capacitor for high voltage circuit
D	Charge amplifier for pressure sensor
D_{in}	Average diameter at the middle of nozzle column
DS	Making switch
$e_{arc}(t)$	Arc energy
$f(t)$	Failure density function
FS	Spark gap

$F(t)$	Probability distribution
h	Specific enthalpy
h_v	Vapour enthalpy
HS	Auxiliary circuit breaker
$I, i(t)$	Arc current
I_{SCi}	Interrupted current
$I_{SC(max)}$	Rated short circuit current
$j(t)$	Current density
k	Stiffness of the spring
L	Tube length, Nozzle length
L_H	Inductance for high current circuit
L_S	Inductance for high voltage circuit
m	Number of measured points
\dot{m}_v	Total ablation
\dot{m}_w	Ablation causing the increase in nozzle diameter
M	Ablation characteristic
Δm	Mass loss
$N_{allow(i)}$	The allowable number of interruption at any fault current
$N_{allow(max)}$	The allowable number of interruption at 100% rated fault current
n_e	Number of electrons
N_f	Number of failed circuit breaker
N_i	The number of interruptions at current I_i
N_0	Fixed number of circuit breaker
N_s	Number of survival circuit breaker
P_r	Radiation power
$q(t)$	Charge generated by an arcing current
Q	Unreliability
R	Receiver
R	Reliability
R	Radius of nozzle tube
R_E	Earthing resistance
R_p	Parallel resistance
r_0, R_0	Radius of nozzle before test or like-new condition

r_n	Radius at each measured points
S	Sender
S	Surface
t_a	Arcing time
t_s	Time at moment of contact separation
T	Voltage probe
T_a	Arc temperature
T_v	Vapour temperature
$\tan \delta$	Dielectric loss factor
$u(t)$	Arc voltage
$u_{elec}(t)$	Voltage over electrode
$u_{noz}(t)$	Voltage over nozzle
V_e	Drift velocity of electrons
V_m	Maximum system voltage
$w_{elec}(t)$	Energy over electrode
$w_{noz}(t)$	Energy over nozzle
Δx_n	Distance between two measured points
Z	Distance along the axis of contacts
ZFS	Triggerable spark gap
α	Time constant of DC component
α	Ionisation coefficient
β	Stefan-Boltzmann constant
σ	Electrical conductivity
δ	Ablation characteristic, ablation factor
ε	Gray factor
ε_r	Relative permittivity
λ	Failure rate
ρ_0	Density of solid material
η	Attachment coefficient
θ	Voltage angle
Φ	Contraction number
φ	Phase angle

10 Appendix

Appendix A: Definition

Availability: The long-term average fraction of time that a component or system is in service and satisfactorily performing its intended function

Continuous monitoring: Monitoring in which the gathered data is transmitted continuously

Defect: Imperfection in the state of an item (or inherent weakness) which can result in one or more failures of the item itself or of another item under the specific service or environment or maintenance conditions for a stated period of time

Diagnostic techniques: All kinds of inspection, measurement and/or monitoring, without actions of dismantling, even when the circuit breaker in service, to indicate the condition of the circuit breaker and/or to detect abnormalities and finally determine the optimum overhaul program

Diagnostic tests: Comparative tests of the characteristic parameters of a circuit breaker to verify that it performs its functions, by measuring one or more of those parameters – carried out with sensors and data processing devices, connected temporarily to the circuit breaker – and comparing the measured value with the specified values or previously measured values

Downtime: The duration that the equipment is taken out of service due to failure, from the occurrence of component failure to the moment it is restored in service

Failure: Lack of performance by an item of its required functions

Failure rate: The mean number of failure of component per unit exposure time (failure per year)

Inspection: Periodical examination of the principal features of the circuit breaker without any dismantling

Major failure: Complete failure of a circuit breaker, which causes the lack of one or more of its fundamental functions

Maintenance: The combination of all technical and administrative actions, including supervising actions, intended to retain an item in, or restore it to, a state in which it can perform a required function

Mean time between failure (MTBF): The mean exposure time between consecutive failures of a component, which is equal to the exposure time divided by number of failures in that period

Mean time to repair (MTTR): The mean time to repair or replace a failed component, which is equal to summation of repair times divided by numbers of repairs

Minor failure: Failure of circuit breaker other than major failure; or any failure, even complete, of a constructional element or a sub-assembly which does not cause a major failure of the circuit breaker

Monitoring: Automatical observation of the characteristic parameters of a circuit breaker to verify that it performs its functions, by measuring one or more of those parameters – carried out with sensors and data processing devices, connected permanently to the circuit breaker – and automatically comparing the measured value with the specified values or previously measured values

Overhaul: Work done with the objective of repairing or replacing parts which are found being below standard by inspection or test or as required by manufacturer's manual, in order to restore the component and /or the circuit breaker to an acceptable condition

Periodic monitoring: Monitoring in which the gathered data is transmitted periodically

Reliability: The possibility of a device performing its purpose adequately for the period of time or number of operating cycle intended under the operating conditions encountered

Repair time: The time uses for repair or replace a failed component

Appendix B: Table

	Charging Voltage	Value at 1 st SW		Value at 5 th SW		Mean value of 5 SW		Increment %	
		5mm	8mm	5mm	8mm	5mm	8mm	5mm	8mm
Peak current [kA]	1kV	2.15	3.70	2.7	4.30	2.50	4.00	6.40	4.05
	1.1kV		4.84		4.65		4.75		-0.98
	1.3kV	3.47	5.83	5.32	6.38	4.86	6.11	13.33	2.36
	1.5kV	5.29	7.38	6.37	7.66	5.97	7.52	5.10	0.95
Max pressure [bar]	1kV	1.66	2.43	2.44	2.22	2.06	2.33	11.75	-2.16
	1.1kV		3.44		2.70		3.07		-5.38
	1.3kV	5.19	5.52	6.55	5.15	6.22	5.34	6.55	-1.68
	1.5kV	8.74	7.60	6.85	6.13	7.56	6.87	-5.41	-4.84
Voltage over nozzle [V]	1kV	481	438	461	429	468	434	-1.04	-0.51
	1.1kV		523		445		484		-3.73
	1.3kV	731	618	689	559	700	589	-1.44	-2.39
	1.5kV	925	686	705	583	787	635	-5.95	-3.75
Voltage over electrode [V]	1kV	658	605	666	594	663	600	0.30	-0.45
	1.1kV		695		611		653		-3.02
	1.3kV	910	769	788	728	850	748	-3.35	-1.33
	1.5kV	1159	888	935	771	1020	830	-4.83	-3.29

Table 1: Measured parameters from 5mm and 8mm nozzle testing

Cumulative energy	Charging Voltage	Curve fitting linear regression			
		5mm		8mm	
		A	B	A	B
Over the nozzles	1kV	-1889.33	8949.57	-787.10	11547.20
	1.1kV			2860.35	13199.95
	1.3kV	-11149.43	22931.11	-2045.15	22326.05
	1,5kV	3501.60	28483.54	2614.40	29020.90
over the electrodes	1kV	-2417.30	12966.70	-710.00	16158.25
	1.1kV			1583.95	19804.85
	1.3kV	3235.00	21698.20	-4121.30	29391.40
	1.5kV	2776.60	37107.69	1608.25	38305.75

Table 2: Curve fitting coefficients for cumulative energy over nozzle and over electrode as a function of the number of switching operations

Charging Voltage	$\int idt$ [As]		$\int i^2 dt \times 1000$ [A ² s]	
	5mm	8mm	5mm	8mm
1kV	19.6	27.7	42.8	91
1.1kV		31.4		117.5
1.3kV	33.3	38.8	132.4	187.5
1.5kV	39.9	47	187.5	280.5

Table 3: Average values of charge and heat generated from the arcing current

5mm nozzle	Charging Voltage	Curve fitting polynomial regression		
		A	B ₁	B ₂
Integral $\int idt$ [Coulomb]	1kV	1.050	16.359	0.573
	1.3kV	6.143	21.012	1.755
	1.5kV	1.930	34.318	0.955
Integral $\int i^2 dt$ [Heat]	1kV	7000.800	25896.004	3053.804
	1.3kV	58670.929	19523.798	15956.262
	1.5kV	16170.190	128020.058	9967.527
8mm nozzle	Charging Voltage	Curve fitting linear regression		
		A	B	p
Integral $\int idt$ [Coulomb]	1kV	-1.98	28.15	<0.0001
	1.1kV	0.46	31.48	<0.0001
	1.3kV	-5.25	40.06	<0.0001
	1.5kV	-1.34	47.25	<0.0001
Integral $\int i^2 dt$ [Heat]	1kV	-13270.50	93877.00	<0.0001
	1.1kV	1137.60	118313.90	<0.0001
	1.3kV	-48882.95	199003.55	<0.0001
	1.5kV	-24696.60	284683.87	<0.0001

Table 4: Curve fitting coefficients for the cumulative charge and heat as a function of the number of switching operations

Cumulative mass loss [mg]	Charging Voltage	Curve fitting linear regression			
		5mm		8mm	
		A	B	A	B
nozzle 1	1kV	-26.733	84.829	-10.75	105.050
	1.1kV			1.950	122.150
	1.3kV	-38.000	191.750	-13.05	189,15
	1,5kV	11.067	227. 886	18.336	232.466
nozzle 2	1kV	-17.000	88.000	-2.950	101.150
	1.1kV			8.600	127.200
	1.3kV	-82.286	173.786	-26.550	188.450
	1.5kV	85.867	205.943	32.250	244.750

Table 5: Curve fitting coefficients for cumulative mass losses of 5mm and 8mm nozzle as a function of the number of switching operations

Cumulative mass loss [mg]	Charging Voltage	Curve fitting linear regression			
		5mm		8mm	
		A	B	A	B
Electrode 1	1kV	3.47	23.20	-3.45	57.25
	1.1kV			-12.60	90.00
	1.3kV			-20.05	174.95
	1,5kV	-42.48	213.15	28.00	233.40
Electrode 2	1kV	17.27	33.11	-1.60	59.00
	1.1kV			-2.65	76.75
	1.3kV			-39.35	180.55
	1.5kV	-20.15	201.44	13.45	247.45
		Curve fitting polynomial regression			
		A	B ₁	B ₂	
Electrode 1 (5mm)	1.3kV	13.57	44.21	13.07	
Electrode 2 (5mm)	1.3kV	15.14	58.12	10.83	

Table 6: Curve fitting coefficients for cumulative mass losses of electrodes with 5mm and 8mm nozzle testing as a function of the number of switching operations

	Charging Voltage	Value at 1 st SW		Value at 5 th SW		Increment [mm]		Increment [mm/kJ]	
		Nozzle1	Nozzle2	Nozzle1	Nozzle2	Nozzle1	Nozzle2	Nozzle1	Nozzle2
D _{in} [mm]	1kV	5.16	5.16	5.73	5.73	0.14	0.14	0.0163	0.0163
	1.3kV	5.15	5.15	6.36	6.35	0.30	0.30	0.0141	0.0141
	1.5kV	5.44	5.39	6.9	6.93	0.37	0.39	0.0128	0.0134
D ₂ [mm]	1kV	5.16	5.17	5.73	5.73	0.14	0.14	0.0163	0.0163
	1.3kV	5.2	5.18	6.72	6.70	0.38	0.38	0.0178	0.0178
	1.5kV	5.41	5.49	7.35	7.28	0.49	0.45	0.0169	0.0155
D _{out} [mm]	1kV	5.17	5.17	5.73	5.73	0.14	0.14	0.0163	0.0163
	1.3kV	5.48	5.44	7.27	7.21	0.45	0.44	0.0211	0.0206
	1.5kV	5.71	5.68	7.82	7.72	0.53	0.51	0.0183	0.0176

Table 7: Expanded diameters and their increment for 5mm nozzle

	Charging	Value at 1 st SW		Value at 5 th SW		Increment [mm]		Increment [mm/kJ]	
	Voltage	Nozzle1	Nozzle2	Nozzle1	Nozzle2	Nozzle1	Nozzle2	Nozzle1	Nozzle2
D _{in} [mm]	1kV	8	8	8.46	8.46	0.12	0.12	0.0105	0.0105
	1.1kV	8.03	8.02	8.61	8.61	0.15	0.15	0.0112	0.0112
	1.3kV	8.01	8	8.92	8.91	0.23	0.23	0.0108	0.0108
	1.5kV	8.09	8.1	9.15	9.15	0.27	0.26	0.0097	0.0093
D ₂ [mm]	1kV	8	8	8.46	8.46	0.12	0.12	0.0105	0.0105
	1.1kV	7.97	7.96	8.85	8.88	0.22	0.23	0.0164	0.0172
	1.3kV	7.94	7.93	9.24	9.23	0.33	0.33	0.0155	0.0155
	1.5kV	8.12	8.14	9.64	9.67	0.38	0.38	0.0136	0.0136
D _{out} [mm]	1kV	7.98	7.98	8.64	8.58	0.17	0.15	0.0149	0.0132
	1.1kV	8.04	8.04	9.18	9.18	0.29	0.29	0.0216	0.0216
	1.3kV	8.03	8.2	9.84	9.94	0.45	0.44	0.0212	0.0207
	1.5kV	8.19	8.17	10.12	10.06	0.48	0.47	0.0172	0.0168

Table 8: Measurement of expanded diameter and its increment for 8mm nozzle

	Charging	Value at 1 st SW		Value at 5 th SW		Mean value of 5 SW		Increment %	
	Voltage	5mm	8mm	5mm	8mm	5mm	8mm	5mm	8mm
Time to max current [ms]	1kV	4.32	4.5	4.18	4.6	4.23	4.56	-0.81	0.56
	1.1kV		4.35		4.6		4.47		1.44
	1.3kV	3.4	4.1	3.66	4.5	3.59	4.3	1.91	2.44
	1.5kV	3.24	4.1	3.84	4.35	3.62	4.23	4.63	1.52
Time to max pressure [ms]	1kV	8.04	7.6	7.8	7.1	7.92	7.35	-0.75	-1.64
	1.1kV		7.5		7.2		7.37		-1.00
	1.3kV	8.16	7.6	7.51	7.6	7.67	7.58	-1.99	0.00
	1.5kV	8.02	7.73	7.5	7.1	7.70	7.41	-1.62	-2.04
Time between P _{max} and I _{max} [ms]	1kV	4.22	3.1	3.7	2.48	3.96	2.80	-3.08	-5.00
	1.1kV		3.2		2.6		2.90		-4.69
	1.3kV	4.69	3.5	3.75	3.07	3.99	3.29	-5.01	-3.07
	1.5kV	4.79	3.62	3.63	2.75	4.07	3.19	-6.05	-6.01

Table 9: Measured time to maximum current (t_1), time to maximum pressure (t_2) and time different (t_2-t_1)

Test conditions	Expanded in diameter of 5mm nozzle after each interruption [mm]					
	D _{in}		D ₂		D _{out}	
	Nozzle 1	Nozzle 2	Nozzle 1	Nozzle 2	Nozzle 1	Nozzle 2
Reference test	0.37	0.39	0.49	0.45	0.53	0.51
Two ignition wires	0.32	0.33	0.41	0.42	0.48	0.47
33kV on HV circuit	0.40	0.41	0.53	0.54	0.63	0.62

Table 10: Increment of expanded nozzle diameter in mm after each interruption under variable test conditions for 5mm nozzle testing

Test conditions	Expanded in diameter of 8mm nozzle after each interruption [mm]					
	D _{in}		D ₂		D _{out}	
	Nozzle 1	Nozzle 2	Nozzle 1	Nozzle 2	Nozzle 1	Nozzle 2
Reference test	0.27	0.26	0.38	0.38	0.48	0.47
Two ignition wires	0.23	0.22	0.35	0.35	0.45	0.44
0.5L Expansion volume	0.27	0.26	0.34	0.34	0.46	0.46

Table 11: Increment of expanded nozzle diameter in mm after each interruption under variable test conditions for 8mm nozzle testing

Curriculum Vitae

Name: Thanapong Suwanasri
Birthday: 14 December 1970
Birthplace: Bangkok, Thailand
Status: Single

Education: 1977-1983 Primary school in Chiang Mai and Nonthaburi
1983-1986 Suankularb Wittayalai Nonthaburi
1986-1989 Vocational certificate in electrical mechanics
King Mongkut's Institute of Technology,
North Bangkok (KMITNB), THAILAND

Academic grade: April 93 Bachelor of engineering (Electrical),
KMITNB, THAILAND
December 95 Master of Science in Electric Power
Engineering,
Rensselaer Polytechnic Institute (RPI), Troy,
NY, USA

Practical: April-June 90 Accumulatorenwerke HOPPECKE Carl
Zoellner & Sohn GmbH & Co KG, Brilon-
Hoppecke, GERMANY

Occupations: August 93-July 01 Electrical engineer at The Electricity
Generating Authority of Thailand (EGAT),
Nonthaburi, THAILAND
Since August 01 Research work (Dr.-Ing.) at Institute for High
Voltage Engineering, RWTH-Aachen
University